THESIS ON INFORMATICS AND SYSTEM ENGINEERING C102

# Analysis and 3D Visualisation of Microstructured Materials on Custom-Built Virtual Reality Environment

EMILIANO PASTORELLI

TUT
PRESS

TALLINN UNIVERSITY OF TECHNOLOGY
Institute of Cybernetics
Laboratory of Nonlinear Dynamics

**This dissertation was accepted for the defense of the degree of Doctor of Philosophy on May 26th, 2015.**

**Supervisor**: Heiko Herrmann, Dr.rer.nat., Prof. Jüri Engelbrecht, PhD, DSc.
Laboratory of Nonlinear Dynamics , Institute of Cybernetics,
Tallinn University of Technology, Tallinn, Estonia

**Opponents**: Prof. Lucio Tommaso De Paolis, PhD
AVR Lab, Department of Engineering for Innovation.,
Università del Salento, Lecce, Italy

Dr. Katja Schladitz, PhD
Fraunhofer ITWM.,
Kaiserslautern, Germany

Defense of the thesis: June 25th, 2015

Declaration:
I hereby declare that this doctoral thesis, submitted for the doctoral degree at Tallinn University of Technology, is my original investigation and achievement and has not been submitted for the defense of any academic degree elsewhere.

Emiliano Pastorelli



Colophon: This thesis was typeset with LaTeX 2ε using André Miede's *classicthesis* style with modifications by David Schryer and Ardo Illaste to conform with Tallinn University of Technology style guidelines. The main font is Libertine (Times compatible). Biolinum is used for sans-serif text.

ISSN 1406-4731
ISBN 978-9949-23-796-8 (publication)
ISBN 978-9949-23-797-5 (PDF)

INFORMAATIKA JA SÜSTEEMITEHNIKA C102

# Virtuaalkeskkonna arendamine mikrostruktuursete materjalide analüüsiks ja kolmemõõtmeliseks visualiseerimiseks

EMILIANO PASTORELLI

TTÜ
KIRJASTUS

# ABSTRACT

The main focus of my doctoral studies has been the work made to design and build a novel type of semi-immersive Virtual Reality (VR) system for scientific visualisation, and the implementation of software that could take advantage of its advanced features. The need for building a Virtual environment (VE) system was indeed strongly connected with the analysis of a 3D physical system, steel fibre reinforced concrete (SFRC), formed by mixing of concrete matrix with short steel fibres.

Semi-immersive multi-screen VE present two main problems: they require a large amount of space in order to provide a reasonable size visualization surface (due to the projectors throw distance) and they are still very expensive. That makes them a tool hardly affordable to many research institutions.
The existing software that can be used for the analysis of SFRC suffers similar drawbacks. They are mostly commercial software with undisclosed algorithms. The researchers face the choice to either acquire expensive licenses of software that cannot be modified to fulfil specific needs, or have the analysis performed by third parts with fees. The few non commercial ones usually tend to lack flexibility on the type and quality of the data they can process, they need the user interaction along the process or have very long processing times (up to three hours for a single dataset).

This work's answer to the above mentioned problems are the following ones:

- The design and building of the Kyb3, a VE representing a unique combination of displaying surface, occupied space and costs.
- The development of the algorithms and the software implementation of a fast, efficient and open source tool for the automated analysis of fibres orientation in SFRC X-ray tomography samples (μTAnS-fib).
- The design and implementation of a VR-ready software to visualize the behavior of fibres orientation tensors during SFRC Computational Fluid Dynamics (CFD) simulation castings, through the use of 3D superellipsoidal glyphs (A.C.T.I.V.E.) .

The VE was necessary as a platform where to both develop and visualize partial and final results of the software. The first task that we undertook was therefore

to design and build one.
In order to have a system that could attract interest on an international ground with its novelty, we decided to design it focusing on obtaining a unique ratio of display surface size, occupied space and costs. The development of our VE, the Kyb3, is described in detail in Publication I and was awarded with a Best Paper Award in the VARE2013 Conference in Tenerife (Spain).

To perform fibres orientation analysis on SFRC X-ray tomography scans we developed the algorithm and software, μTAnS-fib, that we presented on Publication IV. The aim was to obtain a powerful and fast tool for the automated analysis of the samples that could also provide data for the 3D visual inspection of the results.
Through the whole development of the software we used the Kyb3 as a visual debugging platform for the process partial and final results. The decision paid off: the first results, initially difficult to decipher numerically, turned out, once visualized, to be displaying a set of additional information describing features of the fibres orientation usually neglected by the traditional analysis methods.
The contribution of visual feedback to the success of our development process of the software is presented in Publication II.
The software results were validated both numerically and visually: we compared the resulting tensor data with that obtained from an existing method (skeletonisation) on the same large batch of datasets and we displayed them on the Kyb3. Researchers specialized in complex materials analysis could then inspect the results and confirm their validity.
The algorithm performed in the expected way, providing the results anticipated, new information about fibres orientation (described later in this dissertation) and in certain cases an even higher precision than the skeletonisation approach. The computational times have been cut down to less than one sixth compared to the previous method and no additional intervention from the user is required during the process.

To further extend our set of software related to complex materials analysis, we designed and developed a second tool able to work on VE s: A.C.T.I.V.E (see Publication III). Focused on the visualisation of SFRC research as well, the software uses superellipsoidal glyphs to visualise the fibre orientation tensor behaviour in CFD simulations of SFRC during casting time. Its portability and scalability allow it to run both on standard desktop computers and on more complex VE like the Kyb3.

# ANNOTATSIOON

Käesolev doktoritöö käsitleb uudse visualiseerimissüsteemi (Virtuaalse Reaalsuse - VR) projekteerimist ja vastava tarkvara arendamist. Vajadus taolise süsteemi loomiseks tekkis konkreetse kolmemõõtmelise (3D) füüsikalise süsteemi analüüsil, mis vajas visualiseerimist. Füüsikaline süsteem on perspektiivne ehitusmaterjal teraskiudbetoon, mille põhikomponentideks on betoonmass koos lühikeste teraskiududega asendamaks traditsioonilist metallarmatuuri. Kiudude orientatsiooni määramine senituntud meetoditega on osutunud väga tülikaks.

Eksisteerivad VR-süsteemid on väga suurte mõõtmetega, kuna kasutatakse suuri projektoreid ning vastav litsentseeritud kommertstarkvara ei luba paindlikkust andmete töötlemiseks. Seetõttu seati doktoritöö eesmärgiks arendada uus süsteem (nimega Kyb3), mis kujutab endast unikaalset väikesemõõdulist seadet minimaalse hinnaga. Seade pidi võimaldama automaatset kiudude orientatsiooni määramist teraskiudbetooni skaneeritud katsekehadel ja sellega seoses ka vastavate algoritmide ja vabavara väljatöötamist. Kiudude rivistustensorite määramine vajas spetsiifilist arvutusdünaamikal põhineva algoritmi väljatöötamist, mille baaselementideks valiti 3D superellipsoidaalsed glüüfid.

Uuringud algasid vastava VR-süsteemi väljatöötamisega vastavalt doktoritöö eesmärkidele. Süsteemi Kyb3 on kirjeldatud publikatsioonis I, mis sai ka parima artikli auhinna rahvusvahelisel konverentsil VARE2013 (Hispaania). Kiudude orientatsiooni analüüsiks skaneeritud katsekehadel on konstrueeritud algoritm ja vastav tarkvara (μTAnS-fib), mida on kirjeldatud publikatsioonis IV. See võimaldab saada ka andmeid tulemuste 3D visuaalseks kontrolliks. On oluline, et just visuaalne kontroll võimaldas saada täiendavat informatsiooni kiudude orientatsioonist, mis traditsiooniliste meetoditega ei õnnestunud. Taolise visuaalse tagasiside olulisust on kirjeldatud publikatsioonis II, kus võrreldakse numbrilist ja visuaalset analüüsi saadud tensorväljades, kasutades nende võrdlemist väljatöötatud seadmes Kyb3.

Tarkvara arendamise lõppfaas oli pühendatud andmete filtreerimise ja töötlemise parandamisele, arvutuste optimeerimisele ja saadud tulemuste võrdlemisele skelettalgoritmi rakendamisel saadud tulemustega. Väljatöötatud uudne algoritm lubas leida ka lisainformatsiooni kiudude orientatsiooni kohta ning omas mõnel juhul isegi suuremat täpsust kui skelettalgoritm. Oluline on aga suur võit arvutusaegades (kuni kuus korda).

Doktoritöös saadud tulemused on visuaalselt valideeritud Kyb3 süsteemil koos mikrostruktuure uuriva teadusrühmaga TTÜ KübIs. Selle uuringu tulemusena valmis rakendus A.C.T.I.V.E. kompleksstruktuuriga materjalide analüüsiks, mis on rakendatud loodud VR-süsteemis (vt publikatsioon III). Siin on originaalse ideena kasutatud superellipsoidaalseid glüüfe, mis visualiseerivad teraskiudbetooni valamise käigus tekkivaid dünaamilisi muutusi. Vastav tarkvara võimaldab seda kasutada nii standartsel lauaarvutil kui ka virtuaalkeskkonnas Kyb3.

# ACKNOWLEDGEMENTS

To stay focus and work throughout these years of Doctoral Studies would have not been that easy without the support of great friends and colleagues. Hoping to do not forget anyone, this page is dedicated to all of them.

The first thanks goes to Dr.Heiko Herrmann, my scientific advisor, thanks to whom I was able to move to Estonia for my Doctoral studies and be among the Estonian pioneers in a field I always dreamed to work on: Virtual Reality. The support he gave me in the development of the Kyb3 system and the correlated software has been invaluable and conditio sine qua non for the success of my whole research project.

To Prof. Jüri Engelbrecht, my supervisor, goes my unending gratitude for the inspiration he gave me since the beginning of my studies, the support and the cordiality he kept on offering me throughout my whole stay.

Almost four years of Doctoral studies in the Institute of Cybernetics, though, are not only based on research work but on people as well. In supporting me with coffee and chatting, Andrea and Artem absolutely excelled. Another thanks goes to Marika for all the help with translations, bureaucracy and her helpfulness in general. Outside of the Institute, Tiina, Kristiina, Ottavio, all the Perfect Dinner teams and all the Finnish friends also made wonders in making of Tallinn a place in which i loved to spend my working and free time.
It is with endless sadness that while writing this acknowledgements I also have to say goodbye forever to Fabio, that has always been among my best friends since more years that I can remember, and now passed away while still far too young. Rock on forever, my good friend.

A grateful and due special thanks goes to my parents, Lino and Franca, whose unbreakable support is keeping me on the run since more than thirty years, in life and in school. Another no lesser one goes to Rina, my grandmother, for everything she did, she's doing and she will do, and to all my relatives.
To Etta, my aunt, who recently passed away before being able to see me graduating, goes a memory that will last forever.
To Jennifer, for all her love, patience and support, goes a unique thanks for having


been and being with me throughout this exciting part of my life.

Last but not least, a special thanks goes to Prof. Giorgio Delzanno (Universita' degli Studi di Genova) without whom I would have probably never made it to Estonia in the first place.

Financial support from the DoRa 4 Programme sponsored by the Archimedes Foundation, the scholarships and grants from IT Akadeemia, HITSA and IT Doctoral School, and from the CENS Centre of Excellence at the Institute of Cybernetics is also gratefully acknowledged.

# CONTENTS

## LIST OF PUBLICATIONS

I Pastorelli, E; Herrmann, H; **A Small-scale, Low-budget Semi-immersive Virtual Environment for Scientific Visualization and Research.** *Procedia Computer Science*, 25(iii-iv), pp.14-22, September 2013

The author co-designed and built the Kyb3 Virtual Environment, wrote the initial draft of Publication I and presented it at the VARE 2013 conference (Tenerife, Spain).

II Pastorelli, E; Herrmann, H; **Virtual Reality Visualization for Short Fibre Orientation Analysis.** *Proceedings of the 14th Biennial Baltic Electronics Conference (BEC 2014)*, pp.201-204, Tallinn, Estonia, October 2014

The author took part in the design of the algorithm and implemented it, tested it on the Kyb3 Virtual Environment, wrote the initial draft of Publication II, applied the modifications suggested by the reviewers and presented it at the BEC2014 conference (Laulasmaa, Estonia).

III Herrmann, H; Padilla, M; Pastorelli, E; **A.C.T.I.V.E.: A Scalable Super ellipsoid-based CFD Visualization for Virtual and Desktop Environments.** *Eurographics Proceedings of EuroVR 2014 - Conference and Exhibition of the European Association of Virtual and Augmented Reality*, pp.1-4, Bremen, Germany, December 2014

The author supervised the design and implementation of the software, implemented part of it and co-wrote the initial draft of Publication III.

IV Pastorelli, E; Herrmann, H; **Time-efficient automated analysis for fibre orientations in Steel Fibre Reinforced Concrete.** *Proceedings of the Estonian Academy of Sciences*(Accepted)

The author co-designed part of the algorithm, implemented it in the μTAnSfib software, wrote the initial draft of Publication IV and applied the modifications suggested by the reviewers.

# LIST OF FIGURES

## LIST OF TABLES

The interdisciplinary nature of my chosen subject, Scientific Visualization, led me, through the years of my PhD studies, to encounter and deal with a wide variety of topics.

In order to achieve the final goal, it not only became necessary to acquire a good mastery of all of them, but it also implied the need to develop the understanding of how they could be synergistically merged together in order to maximize the results.

This implies therefore that this dissertation not only aims at describing the single modules involved, but also at giving a model of the interdisciplinary method employed. Throughout this whole process, subjects apparently disconnected from each other where developed and used together to enhance the results. This granted not only improvements in the whole project, but also granted me a personal wider understanding of its separate components.

Developing an algorithm (and its software implementation) able to perform the automated analysis on a specific type of complex material, SFRC by granting an effective visual feedback to the user, required at first to familiarize with the multitude of separate subjects involved. This introduction aims at granting the reader a shallow but sufficient background knowledge of most of them, in order to better understand why and how they were used.

In summary, this dissertation represents a concise overview of the work performed during my doctoral studies and its scientific outcomes. In order to examine in further depth the methodologies employed, the results obtained and the background information of the specific topics, the reader is invited to consult the appended publications.

# ACRONYMS

| | |
|---|---|
| SFRC | steel fibre reinforced concrete |
| VR | Virtual Reality |
| VE | Virtual environment |
| VRUI | Virtual reality user interface |
| VRPN | Virtual reality peripheral network |
| CT | computed tomography |
| HMD | Head Mounted Display |
| CAVE | Cave Automatic Virtual Environment |
| 6DOF | six degrees of freedom |
| FOC | field of view |
| DLP | Digital light processing |
| LCD | Liquid-crystal display |
| HID | human interface device |
| ITK | Insight Toolkit |
| VTK | Visualization Toolkit |
| VRML | Virtual Reality Markup Language |
| CFD | Computational Fluid Dynamics |

# 1

# INTRODUCTION AND STATE OF THE ART

## 1.1 MOTIVATION AND CONTRIBUTION OF THIS WORK

As we already introduced in the abstract, this dissertation is about scientific visualization applications using VR systems in the research field of complex materials analysis, in the specific case, SFRC.

This introductive chapter clarifies the motivation and contribution of our research, the outcomes in terms of algorithms and software developed and the related conference presentations. It also provides the background information necessary to full understand the work done by offering a summary of the three main topics involved: Scientific Visualization, Virtual Reality and Steel Fibre Reinforced Concrete.

### 1.1.1 *Motivation of the research*

The fundamental problem faced by our specific choice of topics was related to the nature of multi-screen semi-immersive VE. In order to grant a reasonably large display surface, these systems tend to require large amounts of space and their cost easily reach the hundreds of thousands of euros. What we wanted to have in our research group additionally, was not only a visualization system specifically made to display our research data, but also a system that could become a prototype to develop additional VR-oriented research.

The software tools to analyse and display the results of research on SFRC, showed even more complex problems in terms of flexibility of use (a more detailed overview of the existing ones is presented in section 1.6). The most effective ones are expensive, commercial suites with undisclosed and unmodifiable algorithms. That means they can be used as a tool, but offer no insight or understanding in what they do and how they do it. The alternative of relying on third part services presents the same drawbacks.

What we wanted was a flexible tool with open source code, that could be modified to expand its features while the research on the topic progresses and new areas of interest arise. The existing open access ones (described more in detail in section 1.6) present additional problems. They are first of all often very slow (to analyse a single sample they require approximately 3 hours, at least where timing was mentioned), they take into account well prepared and noise-free datasets (that is unfortunately rarely the real case) and often lack important features as the detection of partially cut or touching fibres.
Moreover, there are features of the fibres that contribute to the material properties of SFRC, as for example the hooks shapes, that are mostly ignored by the existing software.

The work done and presented in this dissertation addresses the above mentioned problems and merges the solutions together in order to highlight the benefits of VR visualization on the research on complex materials.

### 1.1.2 *Contributions of this research in the field of Virtual Reality*

Explained in further detail in Chapter Chapter 2, we can summarize this work contribution on the VR topic with the construction of the Kyb3 VE in:

- The Kyb3 presents a unique ratio displaying surface/occupied space: approximately $2.7\mathrm{m}^2$ of visualization area distributed over 3 screens, in a total occupied space of only $2\mathrm{m}\times1.7\mathrm{m}\times1.9\mathrm{m}$.
- Despite the contained size, the Kyb3 features all the attributes of the largest full-sized CAVE-like [6] VE: multiple screens perpendicular to each other, passive 3D stereoscopy, six degrees of freedom (6DOF) user tracking and interaction and space-saving mirror system for projections.
- Due to the complete design, construction and software implementation disclosure, the Kyb3 is a fully reproducible system.
- With all the above mentioned features, and a total cost of approximately 30.000 euro, it represents one of the most affordable systems of its kind.

### 1.1.3 *Contributions of this research in the field of Analysis and visualization of microstructures materials*

The contributions related to the analysis and visualization of complex materials are summarized in the algorithms and the implementation of the two tools we developed:

- Fibre orientation analysis in SFRC X-ray tomography scans, explained in detail in Chapter Chapter 3.
- Superellipsoidal glyphs-based visualisation of SFRC CFD simulations castings, detailed in Chapter Chapter 4.

To offer the reader an overview of the results obtained, we present here a list of the contributions for each of them.

*Anaysis of fibres orientation on SFRC X-ray tomography scans.*

- Automated analysis of fibres orientation in SFRC.
- Short computational times (Approximately 1/6 of the other existing methods where timing was available).
- Automated separation of touching fibres.
- Capability to filter and analyse even very noisy datasets.
- Data on the contribution of the hooks to the physical properties of the material in its uncracked state.
- Ability to process overnight large batches of datasets without need for user interaction.
- Numerical results (tensor data) and 3D visual data for VE visualization output.
- Released under open source license.

*Superellipsoidal glyphs-based visualisation of SFRC CFD simulations castings.*

- Computes CFD simulations of SFRC casting and visualizes them dynamically using superellipsoidal glyphs to display and highlight the fibres orientation tensors.
- Portable and scalable, can be executed on traditional desktop computer, immersive and semi-immersive VE.

- Extremely optimized to display animated simulations of large amounts of data also on low-performances systems.
- Full control of the visualization parameters and tools to allow in-depth inspection of the data.
- Released under open source license.

## 1.2 RELEASED SOFTWARE

The following software has been developed during the course of the work described in this dissertation and has been released publicly under open source license :

WintrackerIII Vrpn Server – a driver-less Virtual reality peripheral network (VRPN) server for the Wintracker III electromagnetic tracker. The server has been merged into the main trunk of VRPN and is now part of the official download. Available on http://www.cs.unc.edu/Research/vrpn/

μTAnS-Fib – a cross platform tool for the automated filtering and analysis of hooked fibres orientation in SFRC x-ray tomographies. This open-source software constitutes the implementation of the algorithm developed in the dissertation and produced the results explained in Publication II and Publication IV. Available on GIT repository : http://bitbucket.org/VisParGroup/utans-fib

A.C.T.I.V.E. – a scalable tool for Virtual Reality visualization of superellipsoid-based glyphs depicting the orientation equation of SFRC fibres during a CFD casting simulation (see Publication III). The software uses VRUI as framework and is therefore equally suitable for desktop or VR systems. This software would have not been possible without the gratefully acknowledged contribution of Marcel Padilla and Micheal Krause.
Available on GIT repository : http://bitbucket.org/VisParGroup/active

## 1.3 CONFERENCE PRESENTATIONS

The results of our research work have been presented at the following conferences:

- Santa Cruz de Tenerife (Spain) - Virtual and Augmented Reality for Education - VARE 2013
- Lecce (Italy), Salento Augmented and Virtual Reality - AVR 2014, Co-author.
- Tallinn (Estonia), Baltic Electronic Conference - BEC 2014
- Rakvere (Estonia), ICT Doctoral School - ICTDS 2014
- Bremen (Germany), EUROVR 2014, Co-author.

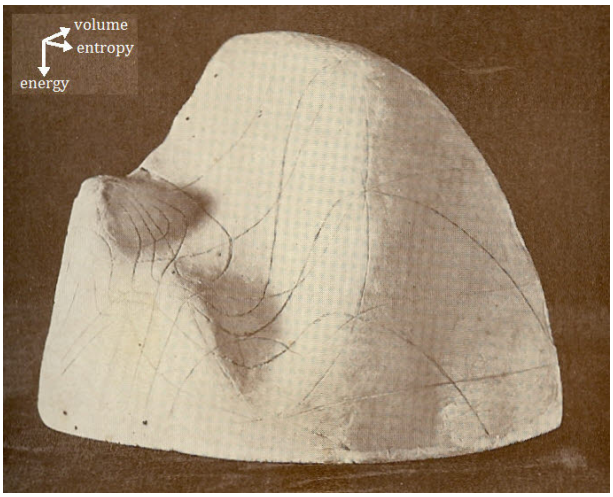


**Figure 1.1** – Gibb's thermodynamic surface of 1873, realized by James Clerk Maxwell in 1874

## 1.4 SCIENTIFIC VISUALIZATION

The incredible evolution witnessed during the last century in all the sciences went hand in hand with an increasing complexity and size of simulations and data.
Already in 1874, by sculpting in clay the famous Maxwell's thermodynamic surface (depicted in Figure.1.1), James Clerk Maxwell forecast the needs that would have developed in the years to come: the first scientific visualisation 3D model was born. Given the predominance of Vision among the human sensory inputs, a complete visualisation of a problem qualifies as an invaluable starting point to stimulate the user through the three separate levels of comprehension: presentation, understanding, and prediction. Vision's purpose is to smoothly introduce the user to the first one, Presentation. It must indeed communicate the data to the user in a way that is easy and fast for him to assimilate. During the last decades traditional visualisation techniques became obsolete in a majority of cases, or simply not sufficient any more to grant a valuable visual understanding of the processed datasets.
Simultaneously to powerful computational machines becoming able to perform more and more complex simulation in shorter times, new graphical algorithms and hardware began having an always growing importance in order to support all the scientific fields requiring visualisation features.
Due to the interdisciplinary nature of this visualisation, graphics algorithms mixed with the need for extreme optimisation and with the specific requirements of the addressed scientific fields. Its growth interwove with natural sciences in such a way to create a new unique branch of information technology: Scientific Visual-

isation.

This discipline specialises in solving visualisation problems in the three dimensional space for all the fields of sciences that might manifest the need.
By granting the possibility for visual inspection of the data (geometry) and relationships (topology), a whole new range of opportunity arises for the analysis of what would otherwise be presented as an enormous flows of numbers only. Hidden features and unexpected behaviours can be discovered more easily and faster, while validation and disclosure of results becomes more accessible for researchers, teachers and students. By merging aspects of scientific visualisation, information visualisation and automated data analysis, the progress of several studies belonging to the most diversified research areas has been boosted by several factors of magnitude.

Among the most interesting examples that we met during our research we find the superellipsoid-based visualisation techniques for liquid crystals alignments [17] the tensor visualisation for MRI imaging analysis [50]; *Crusta*, the virtual globe application able to enable immersive virtual field work using high resolution earth models [4] or the complex but extremely interesting 3D visualisation and interpolations of fractal surfaces [52].
Scientific Visualisation is a field in constant evolution, its pace being dictated by the innovation pursued by other scientific branches, in constant need for new techniques to display newly formed theories and data.

## 1.5 VIRTUAL REALITY

The fundamental drawback of classic 3D graphics (i.e. volumetric data, mesh visualisation, etc.) is due not to limitations in power of hardware and software, but to the nature of the compromise that was considered the only possible paradigm in displaying 3D data: the outcome was always presented on a 2D surface, the display [19].
This represented for years an insurmountable obstacle to the constant attempt of visualisation researchers to make the interaction with the data more and more natural, with the ideal aim of obtaining a quasi-real final result.
By evolving the visualisation and the interaction with the data into a natural process, it is possible to maximise the efficiency while minimising the discomfort caused to the user by being put in contact with an environment too complex to familiarise with. The earlier approaches to dissolve the unnatural interface between man and 3D environment constituted by the display and the traditional interac-

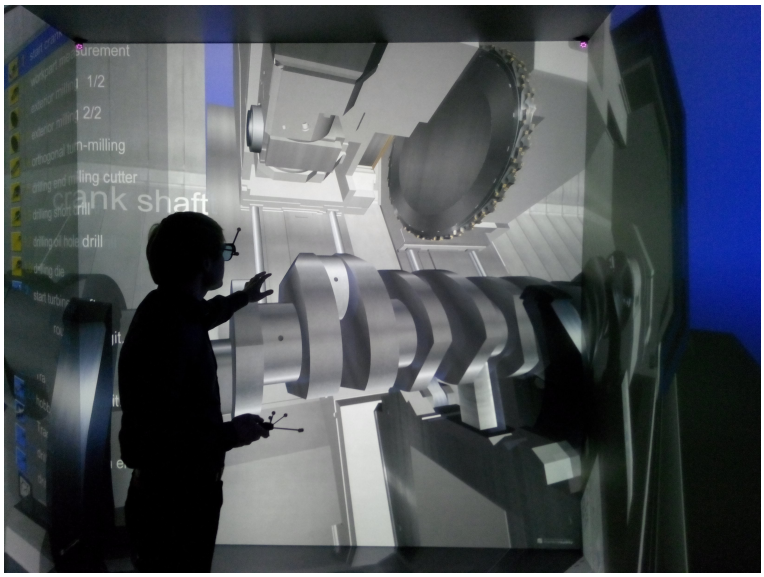


**Figure 1.2** – A semi-immersive multi user CAVE system at the Machine Construction faculty of the Chemnitz Technical University

tion devices (as the mouse (invented in 1960) or the keyboard), followed the input of sci-fi literature in the early 80s, and focused on HMD.
Although the possibility of granting a complete immersion in the simulated datasets and sceneries by occluding the visual of the real world to the user seemed initially to be the ideal choice, the technology of the time had not reached a sufficient development level. The topic gradually faded from the public spotlight.
At the same time, though, researchers did not abandon it at all, focusing instead on a different approach, semi-immersivity. Conceived with a less commercial approach, the first Virtual Environments of this kind, pioneered by the Cruz-Neira's Cave Automatic Virtual Environment (CAVE) (depicted in Fig.1.2) [6] at the University of Illinois in 1992, became huge room-sized systems. Extremely expensive and with large space requirements, the CAVE and its evolutions were anyway the ones that set the path to research in the field of Virtual Reality for the last 20 years.
Due to the large costs of building a CAVE, it was only a few research institutes that began first building room-sized CAVEs, and from there to using them on Scientific Visualisation applications, the step was an obvious one.
In the last ten years, though, the prices of the hardware necessary to run a VR system have decreased quickly, and that allowed a new decision: either spend the same amount of money as before and build systems tens of times more powerful than their ancestors (in performances, resolution, features, etc.) or to build smal-


**Figure 1.3** – Latest customer market VR devices, Virtuix Omni multi-directional treadmill, Oculus Rift HMD and STEM wireless user tracking device

ler systems with very limited budgets.
In the second case, obvious compromises have to be accepted, but on the wave of the latest VR devices (depicted in Fig.1.3), like *Oculus Rift*,*STEM* Tracking system or *Virtuix Omni*, VR is finally on the verge of entering, at least on a single-user level, the fully accessible customer market.

## 1.6 STEEL FIBRE REINFORCED CONCRETE

SFRC is a modern cementitious composite material made of aggregate, cement that incorporates discrete discontinuous fibres. SFRC is bound to gradually substitute the traditional metal bars or grids reinforced concrete for several applications in the construction industry.
The need to reinforce concrete arises from the nature of the material itself. By being brittle, with a low tensile strength and low strain capacity, concrete needs, in order to perform properly, a way to bridge the micro cracks that propagate in its structure.
That method is represented, in the specific case of SFRC, by a certain amount of steel fibres with hooked ends, 50 mm long and 1 mm thick, mixed in the concrete (see Fig.1.4).
Their presence is therefore important in order to improve the mechanical property of the material. They help the concrete in bearing part of the tensile stress and chemically and mechanically transfer the remaining part to more stable regions of the matrix. Multiple factors influence the efficiency of the fibres: shape, volume fraction, aspect ratio, their surface properties and orientation [43].
As the orientation distribution of the fibres within the matrix is non uniform, the properties of the system often tend towards anisotropy. A number of investiga-

**Figure 1.4** – A hooked-ends steel fibre

tions though [13],[53],[27], have been demonstrating the strong influence that the orientation has on the material properties.
One of the most influential causes of isotropic orientation, is for example the so-called "wall effect", i.e. the influence of the bounding mould in generating nearby regions of fibres with dominant orientations.
Due to such a variety of different mould shapes and casting conditions and methods, non-destructive testing becomes a necessary approach in order to identify the relations cause-effect that generate specific fibres orientation. Such a knowledge represents an invaluable asset in order to improve the existing industrial techniques and machines and properly train the construction workers.
The state of the art of the research on SFRC, focuses nowadays on non destructive analysis methods. This approach, considered to be the ideal one as it preserves the internal state of the concrete without any intervention that might influence it, has been developed by several research groups through the use of different techniques.

The majority though, employed the same approach (even if with slightly different equipment) in order to acquire the data from the SFRC: x-Ray tomography [39], [43], [47].
Through a computed tomography (CT)/micro-CT scanner, the samples of concrete are scanned and reconstructed to be later analysed through specialised software.
Among the disclosed analysis techniques, the most recent ones are :

- The fibre skeletonisation approach developed by a collaboration between the Institute of Cybernetics of Tallinn University of Technology (Estonia) and the Helsinki University (Finland) [43]. This method is based on reconstructing each fibre skeleton and determining its orientation value.

- The method presented by the researchers of the Department of Civil Engineering of the University of Burgos (Spain) [47] that employs linear regression for each fibre in order to extract its orientation data.

Other approaches have also been developed without the use of x-Ray scanners, for example DC-conductivity based [8], AC-impedance based [31], magnetic methods [11] and slicing photometry [8], [42].

# 2

# VIRTUAL REALITY - THE DESIGN AND BUILDING OF THE KYB3 VIRTUAL ENVIRONMENT

In the previous chapter we introduced VR as a more natural and articulate way of interacting with the data. A wide amount of scientific work revolves on the correct understanding of multivalued data. Correlations among those values can often be spotted and then further investigated more easily through human direct inspection. The human vision system, often able to beat the most advanced algorithms in the detection of visual patterns and anomalies, grants the scientists an incredibly fast method to peek into hints that often lead to further research developments [46].
Visual inspection, as introduced in section Chapter 1 provides the user with a quick means to narrow down research so as to address specific areas or behaviours in the data.

This chapter will first introduce the reader to the multifaceted aspects of VR and then descend into the details of the design choices and implementations, both hardware and software, that lead us to the construction of the Kyb3 VE.

Since its first appearance,the study of VR impact is based on the two main concepts that describe how the user is affected physically and psychologically by the surrounding VE: Immersion and Presence.
Immersion is the factor that arises from the physical configuration of the VR system and from its user interface. According to how much the VR scene "wraps" the user, the systems can be classified as immersive (HMD), semi-immersive (CAVE-like VEs) or non-immersive (desktop environments).
A more subtle and more difficult to define factor is the sense of presence that the system manages to transmit to the user. Currently the subject of several ongoing researches, presence is generated by a mix of still partly unknown stimulations of the brain and grants the user the illusion of really being in the VE. The higher the amount of presence, the more the user will behave and feel in the VE as if being in a similar real-life situation.

This has not only been a reason why several researchers are currently employing VR as a method to treat phobias and other mental dysfunctions, but also one of the governing factors that motivate our full research. From the naturalness with which the user can interact with a 3D VR scene, arises several of the benefits to visualization that we depicted in section Chapter 2 [15].

Some years ago, in 2012, VR had not yet entered the spotlight with customers devices as it happened during the last year. Despite that, a large number of institutes and companies all over the world already bought or built their own expensive room-sized VE. Most of the European largest car companies such as Mercedes, VW and BMW already have built, in the last 4-5 years, semi-immersive CAVE-like systems, employing them both in the design, testing and customer presentation of their products.
In Germany, the Leibniz Supercomputing Centre (LRZ) and the RWTH Aachen University already owned two of the largest VE in Europe and were developing their technology for several years. The European Space Agency (ESA) built its VR Theater in 2004, while NASA is employing an ever growing variety of room-sized and personal VR simulators since the appearance of the first CAVE system.
The common trait that the above-mentioned institutions have in common is the large availability of money and space: two among the most critical factors for the development or acquisition of a large multi-user VE.
Upon my arrival in Estonia nothing had been done yet until that moment in the country in the field of VR, and that offered a unique chance.
Being the first attempt at VR in Estonia, and having decided that the only way that could have really started research in that direction was to design and build the whole system by ourselves at the Institute of Cybernetics, we realized that we had to begin with small steps. A room-sized CAVE-like system worth several hundred thousands of Euro was out of the question and would not have made much sense.
The aim was to conceive a VE that could carry out multiple objectives according to a number of specific needs and constraints.
We therefore decided to design a system that:

- Was budget and space-contained and run exclusively with open source software, in order to design an affordable and easily accessible visualization tool.
- Had, on a smaller scale, all the features of a room-size VE: 3D stereoscopic visualization through projector-mirrors system, multiple screens in a corner-like setup (i.e. at least 3 screens) and full 6DOF user tracking and interaction.

- Could be used in multi-users Scientific Visualization.
- Was flexible enough to be used in a variety of other applications fields like Medicine, Cultural Heritage or Engineering and Design.

The above mentioned choices dictated the whole design process and all the decisions we made, as explained in Publication I.

In order to better understand the nature of the Kyb3 and its peculiar characteristic, it is necessary to go more into detail through its separate components. This will grant the reader not only a better understanding of the VE itself, but also a semi-complete guide on how to design a similar system. We will now narrow down each of the following subsections onto the components of the Kyb3:

- Projectors, Mirrors (Section 2.1)
- Circular polarization-based 3D Stereoscopic Vision (Section 2.2)
- User tracking (Section 2.3)
- Frame and screens (Section 2.4)
- Software infrastructure (Section 2.5)

## 2.1 BUILDING THE KYB3: PROJECTORS AND MIRRORS

Ever since the Cruz-Neira CAVE [6], VR researchers realized that using direct projection to generate the images from the beamers implied too large a waste of space.
This became even more relevant to the specific case of a room-size CAVE-like system, where each screen side is usually between 2.5 and 3 meters, whereas a direct projection would have implied a necessary throw distance of at least 5-6 meters for each wall, that summed all together and taking into account the $3\mathrm{m} \times 3\mathrm{m}$ area of the CAVE would have meant the need for a $15\mathrm{m} \times 15\mathrm{m}$ room, folding the projector beam through the use of mirror surfaces halved that space requirement.

In our specific case, the space constraint was even tighter, and we had to take some specific measures in order to achieve a large enough projected image while minimizing the required throw range.

The only viable option offered by the market, in order to achieve a large image with a short throw distance, were the so-called Short-throw projectors. The selection narrowed further because of the requirements described in section 2.2,

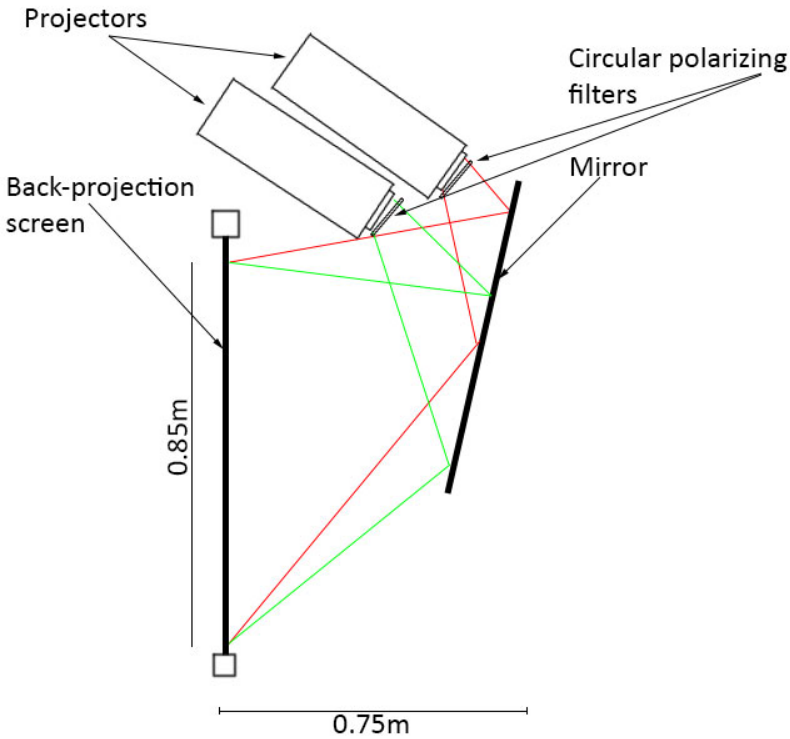


**Figure 2.1** – Projectors and mirrors setup in the Kyb3

that forced us to exclude LCD Projectors, whose light is inherently polarized and would therefore conflict with the stereoscopic effect [36].
A search on the best compromise of quality and price led us to the choice of the Acer S5201B Digital light processing (DLP) model.
With a $1024 \times 768$ resolution, 3000 ANSI lumen of luminosity, a throw range that allows to project a $1.3\text{m} \times 1\text{m}$ image from a distance of approx 0.9 m and an easily accessible price of approx 700 euro, this model was a perfect fit to our specific needs.

The sum of throw range plus the length of the projector though, was reaching a total length of approximately 1.5m and that was far too high for us to stick to our space constraints.
We therefore resorted to the above mentioned mirrors-based system (depicted in Fig.2.1). For each pair of projectors, a single mirror was set up. With a 100% distortion free image and an almost perfect reflectivity, the professional foil-based

mirrors where the only choice.
Able to preserve the polarization and granting a much higher reflectivity than traditional glass-coated ones, these mirrors consist of a thin reflective foil tensed on top of an aluminium structure. They are extremely fragile and prone to accidental damage; but represent the only possibility for a flawless projection.
For the projectors to be able to cast such a large image with such a short distance, their lenses have to be strongly round-shaped, in order to "spread" the image onto a larger surface. This is the main advantage of short throw projectors, but it generates additional problems in their setup.
Each slight movement of the projector indeed, be it a translation or a rotation, has very large repercussions on the cast image; this is easily cause for unwelcome deformations of the image.
Additionally, the customers market projectors, different from the professional ones, often tend to have an imprecise projection beam alignment, i.e. it is not uncommon that two identical projectors, with the exact same settings and positioning, generate slightly different images on a surface at exactly the same distance.
Due to the above mentioned characteristics of the hardware and the Stereoscopy requirements described in section 2.2, even with the fine tuning structure we built (see section 2.4) the precise alignment of each pair of projectors required no less than 20-30 hours of two people's work.

## 2.2 BUILDING THE KYB3: CIRCULAR POLARIZATION-BASED 3D STEREOSCOPIC VISION

With its spread on the customer market with 3D movies in the cinemas and 3D televisions, stereoscopic vision is nowadays a quite well renowned topic.
Differently from the projection of a video stream on a single display though, employing stereoscopy on a multi-screen interactive system has a variety of additional factors to be taken into account while deciding for the exact techniques to be used.

The fundamental concept behind 3D visualization is stereoscopy. Based on the exploitation of the anatomical properties of the human vision system, stereoscopy provides each eye with a separate 2D image, taken from the same angle and perspective from which that eye would be looking at the scene.
This results in two images, only slightly different from each other, but produced in a reliable approximation of how human eyes process the visual information in

the real world.
By feeding the brain the two separate images, the stereoscopic device takes advantage of the binocular vision of the user [34], in which the simultaneous perception and consequent fusion of them during the brain processing result in the perception called Stereopsis [35], i.e, the perception of depth and 3-dimensional structures in space.

The two main approaches in stereoscopy are divided into Active and Passive.

First appearing in 1986 [45] the active stereoscopy approach, also called alternate frame sequencing mode, is based on displaying the images by alternating the one from the left eye and the one from the right eye while simultaneously blocking the vision on the eye not in use for a given frame.
This process is usually achieved through Liquid-crystal display (LCD) shutter glasses that rapidly darkening one of the two eyes at a time, while the projector beams the alternate images.
A timing device is usually in charge of controlling the synchronization between the shutters and the refresh rate of the projected image.
In order to produce the alternated images stream flawlessly, so that the user's eyes will not perceive any flickering, projectors and monitors for active stereo need to perform at at least 120Hz.

Passive stereoscopy on the other hand, uses the evolution of an even older approach, the red-cyan anaglyph invented by Wilhelm Rollmann in Leipzig, in 1852, to deliver the stereoscopic perception [38].
Whereas the red-cyan is still used nowadays only for a small range of simple applications, its load-bearing concept fathered the modern passive stereoscopy: the system displays two superposed images, that represent the left and right eye separated point of view, and the user is equipped with glasses whose lenses are able to filter the visual input, allowing each eye to only perceive the image meant for it [51].

In the specific case of the Kyb3, our chosen filtering principle is based on circular polarization [29].
Linear polarization means that each projector is fitted with a polarizing filter, and for each couple of projectors light is polarized on a perpendicular direction (i.e. one of the filters will be horizontally polarized and one vertically).
The user's glasses will then have the lenses polarized in corresponding ways, so that each eye will only see the image intended for it.
Such a linearly polarized setup would be perfectly usable and relatively cheaper on a wall-like screen or on a setup with only two screens perpendicular to each other on only one axis. In our specific case, given the presence of the table display, linear polarization would result in a major problem: according to the position of

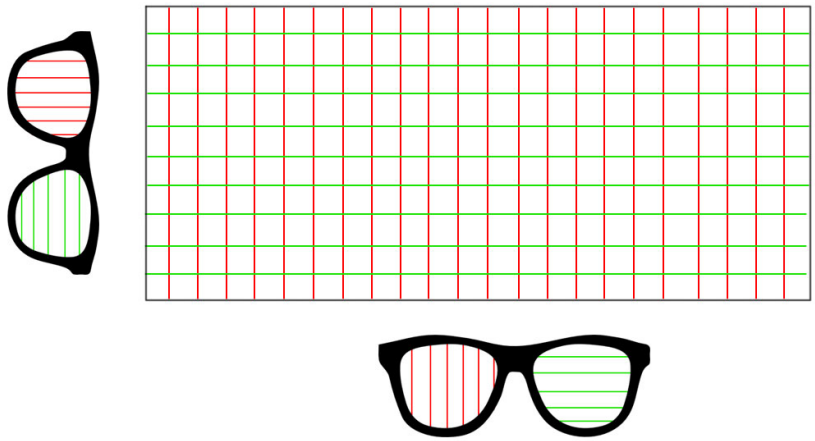

**Figure 2.2** – The image for the left eye, vertically polarized (red grid lines) would swap with the one for the right eye, horizontally polarized (green grid lines) in the moment the user would reach the side of the table

the user around the table screen, in the moment the user would move around the table, as explained in Fig.2.2 , the images would be first partly merged and then swapped to his eyes. A similar problem would appear in case of the user tilting their head.

The circularly polarized filters that we used on the Kyb3 (see Fig.2.3) solves this problem by giving a rotational polarization to the light waves. Each of the filters for each pair of projectors will be applying an opposite rotation direction to the light (i.e. one clockwise and one counter-clockwise) so that the polarization effect will not be influenced any more by the position of the user and the alignment of their glasses [29].

## 2.3 BUILDING THE KYB3: USER TRACKING

The real world vision paradigm implies that accordingly to the view point position and rotation, the objects will be perceived according from a different angle, therefore displaying different sides and features of the visualized objects.
To achieve the same result in a VE, and in order to maintain the correct 3D stereoscopic perspective described in section 2.2, the system needs a way to be constantly aware in real time of the user's head position and orientation.
Not only that, but also in order to grant a possibility of interaction in the 3D space, traditional input devices like the mouse would not be sufficient any more.

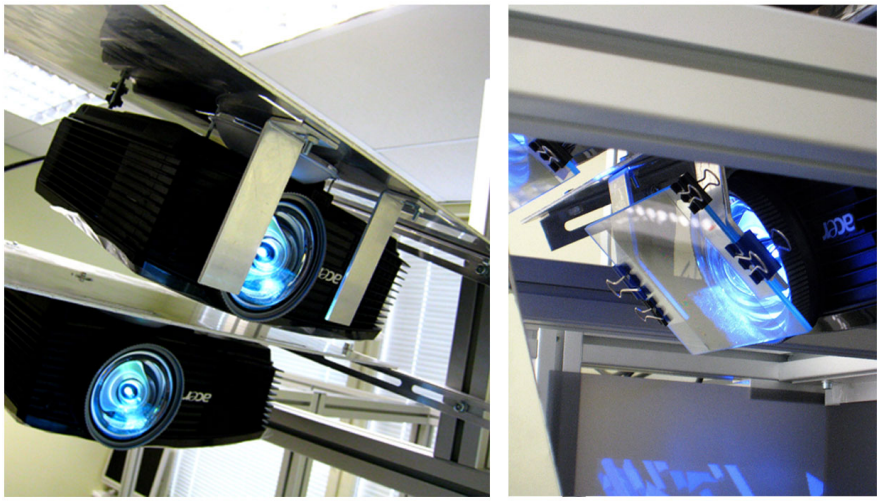

**Figure 2.3** – Filter support and installed polarizing filter

The approaches to user tracking are usually divided into two main categories: optical and electromagnetic [37].
In short, the first ones employ a number of cameras to track position and rotation of one or more set of markers placed on the user and their interaction devices. The second ones are composed of an emitter of an electromagnetic field and a number of sensors whose position is tracked inside the magnetic field.

Although the first ones became nowadays, in terms of user appreciation the most commonly used ones (the user doesn't have to have any wire impairing his movement in the system), those systems still tend to be exceptionally expensive. In order to correctly track the user and the interaction tools in the whole scene, the tracking device needs to employ an amount of cameras that varies, according to the system size, between 2 and 8.
Even though 3 would have probably been sufficient to follow the user all around the Kyb3, each of the cameras usually costs approximately 10.000 euro. That would have made the device, considering also the need for the interaction wand and markers, more expensive than the whole Kyb3.

Cheaper optical user tracking solutions, realized for example by employing the skeleton tracking features of the Kinect-like cameras, were quickly excluded due to a variety of problems they would pose in our specific case [48] [2]. The lack of rotations information on the skeletal joints (including head), the very tight constraints in terms of luminosity of the room, range and view angle and finally the

extreme data flooding of the USB BUS in order to transfer the whole amount of video and data made us discard it as a choice. The Kinect would have caused a much higher amount of new problems to solve than what the low price of the device would have been worth.

The only remaining alternative at that point was for us to decide for electromagnetic tracking. Although partly despised because of the need for wires connecting the user to the tracker and because of the variety of factors able to distort the magnetic field of the device and therefore the measurements [23], [54], [1], the electromagnetic trackers offer a precise and quite reliable 6DOF in a range of prices several times lower than the optical ones.
After a long survey on the available ones, comparing prices, range of action, number of sensors and additional features, our choice fell on the VRSpace WintrackerIII (displayed in Fig.2.4(a)). Provided with 3 sensors and effectively working in a range of 0.3m to 1.3m from the emitter, the WintrackerIII comes with an additional range extender, effectively doubling that range if the need arises (both the minimum and maximum range are extended) .

By using a USB cable and a human interface device (HID) interface, the WintrackerIII offers a minimal, almost non existent drivers-free development interface for software to obtain the 6DOF data. By using the LibUSB libraries we developed a C++ VRPN [44] server that later on became part of the VRPN main trunk. After that, the WintrackerIII was usable with the large majority of the VR-related software thanks to the wide spread of VRPN as device manager for VEs.
The main head tracking sensor is used to determine the perspective of the scene and its stereoscopic properties. In order to obtain an interaction tool or wand as they are usually called, we decided to hybridize one of the unused sensors of the WintrackerIII with the Wiimote, a gaming device produced by Nintendo. Usually autonomous in motion sensing through the use of an integrate infra-red camera and an accelerometer, the device native features immediately proved to be too limited in a system like the Kyb3 . We therefore connected the spare sensor of the Wintracker to the Wiimote, in order to obtain from the electromagnetic tracker the 6DOF data, and from the Wiimote the flexibility offered by the 11 clickable buttons.
A few months later, the Wiimote wand was substituted by another gaming device, the Razer Hydra (shown in Fig. 2.4 ,a). Basically structured as an autonomous electromagnetic tracker, the Hydra offers two 6DOF wands, each endowed with 7 buttons and an analogue controller for additional interaction options.


**Figure 2.4** – (a) Wintracker III (with wiimote wand), (b) Razer Hydra 6DOF controller

## 2.4 BUILDING THE KYB3: FRAME AND SCREENS

Among the most influential design decisions that we had to take there was the one related to the "shape" of the screens system and of the whole structure bound to support it.
As mentioned in the beginning of this chapter, among the requirements we defined for the Kyb3, there was the fact of being multi-screens built, possibly with corner-like screens setup as real CAVE. This decision derived from a dual need. On one hand, we needed to create a focusing and space-optimized area of visualization, fitting scientific visualization applications and at the same time presenting an opportunity to learn all the construction and configuration problems related to such a specific setup.

A variety of studies [30], [32], [20] conducted on the psychological benefits of VR environments on the perceptual attention focus of the user, usually tend to define the user in a span of 190° horizontally and 90° vertically. That implies that in order to obtain the given amplitudes with a single flat screen without forcing the user to be really close to the screen, would require a very wide and high screen. On a multi-screen VE on the other hand, that can be achieved more easily with a proper corner shaped disposition of the screens themselves.
Taking into account the previous considerations, we therefore decided to have 3 screens on our VE. After several evaluation tests, also in order to reproduce the most specific features of CAVEs, we chose a corner-like setup, with all the screens perpendicular to each other (two wall-like and one table-like) .
To produce a single image spanned across multiple displays has a primary requisite: the separate projections of each screen must be joined seamlessly. Even a small gap of a few millimeters is sufficient to break the stereoscopic effect and

**Figure 2.5** – 3 Screens support frame details

immediately nullify the immersion feeling of the user.
We therefore designed the frame of the whole system with the screens positioning as a first constraint. We made it so as to offer the screens a solid fixed position and, for the horizontal one, a sufficient supporting surface to avoid bending effects (depicted in Fig. 2.5).

The choice to use the whole projectors-mirrors paradigm described in 2.1 in order to reduce the necessary space occupied by the Kyb3 in the room, had a large influence on the design of the frame.
In order for the two projectors to cast their images onto the mirror and from them having it reflected back onto the screen so that the two projections superpose with the highest possible precision, some fundamental features were necessary:

- A support post on which the two projectors could hang upside down and that allowed the full configuration (translations and rotations) of each projector independently from the other.
- The projector supports also needed flexible fixing points on which to attach the polarizing filters plates.
- A support structure for the mirror, able to translate horizontally and vertically and to allow the tilting on the horizontal axis

In order to achieve the above mentioned flexibility, we designed the supports for the projectors as sliding metal plates supported by rails mounted on vertical rails (as shown in Fig.2.6). This, together with the particular shape of the plates, allows millimetre-wise and degree-wise configurations and was invaluable to achieve the final alignment result.
In order to achieve the same results with the mirror, and therefore to grant the

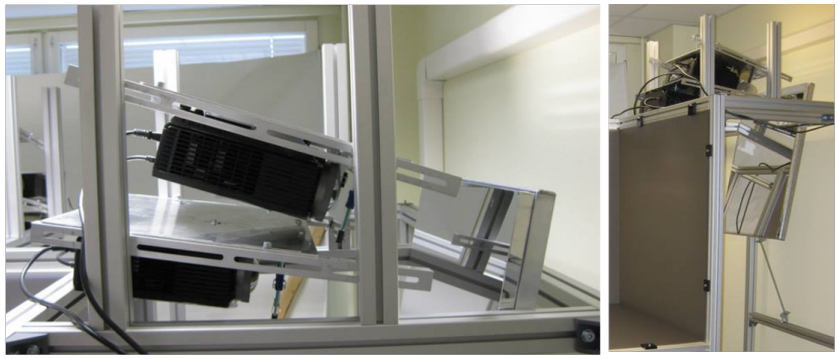

**Figure 2.6** – Details on the projectors and mirror mounting posts

system an additional level of flexibility during the setup, we fixed the upper part of the mirror frame on sliding metal posts, and the lower part to an adjustable threaded rod (displayed in Fig.2.6).

As mentioned in section 2.3 the material on which the frame had to be built was an important decision. It implied an investigation on the material properties (heat resistance, stability and robustness)and was strongly influenced by the choice of the Electromagnetic Tracking System as a tracking method. To minimize the distortion of the magnetic field generated by the tracker emitter [23], [54], [1] a non metallic material would have been the best choice. Unfortunately, most of those with an accessible price were too easily subject to deformations due to heat, or simply not robust enough. The choice became therefore aluminium that, being a non ferromagnetic metal, was one of the materials with the right physical properties and still able to minimize the distortion of the electromagnetic field.

Once the design of the frame was complete in every single detail, a local Estonian company, Dimentio OÜ built all the separate components, that were then assembled in approximately 5-6 hours of work.

## 2.5 BUILDING THE KYB3: SOFTWARE INFRASTRUCTURE

In order to design an affordable system that could also offer the ideal prototype on which to learn the whole variety of factors involved in the design of a VE, we decided that the Kyb3 would have been employing only open source software.

This choice granted us that, throughout the whole process, we would have had access to each single component of the software infrastructure in order to enhance our learning and the flexibility of the whole system.

The current operating system of the Kyb3 is Linux Debian 7.0 "Wheezy", even though different releases of Linux "Ubuntu" were successfully tested as well. Compared to the more user-friendly Ubuntu, the Debian release of Linux grants a higher amount of flexibility and a better decoupling of operative system logics and interfaces, a fundamental feature for a multi-screen environment.

The first step to prepare the Kyb3 after the operative system and the visualization devices (graphic cards and projectors) were properly configured, was to set up the communication between the interaction devices described in section 2.3. As already mentioned, we decided to adopt VRPN [44] as foundation of the interaction between tracking devices and the Kyb3. Once we wrote and configured the VRPN server for the WintrackerIII and Razer Hydra, through which the majority of the software we employ manage their input, we decided for Virtual reality user interface (VRUI) [25] as development platform of choice.

Compared to another variety of available frameworks that can be used to develop software for VE, VRUI offers a set of valuable features that made the choice an obvious one:

- A very optimized and performing wrapping of the OpenGL libraries
- A smart system to maintain the context data commonly available to all the display avoiding computationally heavy replication of the data among the separate screens
- An integrated interaction system that takes care of most of the problems related to the visualization, allowing developers to focus on the scope of their software while the surrounding environment is already managed
- An optimal scalability that allows the same software to be run without any modifications on a desktop system, a multi- screen VE or even on a HMD.

## 2.6 CHAPTER CONCLUSIONS

In this chapter, we explained in detail how we designed and built the Kyb3 infrastructure, both in terms of hardware and software. The accurate choice of particular components and the use of the multiple combined techniques that we applied, allows the Kyb3 to feature a unique ratio of display surface, occupied space and costs. By illustrating the full design details and measurements, and thanks to the use of open source software only, we provide the possibility to reproduce a VE

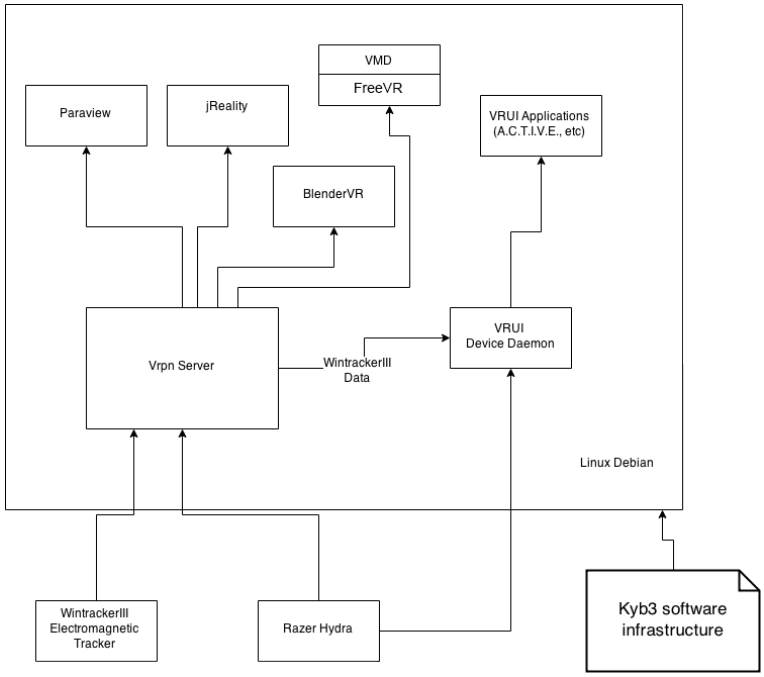


**Figure 2.7** – Kyb3 basic software infrastructure

of the same kind to any other research institution with needs similar to ours. Addressing budget and space availability, often the major constraints in the decision of having a visualization infrastructure it is our aim to promote the diffusion of such systems.

# 3

# STEEL FIBRE REINFORCED CONCRETE CT AUTOMATED ANALYSIS

In the introduction we presented the complex material that constitutes the main application field of the algorithms and methods developed in this dissertation. The core of the software development on the Kyb3 is indeed centered on SFRC and originates from a specific need: non-destructive testing.
Throughout section 1.6 we described briefly the reasons motivating the importance of the fibre orientation and distribution and in the next chapter we will explore the process that leads to such a physical configuration of the steel fibres.
As in many research processes, the analysis of large amounts of data represents a vital starting point in order to deduce the causes and predict the possible effects of different setups of SFRC.
The concrete itself represents a very physical obstacle to this same analysis: the fibre are embedded in a solid block of cement and any attempt to extract them would disrupt their state, therefore invalidating the analysis.

In this chapter we will go in detail through the approach for a non destructive analysis performed using an x-ray tomography scanner [43] and a self developed algorithm and software (as described in Publication IV). The analysis process produces the fibres orientation data used to determine the physical properties of the material and the appropriate file formats to visualize such results. Through the following sections we will describe in detail the acquisition of the data, the filtering of the radiographies and the extraction of the orientation data.

## 3.1 DATA ACQUISITION

The first step in order to obtain the datasets consisted in drilling some cylindrical samples out of specific areas (edges and center) of large SFRC floor slabs (shown in Fig. 3.1) ( $H \times W \times L$: $25\text{cm} \times 100\text{cm} \times 500\text{cm}$) [43].
The slabs were cast with class C30/37 self-compacting concrete and reinforced

**Figure 3.1** – SFRC samples drilled out of the floor slab

with 50 mm long and 1 mm thick fibres with hooked ends (depicted in Fig.3.3) made out of steel wire (C4D/C7D steel according to EN 10016-2 standard).
The amount of fibres in the mixture was 80 kg/m$^3$, with an approximate number of fibre per dm$^3$ of 250.

The cylinders were scanned in the laboratories of Helsinki University (Finland) through a μCT Nanotom 180 NF supplied by Phoenix Xray Systems + Services GmbH (Wunstorf,Germany) (depicted in Fig. 3.2).
The scanning process resulted in 360 projection images of $1127 \times 576$ pixels (for an effective pixel width of 128.3 μm). The reconstruction of the tomography was then performed by an FDK-algorithm-based [10] software supplied by the scanner manufacturer. Figure 3.4 shows top (a) and side (b) view of the reconstructed data. Throughout the reconstruction, a beam hardening (attenuation in grey level contrast due to the loss of correction module was applied in order to equalise the grey scale values between the central part of the cylinder and its edges. Due to the absorbing nature of the concrete though, the intensity values from the core of

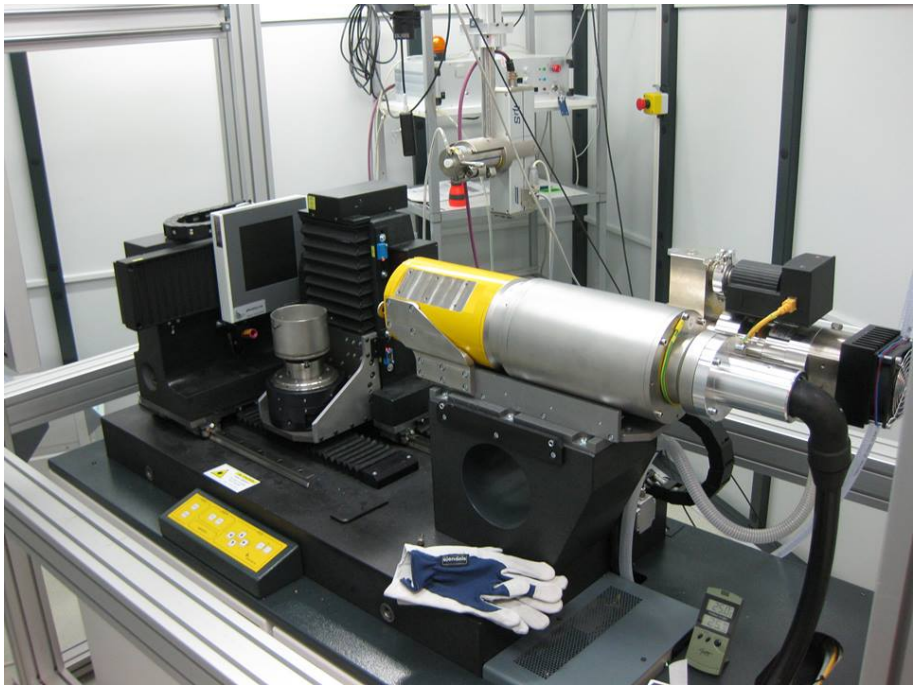

**Figure 3.2** – Custom-build SFRC x-ray scanner

the cylinder were too low for the algorithm to perform correctly, and a number of artefacts were therefore generated during the process.
The resulting raw data, describing a volume of $900 \times 900 \times 576$ voxels (the 3-dimensional equivalent of the pixels in 2D) was then used as input for the filtering.

## 3.2 DATA FILTERING

Due to the nature of the concrete, as already partly described in section 3.1, the volume datasets were not in ideal conditions for the analysis. The first step had to be a massive filtering process to prepare them.

**Figure 3.3** – Hooked end steel fibre used in the analysis datasets

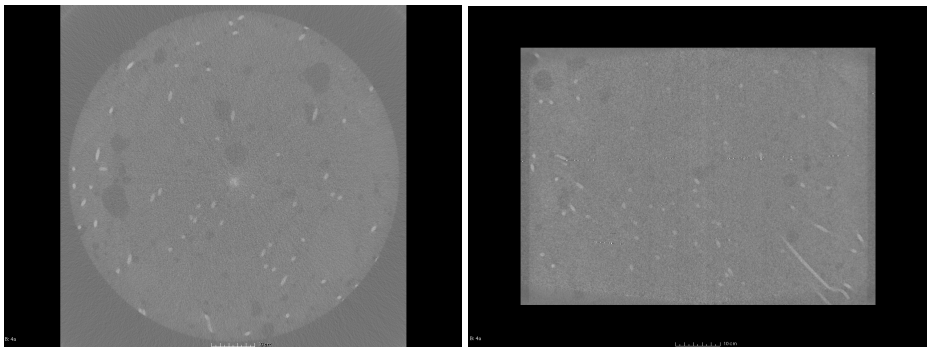

**(a)** **(b)**

**Figure 3.4** – (a) Top view and (b) side view of the reconstructed sample.

Not only could the scanning artefacts spoil the analysis, but also the concrete matrix itself as well. Sprinkled with air bubbles and gravel aggregates that might have similar density values of the fibre it would requiring a complex thresholding in order to be excluded from the data.
In order to save time and optimise the computational times, we decided to use one of the most widespread and known libraries for image processing, Insight Toolkit (ITK) [18]. Originally created for medical applications, ITK features a C++ based API of functions (most of them optimised for parallel processing) based on complex but optimised image processing algorithms. Moreover most of the library functions are supported by publications that explain in detail their algorithms and scientific basis.
ITK has an intuitive pipeline oriented structure, with the input data flowing through the separate filter modules in sequence, being each time processed and sent further along the next one until ready.

The idea for the first and most important step in the filtering processing came from two sources: medical analysis and Redenbach et al. work [33]. In the last two decades the biomedical imagery field has been one of the most innovative and advanced ones among those dealing with image processing. Due to the benefits produced by the results of the analysis of tomographies and medical data, wide amount of investments pushed researchers to develop very specific and powerful tools, ITK among them.
The parallelism that we found between a human tomography and our dataset was the presence of cylindrical/tubular shapes in both of them. Biomedical imagery developed in the years a variety of techniques to detect such shapes belonging to one of the most important and more difficult features to detect in the human

body: the circulatory system. Despite not belonging to a unique connected network, the steel fibre in the SFRC roughly share their shape with the blood vessels.

One of the most effective techniques to highlight the circulatory system, is based on the Frangi Vesselness filtering [12] and it is available in ITK as a combination of two filter modules: HessianRecursiveGaussianImageFilter and Hessian3DToVesselnessMeasureImageFilter [26]. By using the analysis of the Hessian matrix for each voxel (the Hessian-based algorithm is explained in detail in section 3.3 , the algorithm detects which voxels belong to tubular-shaped structures and extract them from the dataset.

With this method it is sufficient to just specify two parameters for the filtering: the diameter of the cylindrical elements of interest (a given measure derived from the type of fibres used and known from the specifications of the samples) and a threshold value that is only dependent on the scanning/material properties (and remains constant for a full batch of similar samples acquired with the same settings).

Once the tubular shapes are isolated from the rest of the dataset, a median filtering is applied in order to clean up leftover noise in the dataset i.e. very small noise aggregates that accidentally happened to have a semi-cylindrical shape. The MedianImageFilter (belonging to the family of the non-linear filters processes an image (or volume) so that a given pixel is the median value of the the pixels in a neighbourhood around the corresponding input pixel. In practical terms, the noisy little elements are flattened on the background value and removed.

At this point of the process, the data is ready to be binarised, so to clearly segment it into two values: foreground (fibre elements) and background (everything else). ITK offers a filtering module, BinaryThresholdImageFilter, that performs that in a few seconds even for large datasets.

To ensure that only the correct shapes have been extracted, and to remove, where possible, larger artefacts that might have been originated by the smoothing performed by the Vesselness filtering, we then process the whole binarised dataset through a morphological filter, the itk::OpeningByReconstructionImageFilter. As described in [41], the filter only preserves unmodified regions that can completely contain a predefined structuring element (a sphere of diameter slightly smaller than the fibres section diameter). This filter eliminates all other regions of foreground voxels that don't match the condition above.

Now the data is ready to be forked into the final steps that will produce the input for the analysis (see section 3.3).

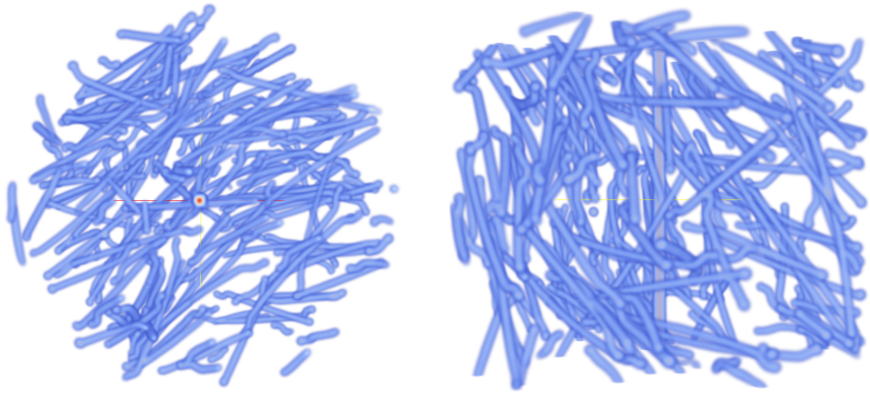

**Figure 3.5** – Top and front view of a SFRC filtered dataset

The first branch is based on the labeling of separate regions among the binarised data. By assigning a unique label to each non-touching region, that can represent a single fibre or a cluster of interconnected fibre, this represents the first step in isolating each fibre for the analysis, to later compute their separate orientation vectors.
Through the use of the BinaryImageToShapeLabelMapFilter module [28], we save a parameter file containing, for each voxel of the dataset, the region to which it belongs. Regions composed of a too small amount of voxels (i.e 4500, corresponding to a bit less than 1/4 of a fibre) are dropped along the process. The voxels composing them might be leftover noise or belong to partially cut fibres too small to be relevant for the given sample.

The second branch of the filtering, produces instead the raw data for the analysis. It smooths the clean and binarised data through SmoothingRecursiveGaussianImageFilter and finally saves it into raw format (header + volume files) (the results are depicted in Fig. 3.5).

The whole filtering process requires 109 minutes to reach completion for a 900x900x576 dataset if executed single-threaded on a Opteron4284 3.0GHz core and 23 minutes on two Opteron 4284 3.0GHz 8-cores CPU by taking advantage of ITK parallelisation features. The process requires at its highest consumption peek, during the Frangi Vesselness phase, approximately 32 GB of RAM.

Mainly thanks to the use of the Frangi Vesselness algorithm, that removes the need for a manually entered threshold for each dataset, the data filtering only requires in input the diameter in voxels of a fibre (8 in our specific case), and the binarisation thresholding that depends on the material and on the scanning process, that, as already mentioned, remains constant for all the datasets acquired

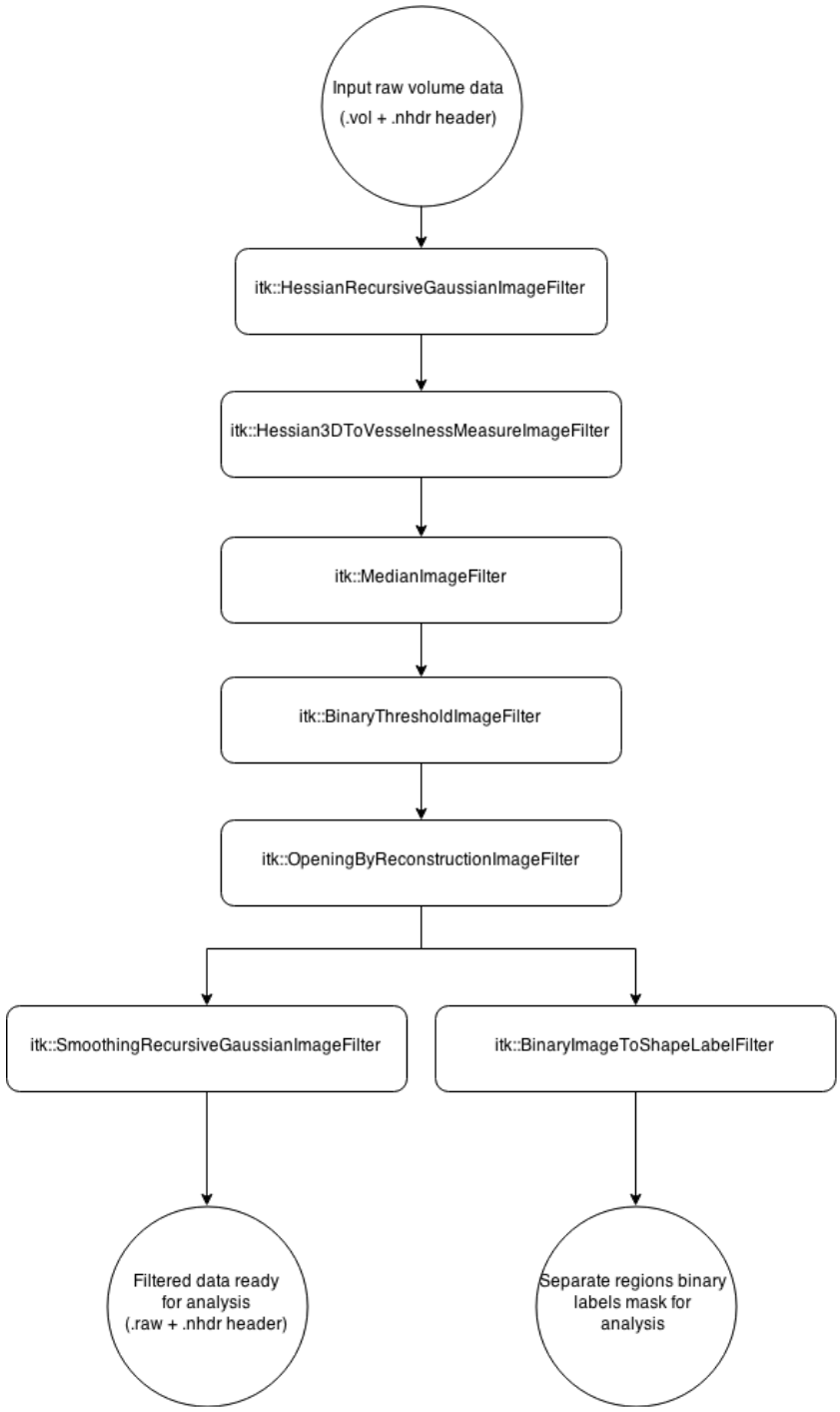


**Figure 3.6** – ITK-developed filtering pipeline for the preparation of SFRC datasets

with the same method. The need for no further input parameters has proven extremely useful in order to perform overnight processing of large batches of datasets. In a single night more than 25 datasets can be filtered and automatically prepared for the following analysis. Fig. 3.6 summarises the whole filtering process just described.

## 3.3 FIBRE ORIENTATION ANALYSIS

All the steps described in the previous section produced the data to be used in the analysis of the fibre orientation: a clean filtered dataset containing only the fibres and a set of labels that identify the non touching clusters of fibres.

The main analysis we developed for the orientation of the SFRC, self-written and only employing Eigen as support library [14] was initially inspired by the method described in [33]. In the paper, the researchers analyse a method to extract the alignment of plastic fibres in a dense fibre-composed material through the use of a greyscale-built Hessian matrix.

The Hessian matrix (already mentioned in the filtering section) is a square matrix of the second-order partial derivatives of a function.
When such a matrix is calculated for each pixel/voxel of a greyscale image (be it 2- or 3-dimensional), its eigenvalues and eigenvectors contain an important set of information about the pixel/voxel: the intensity of the grey level variation in all the 8 directions.
In Fig. 3.7 we can observe this concept when applied on the 2-dimensional section of a cylindrical shape as for example one of our fibres. On the left side of the image, the blue arrow represents the eigenvector of the highest eigenvalue for the variation on the grey scale (from the core of the fibre towards the outside) while the white arrow shows the direction of the eigenvector of the smallest eigenvalue, i.e. the direction of the fibre itself in that given voxel.

The underlying idea for the fibres orientation detection is based on the Hessian matrix method described in Redenbach et al. [33]. The fibres analysed in the paper, though, where straight, thin plastic fibres with a much higher density than those in the SFRC. In order to make sure the method would have also worked on hooked fibres, we created a set of artificial volumetric data on which to test the algorithm: one straight cylindrical shape and one emulating the shape of a real fibre (depicted in Fig. 3.8).

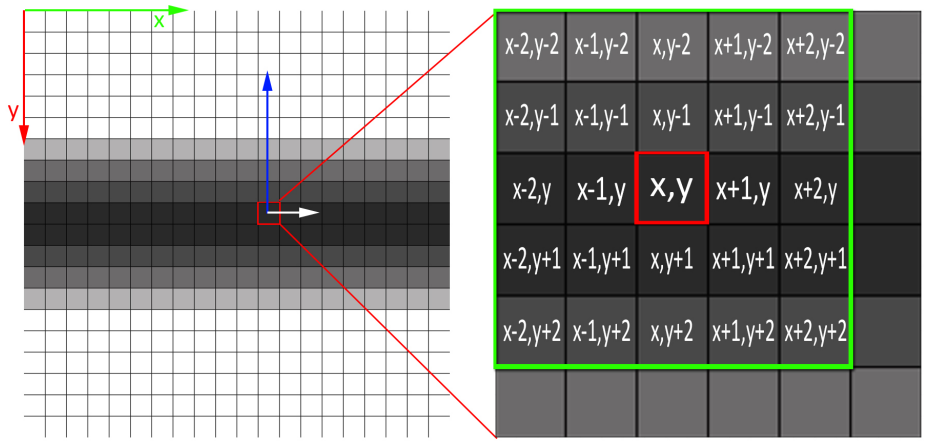


**Figure 3.7** – Pixels used for the construction of the 2D greyscale-based Hessian matrix. The direction of the eigenvectors of the matrix in one point is also indicated.

Although the two test fibres had the same size and same main alignment, the orientation tensors describing them differed by a factor of 5 to 10%. In order to understand the reasons behind the difference we stored the per-voxel data of the two artificial datasets in Visualization Toolkit (VTK) [40] files for visualisation, and visualised them with ParaView [16] on the Kyb3 VE.

The visual inspection validated on the first attempt the Hessian method: for each voxel there was a vector that described precisely the direction of the fibre in that point ( as shown in Fig. 3.9).
Once we proved the correctness of the results, the cause for the differences in the tensors built on the averaged sum of the voxel tensors became obvious: the hooks (see Fig. 3.10).

In next step we applied the algorithm to the full datasets and compare the results with the skeletonisation method [43] for the same data. The results were the ones expected: the two processes resulting orientation tensors had a difference of 5% to 10% (the skeletonisation approach does not take the hooks orientation into account while calculating the fibres orientation).

We discarded detection of the hook shapes from the options as practically complex and too prone to a variety of errors in our datasets. Not only are the hooks bent with a varying angle between 30 and 45 degrees, but the several touching fibres might generate in their contact points a variety of similar angles, making the search for bending points very difficult. We therefore approached the problem

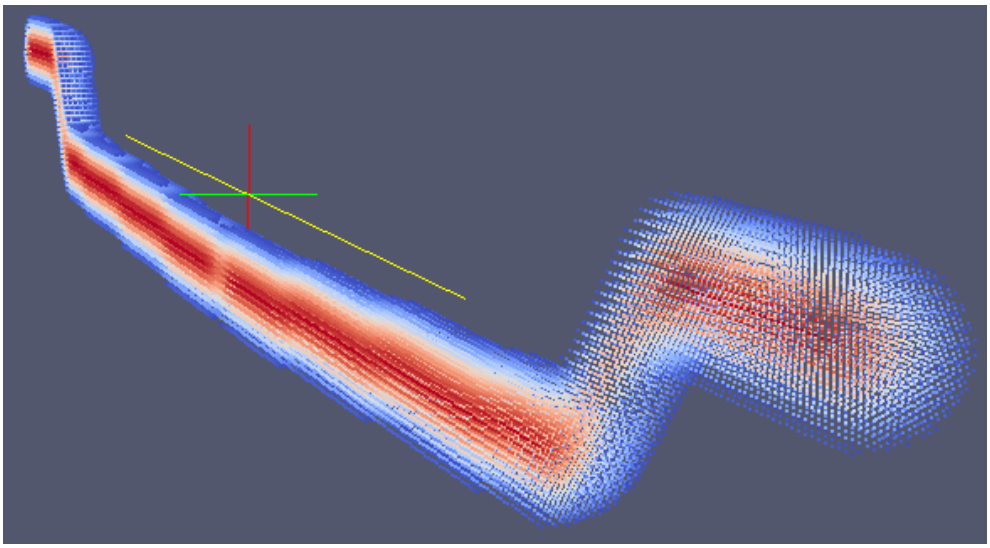

**Figure 3.8** – Artificial fibre volume sample for testing and development

from a different point of view.

An individual fibre has, after the above mentioned per-voxel analysis, an amount of approximately 18000 vectors describing the orientation of the fibre in each of its voxels (depicted in Fig. 3.9). Although strong enough to compromise the results of the pure application of the [33] method, the amount of those vectors belonging to the hooks is very limited compared to those belonging to the fibre main shaft (as shown in Fig. 3.10).

The idea we decided to apply was therefore the following one: detecting the dominant directions in a fibre (or cluster of fibre) that could be proportionally large enough to only belong to the main fibre orientation.

First of all, to facilitate the clustering, we converted all the voxel vectors of a region from Cartesian to spherical coordinates. we used the Theta ($\theta$) angle to represent the rotation on the $z$ axis (polar angle) and the Phi ($\phi$) angle for the rotation on the $xy$-plane (azimuthal angle). Thanks to symmetrical properties we constrained the angles so that $\theta \in [0, 90]$ and $\phi \in [0, 360]$. With this approach it was possible to store the whole region vector data in a 2-dimensional $90 \times 360$ matrix. Each cell index would then represent one of the two angles, while the integer value stored in the cell would store the amount of vectors that are represented by those angles.

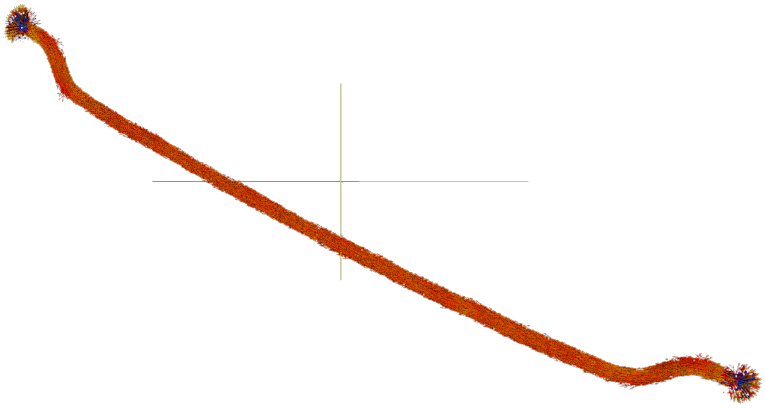

**Figure 3.9** – Fibre voxels vectors analysis

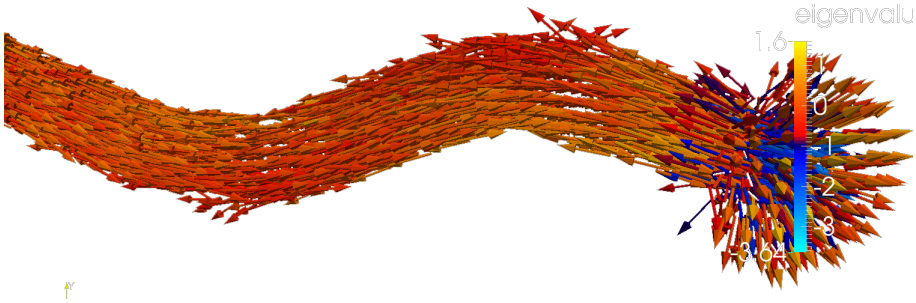


**Figure 3.10** – Zoom on the fibre hook voxel vectors analysis

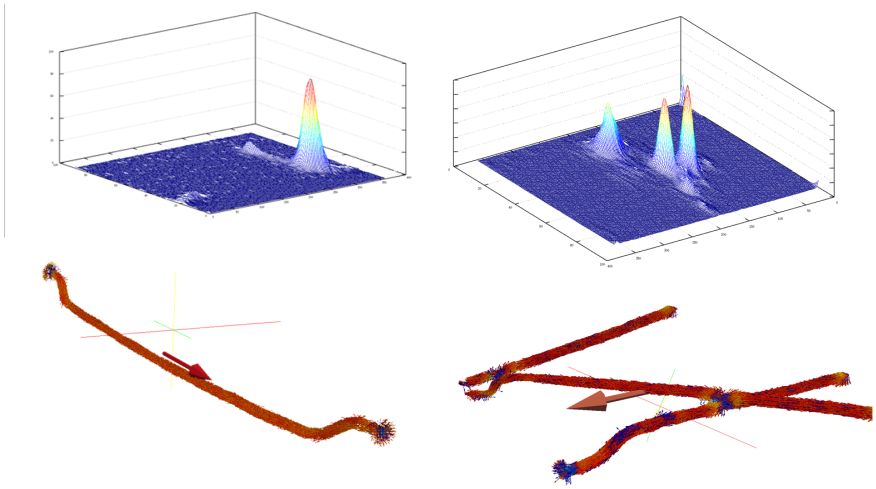

**(a)** **(b)**

**Figure 3.11** – (a) Single fibre region peak detection and (b) complex multiple touching fibre detection.

The next step consisted in smoothing the matrix through a simple gaussian [5] filter. This allowed to solve small errors that the analysis vector retrieval and successive spherical coordination conversion might have caused in the values. An alternative option to the smoothing, clusterisation, might have too often resulted in excessive approximations.

On a simple isolated single fibre region (a quite rare occurrence in the SFRC datasets), the extraction of the fibre alignment corresponds to a straightforward detection of the highest peak in the θ-ϕ matrix (displayed in Fig. 3.11, a). The majority of the regions in the datasets, though, partly due to the scanning artefacts and partly as a consequence of the filtering and smoothing, are composed of two or more full or partly cut fibres touching each other in one or more contact points. This results in a more complex theta-phi matrix (depicted in Fig. 3.11, b).

By analysing the data displayed in Figure .3.11(b) it became obvious that it was necessary to use more advanced data mining techniques in order to extract the information from the polar coordinates clustering matrix. The visual inspection of several similar datasets revealed that the orientation peaks were split into quite cleanly separated regions.The only exception to that were for a rare number of cases (<10%) were separate orientation peaks merged into a single one due to an almost identical orientation of the two touching fibre. From the outcomes of the

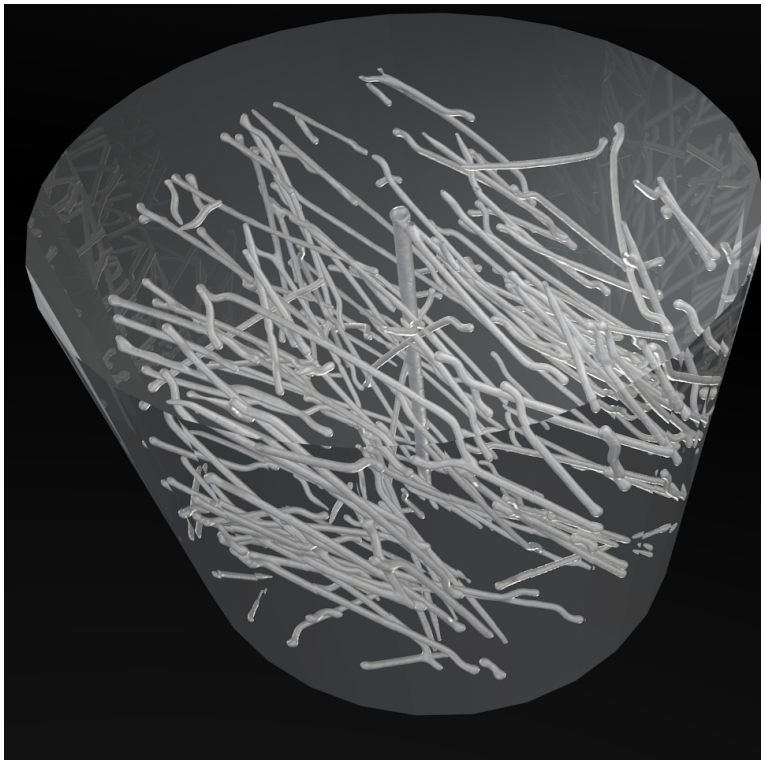

**Figure 3.12** – Post-processed rendering of the filtering process

visualisation we got the idea of using a connected regions labeling [7] similar to the one employed in separating the fibre clusters in section 3.2.

By imposing a fixed threshold in order to allow the algorithm to ignore very low values on the matrix (usually generated by noisy vectors of each region), we labeled each separate cells region with a different value. The results of the method were very good (as shown Fig. 3.13). In order to also obtain the centre position of each fibre, the algorithms calculates and stores the average coordinates of all the vectors contributing to generating each peak. As a last step, the coordinates are converted back to the Cartesian system and saved into a VTK file for a flexible visualisation.

Figure 3.15 shows the same dataset as Figure 3.11 (b) from a different perspective and with the orientation vectors extracted separately. Each of the light-blue arrows represents the orientation of one of the three fibres of the interconnected region. Additionally we visualised the fibres data in several ways in order to validate its correctness (as shown in Fig. 3.12).

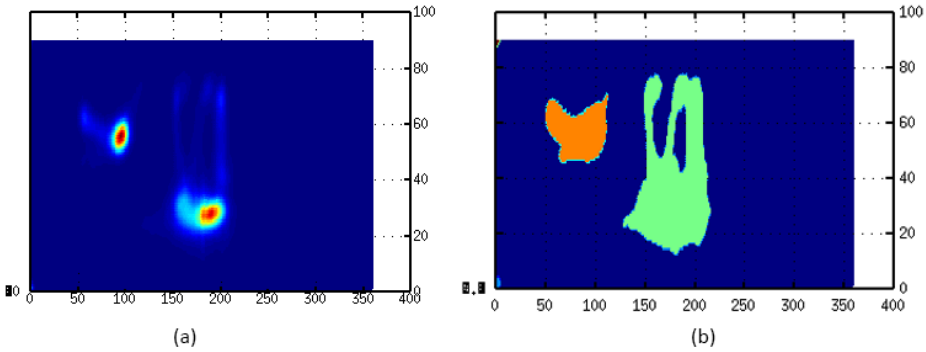


**Figure 3.13** – (a) Top-down view of a theta-phi matrix with two fibre peaks and (b) labeled regions for separate peaks detection.

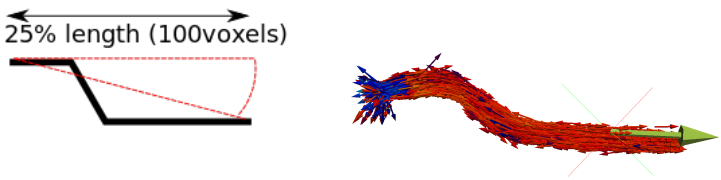


**Figure 3.14** – Different behavior in the processing of cut fibre orientation for the (a) skeletonisation method and (b) the method presented in this dissertation.

Along the development, the constant visualisation feedback allowed us to highlight and understand one very unique and important feature of the algorithm: the per-voxel vectors ( depicted in Fig. 3.9 and 3.10), were not only a step of the process, but they also had an important meaning in the understanding of the material. While the majority of approaches often focuses on the main fibre orientation values only, the simple fact that there is a difference between the total value obtained by the single fibre orientation and the per-voxel vectors orientation, clearly states that also the hooked ends influence the mechanical behaviour of the uncracked state of the material.
This means that until the moment in which the bond between fibre and concrete matrix is broken, the hooked ends also give a contribution. After the cracking, though, only the main fibre orientation will be responsible for the fracture bridging.

An additional advantage of the method discussed in this dissertation compared to the skeletonisation method [43] is related to the orientation calculations for partially cut fibres. While the skeletonisation method calculates the angle based on the vector connecting the two ends of the fibre ( as shown in Fig. 3.14, a), our method retains the correct main fibre orientation ( as depicted in Fig. 3.14, b)

The whole analysis process described above is performed with a $900 \times 900 \times 576$ input dataset on a desktop computer (Intel i5-3350P quadcore CPU 3.10GHz, 16 GB RAM) in an approximate time of 3.5 minutes. Slight variation in the duration (+/-30 seconds variations might occur depending on the amount of fibre and their interconnectedness).

Summing up the filtering and analysis time, the whole process requires approximately between 28 and 33 minutes per sample, versus the approximate 3 hours required by the skeletonisation method [43] and the linear regression method [47].

Once the software was ready and polished, we named it μTAnS-Fib (Micro Tomographies Analysis Software for Fibres).

## 3.4 VALIDATION AND VISUALISATION OF THE RESULTS

We validated the correctness of the results of the algorithm and implementation described in section 3.3 in two different ways: by numerical comparison with the results obtained by the skeletonisation method [43] on the same datasets, and visually on the Kyb3 system (see section Chapter 2).
The visualisation was also used through the entire development (as described in

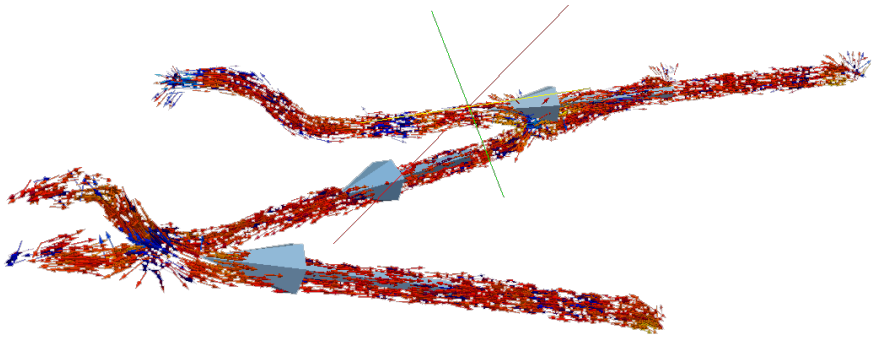

**Figure 3.15** – Separate orientation peaks extraction for a cluster of 3 partially cut touching fibres.

Publication II) for a constant fast feedback on the outcomes of the various steps. Its contribution was extremely beneficial in terms of time saved and understanding of the data.
A variety of important features, some of them already implemented in the algorithm described in this dissertation and other ones being still developed, only emerged thanks to the in-process visual inspection.

The numerical validation of the method is performed through the one-to-one comparison of the results of the analysis on a same dataset, carried out with both the skeletonisation method and the one presented in this dissertation (displayed in Fig. 3.19).
Tables 2 and 1 report the numerical results on the dataset for the skeletonisation, for the single fibre orientation and for the voxel-vectors based orientation.

The orientation is quantified according to three parameters as in [43]: director, order parameter and orientation number. The director is the eigenvector corresponding to the largest eigenvalue (according to amount) of the second order alignment tensor $A$ that is described as:

$$A = \frac{1}{N} \sum_{i=1}^{N} n_i \otimes n_i \tag{3.1}$$

$n_i$ represents the direction of the $i$-th fibre, $N$ the total amount of fibres and $n_i \otimes n_i$ the symmetric traceless tensor product. The order parameter is given as

$$S = \frac{3}{2}\lambda_1 \tag{3.2}$$

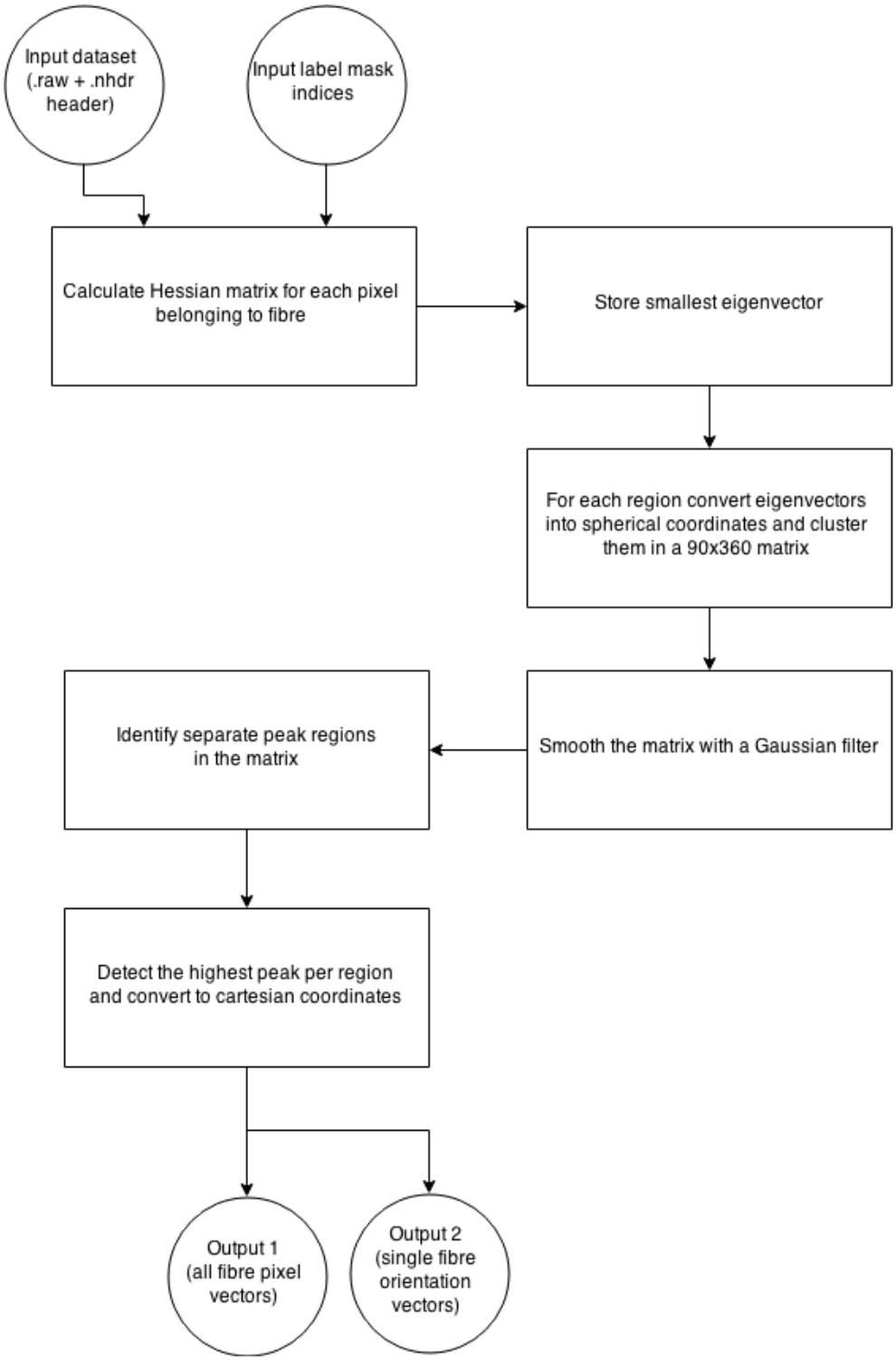


**Figure 3.16** – Diagram of the complete analysis process described in this section

| | skeletonisation | | | | hessian fibre | | | hessian voxel | | |
|---|---|---|---|---|---|---|---|---|---|---|
| Sample | # fibres | % vol. | S | $\mathbf{d} = (\Phi, \Theta)$ | # fibres | S | $\mathbf{d} = (\Phi, \Theta)$ | % vol. | S | $\mathbf{d} = (\Phi, \Theta)$ |
| 1A middle | 167 | 0.78 | 0.52 | (70,70) | 182 | -0.44 | (185,43) | 0.9 | 0.38 | (64,62) |
| 1B middle | 201 | 0.89 | 0.53 | (344,88) | 175 | 0.51 | (345,87) | 0.6 | 0.4 | (344,87) |
| 2A middle | 201 | 0.9 | 0.42 | (5,41) | 217 | -0.42 | (184,48) | 0.9 | 0.37 | (2,38) |
| 2B middle | 192 | 0.83 | 0.46 | (2,89) | 243 | 0.48 | (1,88) | 0.2 | -0.19 | (94,17) |
| 3A middle | 168 | 0.77 | 0.52 | (25,36) | 189 | 0.57 | (17,37) | 0.7 | 0.54 | (25,35) |
| 4B middle | 186 | 0.84 | 0.62 | (181,79) | 216 | 0.59 | (185,82) | 1.1 | 0.46 | (180,77) |
| 5A middle | 189 | 0.89 | -0.44 | (169,59) | 181 | -0.41 | (168,57) | 1.2 | -0.35 | (167,60) |
| 5B middle | 198 | 0.92 | -0.39 | (280,17) | 200 | -0.4 | (281,11) | 1 | -0.28 | (278,24) |
| 6A middle | 138 | 0.7 | 0.65 | (29,51) | 169 | 0.63 | (25,53) | 0.8 | 0.56 | (331,47) |

**Table 1** – Summary of properties of the samples. The "# fibres" means parts of fibres longer than 25% fibre-lenght; the expected number of whole fibres from the real volume fraction would be 143. In the hessian cases, the "% vol" are calculated from the voxel analysis and would be equal for both cases, the "# fibres" make only sense in a per-fibre analysis. The director $\mathbf{d}$ is given as a tuple $(\phi, \theta)$ and defined by equation (3.3) and the order parameter $S \in [-\frac{1}{2}, 1]$ is defined in equation (3.2).

or as

$$S = \left\langle \frac{3}{2} \cos^2 \alpha - \frac{1}{2} \right\rangle \tag{3.3}$$

with $\lambda_1$ the largest eigenvalue of $A$ (according to value) and $\alpha$ is the angle between the individual fibre and the director.

$$\eta_\xi = \frac{1}{N} \sum_{i=1}^{N} \cos \alpha_i^\xi \tag{3.4}$$

defines the orientation numbers with respect to pre-defined axis $/xi$, with $\alpha_i^\xi \in [0\,\mathrm{deg}, 90\,\mathrm{deg}]$ as the angle between the $i$-th fibre and the $\xi$ axis ($\xi$ can be for example the X,Y or Z axis) .

It is easy to immediately notice the similarity of results by comparing the output of the two different methods. Differences arise from a variety of factors:

- the evaluation of orientation angles belonging to partially cut fibre (as shown in Fig. 3.14)
- differences in how the two methods deal with touching fibres regions, that depending on each specific case might be slightly more optimal with one or with the other approach

It is also possible to identify in the table 1, some sign inversion in the tensor order-parameter S even while the value remains otherwise similar if not identical

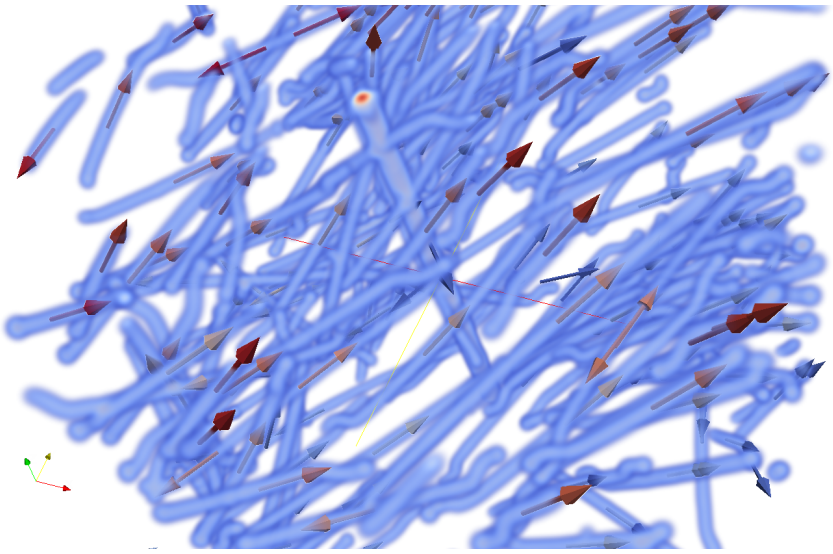

**Figure 3.17** – The filtered fibres volume and the single fibre orientation vectors

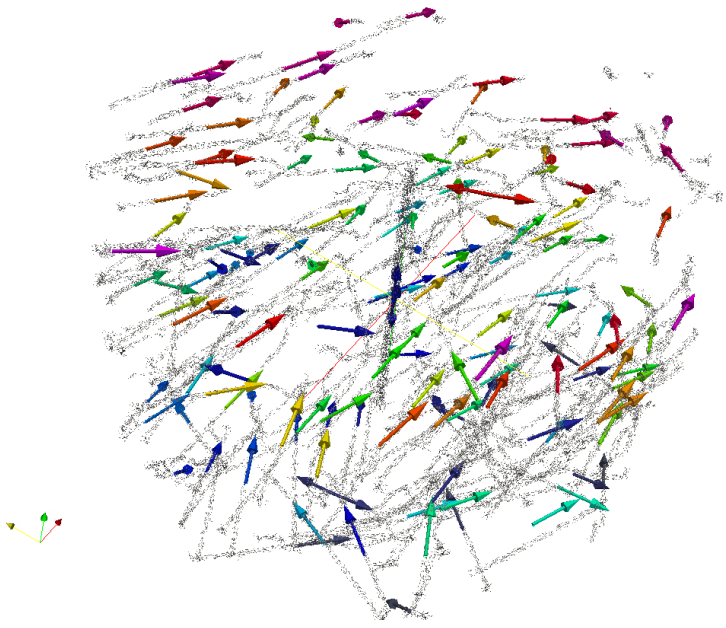

**Figure 3.18** – Full SFRC volume with fibres orientation extraction

| | skeletonisation | | | hessian fibre | | | hessian voxel | | |
|---|---|---|---|---|---|---|---|---|---|
| Sample | $\eta_X$ | $\eta_Y$ | $\eta_Z$ | $\eta_X$ | $\eta_Y$ | $\eta_Z$ | $\eta_X$ | $\eta_Y$ | $\eta_Z$ |
| 1A middle | 0.38 | 0.72 | 0.4 | 0.42 | 0.69 | 0.4 | 0.42 | 0.64 | 0.46 |
| 1B middle | 0.77 | 0.44 | 0.22 | 0.77 | 0.42 | 0.23 | 0.7 | 0.42 | 0.32 |
| 2A middle | 0.49 | 0.48 | 0.56 | 0.5 | 0.47 | 0.54 | 0.47 | 0.47 | 0.57 |
| 2B middle | 0.76 | 0.44 | 0.25 | 0.77 | 0.42 | 0.21 | 0.54 | 0.55 | 0.39 |
| 3A middle | 0.44 | 0.48 | 0.64 | 0.49 | 0.42 | 0.65 | 0.45 | 0.43 | 0.66 |
| 4B middle | 0.82 | 0.34 | 0.25 | 0.81 | 0.35 | 0.22 | 0.73 | 0.37 | 0.33 |
| 5A middle | 0.37 | 0.58 | 0.58 | 0.42 | 0.55 | 0.56 | 0.39 | 0.54 | 0.57 |
| 5B middle | 0.65 | 0.53 | 0.25 | 0.68 | 0.53 | 0.19 | 0.6 | 0.51 | 0.34 |
| 6A middle | 0.59 | 0.41 | 0.57 | 0.62 | 0.39 | 0.53 | 0.55 | 0.4 | 0.59 |

**Table 2** – Comparison of the orientation numbers calculated from different analysis methods. The orientation numbers are given by equation (3.4).

between the skeletonisation method and ours. This inversion is determined by small variations in the fibres angles distribution but sufficiently like to have the resulting tensor being classified in a different distribution.

The scatterplots displayed in Fig. 3.19 represent the fibre angles for each dataset analysed through and the comparison of the values produced by the two methods and describing the fibre behaviour in the single dataset. By displaying the two separate results and their superposition the figures show with clarity the high similarity in results of the two different methods.

As already mentioned, a very important contribution to the development of the algorithm and related software was offered by visualisation. Using ParaView [16] on the Kyb3 VE and having each step of the process producing VTK output for the partial and final results, we could constantly monitor and inspect the development of the process visually. Implementation mistakes could therefore be quickly corrected before propagating to the next steps. Moreover, the visualisation of the final software results (depicted in Fig. 3.17 and 3.18) offers an insightful and easily understandable picture of the scope and quality of the whole development process.
The visual output, in its clarity can in the future, be used for educational reasons, both in the academic environment and in teaching to company owners and workers the outcomes of different SFRC productive processes.

The added value of stereoscopic VR-based visualisation on the Kyb3 amplifies the benefits of visual feedback. Complex datasets like the fibres volumes, with a very large number of thin objects, can be extremely difficult to inspect on standard 2D display: the loss of depth information tends to flatten the whole data on a single plane.
On a VE on the other hand, inspection is easier and more complete and, also thanks to a more natural interaction, the whole process productivity increases.
Also in the popularisation of the results and presentation of the work done, the increased interest raised in the audience by a VR-visualisation showed a very positive effect: students are more easily attracted by the topics presented, and the non-academic viewer tends to focus on the data with much more ease.

## 3.5 CHAPTER CONCLUSIONS

In this chapter we presented the detailed development of the whole analysis of SFRC X-ray tomography samples. We described the complete implementation of the algorithm from the filtering to the production of the final results and we highlighted its novel contributions :

- Does not require any user intervention during the process and the user input is limited to the preliminary insertion of the parameters defining the analyzed material and scanning specifications. It allows overnight batch processing of several datasets.
- It is much faster than the other existing approaches to obtain the orientation data (it requires approximately 1/6 of the time of the existing similar processes, where timing is mentioned).
- Through filtering and pre-processing, is able to operate correctly even on very noisy datasets.
- Handles correctly the separation of the fibres and the analysis of partially cut ones.
- Provides data almost always neglected by other methods that describes the fibres hooks contribution to the material properties of the uncracked SFRC.
- It produces results both in numerical form and in a format that can be visualized on a standard monitor or on a VE.

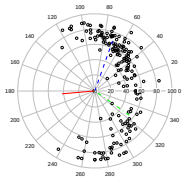

**(a)** Sample 1A middle (hessian)

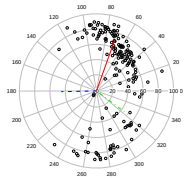

**(b)** Sample 1A middle (skeleton)

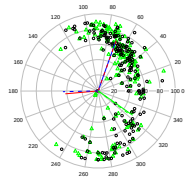

**(c)** Sample 1A middle (green skeleton, black hessian)

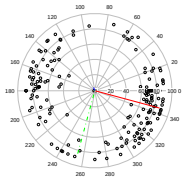

**(d)** Sample 1B middle (hessian)

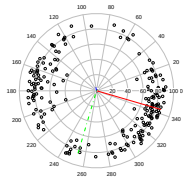

**(e)** Sample 1B middle (skeleton)

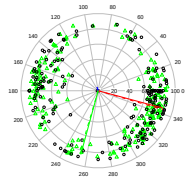

**(f)** Sample 1B middle (green skeleton, black hessian)

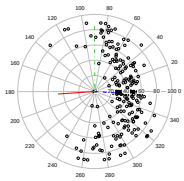

**(g)** Sample 2A middle (hessian)

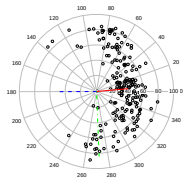

**(h)** Sample 2A middle (skeleton)

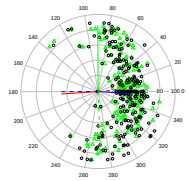

**(i)** Sample 2A middle (green skeleton, black hessian)

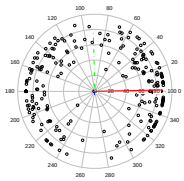

**(j)** Sample 2B middle (hessian)

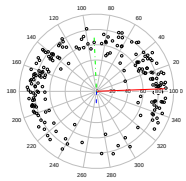

**(k)** Sample 2B middle (skeleton)

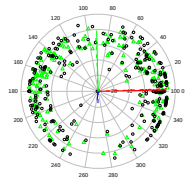

**(l)** Sample 2B middle (green skeleton, black hessian)

**Figure 3.19** – Scatter plot of fibre orientation, radius is inclination angle Θ in degrees. View antiparallel to Z-axis (from bottom to top of cylinder). The solid lines show the director (eigenvector) of the existing distributions.

# 4

## A.C.T.I.V.E

This chapter presents an additional tool we developed to further support the research on SFRC: A.C.T.I.V.E. Developed to be VR-ready, the software uses superellipsoidal glyphs to visualize CFD simulations that describe the SFRC behavior at casting time. We first clarify the nature of tensor visualization through geometrical glyphs, we detail the algorithm to obtain the superellipsoidal shapes from the CFD tensor data, and we finally explain the features and portability properties of the developed software.

Ever since we completed the construction and the configuration of the Kyb3 VE, in December 2013, we worked on finding and developing applications that could take advantage of its features.
Among the development platforms able to grant the maximum flexibility and scalability of software, VRUI [25] was since the beginning our favoured one.
In addition to offering a variety of already implemented software (Mesh Visualisation, Volume Rendering, VRML navigators, etc) that were among the first ones to be run on the Kyb3, VRUI has several features that make it a very good development tool:

- Scalable - With different configuration files only, the same software will run on a desktop computer, on a multi-screen or on a HMD-endowed VE.
- Optimised - VRUI offers a complete OpenGL wrapping with maintenance of rendering contexts in order to avoid replication of data in case of multiple displays
- Complete - the development toolkit offers a full user interaction management already implemented (head tracking, interaction tools and menu-based GUI)
- Well documented - VRUI has a complete documentation and Oliver Kreylos (University California Davis), its creator, always answers with fast and complete feedback and support.

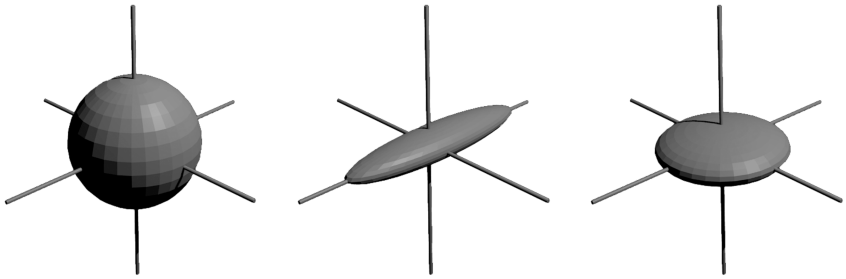


**Figure 4.1** – Ellipsoidal diffusion tensor shapes : (a) Isotropy, (b) Linear anisotropy and (c) Planar anisotropy.

The mentioned properties and the variety of helpful existing open source software to be used as an example, make VRUI an excellent development framework.

## 4.1 TENSOR VISUALISATION WITH SUPERELLIPSOIDAL GLYPHS

As part of our research to improve the visualisation techniques related to SFRC, a large focus has always been towards an easily understandable way to display tensors. Due to the amount of information contained in these mathematical structures, the more classical glyphs used for vector visualisation fall short of describing features.
The visualisation outcome of the fibre analysis algorithm and software described in the previous chapter performs perfectly when displaying the orientation vectors of the voxels and fibres, but does not provide a way to properly describe the average orientation tensor for the analysed sample. Already in my masters thesis, "Liquid Crystals Tensor visualisation with Virtual Reality Displays" (University of Genova, Italy, 2011) I have been dealing with the complex needs of tensor visualisation, and we therefore decided to port the same approach used there to the SFRC VR visualisation on the Kyb3.

If properly visualised, alignment tensor (as the ones that can be used to describe the fibres alignment in the SFRC) can describe unambiguously isotropic and anisotropic characteristics (as depicted in Fig. 4.1).

The low-level visual inspection of single tensor shapes is often a necessary step in tensor data understanding. Among the several shortcomings of the traditional shape, one of the most relevant ones is visual ambiguity. Two ellipsoidal glyphs

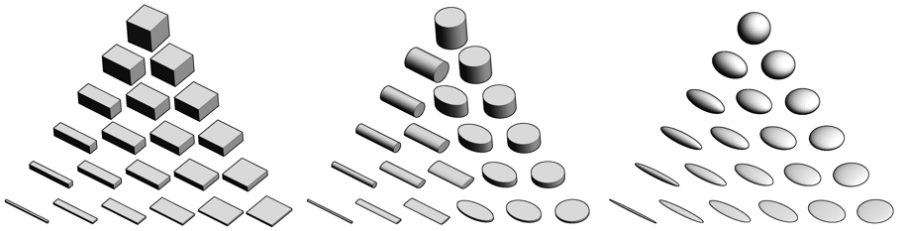

**Figure 4.2** – Cuboid, cylinders and ellipsoid shapes produced by the Teem software [22]

with different tensor shapes might exhibit very similar image-space shapes due to the viewpoint, forcing the user to a longer and more thoroughly unnecessary inspection. Furthermore, e.g. cylinder-shaped glyphs lack multi-axis symmetry and would fail in depicting isotropy as instead an ellipsoid would. Traditional shapes (shown in Fig. 4.2) are therefore not ideal for a correct visualisation.

Probably the most renown technique for tensor visualisation originates from the work of Gordon Kindlmann [21] that was the first to extend the traditional ellipsoid, cuboid and cylindrical way of visualising tensors with a more complex geometrical primitive: superquadrics.

Superquadrics [3] are 3D extensions of Piet Hein's 2D superellipses [9]. Their shape changes according to six parameters, that determine roundness/squareness along the horizontal and vertical axis, length, width and depth (and for the superquadrics toroids, the diameter of the internal hole) [24]. In the specific case of Kindlmann's work, a subset of the whole family of primitives was used.

Our work, (and my MSc Thesis before) is based though on an assumption that requires a slightly different family of glyphs than those used in Kindlmann's work [21]: the Superellipsoids as defined and built in the Jankun-Kelly,Mehta paper [17] (depicted in Fig. 4.3). Originally thought for liquid crystals tracelss tensor alignment visualisation, the Jankun-Kelly,Mehta's glyphs begin the glyphs construction by defining the **Q** tensor that represents the director and the average alignment with the director simultaneously:

$$\mathbf{Q}(x,t) = S(x,t)(n(x,t) \otimes n(x,t)) - \frac{1}{3}S(x,t)I \tag{4.1}$$

the Q tensor is built by extracting the eigenvalues and takes it into account a certain amount of biaxiality, represented as the divergence $b$ from the uniaxial tensor:

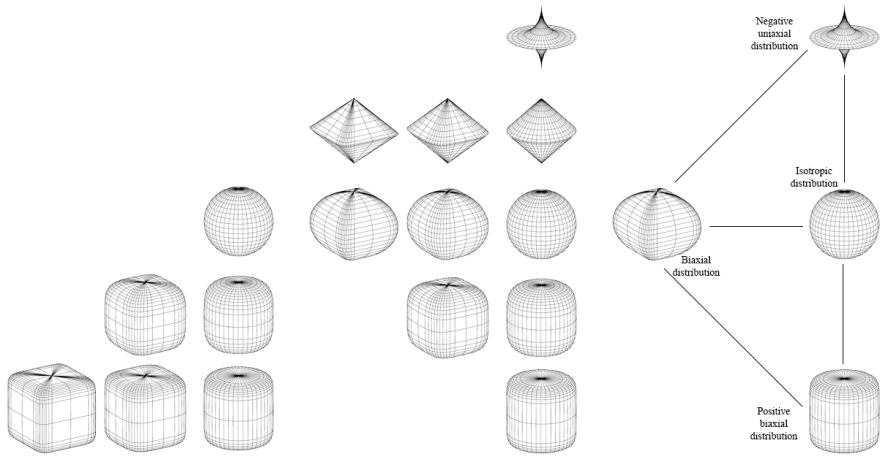


**Figure 4.3** – (a) Superquadrics subset used in Kindlmann's method [21], (b) the subset used in Jankun-Kelly,Mehta method [17] and (c) the distributions represented by glyphs shapes in an image produced with the Teem software [22]

$$[Q]_\epsilon = \begin{pmatrix} \frac{2}{3}S & 0 & 0 \\ 0 & -\frac{1}{3}S - b_s & 0 \\ 0 & 0 & -\frac{1}{3}S + b_s \end{pmatrix} = \begin{pmatrix} \lambda_1 & 0 & 0 \\ 0 & \lambda_2 & 0 \\ 0 & 0 & \lambda_3 \end{pmatrix} \tag{4.2}$$

with the eigenvalues sorted as $|\lambda_1| \geqslant |\lambda_2| \geqslant |\lambda_3|$.

The shapes of the superellipsoidal glyphs offer, in my opinion, a more understandable visualisation of our tensors shapes of interest while retaining the full flexibility of superquadrics. In particular, the spiked disks they include, one of the most notable differences when compared to the superquadrics, are in our specific case an unambiguous and recognizable sign of certain specific tensor configurations.

By processing the results produced by the SFRC analysis software, it is possible to calculate a single orientation tensor for each dataset, based on the averaged sum of all the single fibres orientation vectors. Extracting the eigenvectors from the orientation tensor is the first step toward understanding its meaning and visualising it. The eigenvectors represent indeed the general orientation distributions of the fibres in the sample.

The data extraction process from the alignment tensor [17] defines four metrics:

$$\mu_{u^+} = \begin{cases} -3\lambda_3 & S \geqslant 0 \\ 0 & S < 0 \end{cases} \tag{4.3}$$

$$\mu_{u^-} = \begin{cases} 0 & S \geqslant 0 \\ 6\lambda_3 & S < 0 \end{cases} \tag{4.4}$$

$$\mu_b = 6b = |3\lambda_1 + 6\lambda_3| \tag{4.5}$$

$$\mu_i = \begin{cases} 1 - \frac{3}{2}\lambda_1 & S \geqslant 0 \\ 1 + 3\lambda_1 & S < 0 \end{cases} \tag{4.6}$$

where $mu_{u^+}$ (4.3) defines the strength of the positive uniaxial alignment,$mu_{u^-}$ (4.4) the strength of the negative uniaxial alignment. $mu_b$ (4.5) represents the amount of biaxiality and $mu_i$ (4.6) describes the amount of isotropy of the collection.

Superellipsoids shapes are defined using the same shape parameters as the traditional superquadrics [21], using shape parameters $\alpha$ and $\beta$ according to the following definition:

$$e(\theta, \phi, \alpha, \beta) = \begin{pmatrix} \cos_s^\alpha\theta\cos_s^\beta\phi \\ \sin_s^\alpha\theta\cos_s^\beta\phi \\ \sin_s^\beta\phi \end{pmatrix} \begin{matrix} -\pi \leqslant \theta \leqslant \pi \\ -\frac{\pi}{2} \leqslant \phi \leqslant \frac{\pi}{2} \end{matrix} \tag{4.7}$$

where $x_s^y = sgn(x)|x|^y$.

The $\alpha$ and $\beta$ shape parameters are extracted from the shape metrics (4.3, 4.4, 4.5 and 4.6) according to:

$$\begin{aligned} mu_{u^+} \geqslant 0, mu_{u^-} = 0 \Rightarrow \begin{cases} \alpha = (1 - mu_b)^{\gamma_b} \\ \beta = (1 - mu_{u^+})^{\gamma_u} \end{cases} \\ mu_{u^+} = 0, mu_{u^-} > 0 \Rightarrow \begin{cases} \alpha = (1 - mu_b)^{\gamma_b} \\ \beta = 1 + 3(mu_{u^+})^{\gamma_u} \end{cases} \end{aligned} \tag{4.8}$$

with $\gamma_b$ and $\gamma_u$ as parameters to define the sharpness of the superellipsoids[21].

The last two steps in defining the glyphs are scaling and orientation. Due to the traceless nature of the tensors, eigenvalues cannot be used to properly scale the glyph as some of them might be negative. The scaling is therefore determined so that the magnitude of the axes orthogonal is inversely proportional to the uniaxiality order of the tensor. The two minor axes of the glyph are additionally inversely proportionally to biaxiality. The orientation can be then easily applied by aligning each of the glyphs axes with the corresponding tensor eigenvectors according to scale.

An uniaxial fibres distribution, represented by an SFRC sample in which the majority of fibres have a well aligned orientation along an axis is, as shown, depending on their distribution (linear or ring-like shaped) in Fig. 4.3(c) either as an elongated shape (positive uniaxiality, linear, as depicted in Fig. 4.4,a and Fig. 4.4,b) or as a spiked disk (negative uniaxiality, ring-like as shown in Fig. 4.4,b and Fig. 4.4,d). Such is the case of a tensor with a strongly dominant eigenvector.

In the specific case of the SFRC tomographies from the previous chapter, the glyphs-based visualisation, has an even more relevant efficacy when used to visualise the fibres orientation distribution superposed to the concrete slab from which the samples were taken. Different behaviours will be therefore displayed visually in the different areas of the slab, giving an understandable way of inspection in order to analyse the outcomes of the casting techniques and the different materials used for the mould.

## 4.2 THE ACTIVE SOFTWARE

This whole set of features, pushed us to further expand our set of tools with the A.C.T.I.V.E. (Anisotropic Composite Tensor Interactive Visualisation Environment) software. Thanks to the contribution of two interns from the German DAAD - RISE Worldwide project, Mr. Marcel Padilla (TU Berlin) and Mr. Michael Krause (RTWH Aachen), we decided to proceed in developing the software towards an SFRC-related but completely new visualisation function: a CFD simulation visualisation representing the coupling of the fibres orientation equation and the casting of the SFRC concrete.

The simulation, developed in OpenFOAM [49], represents a two-fluids mixing (air and concrete) during the casting procedure, with the fibre orientation equation being coupled to the concrete rheology for each step. The concrete is poured

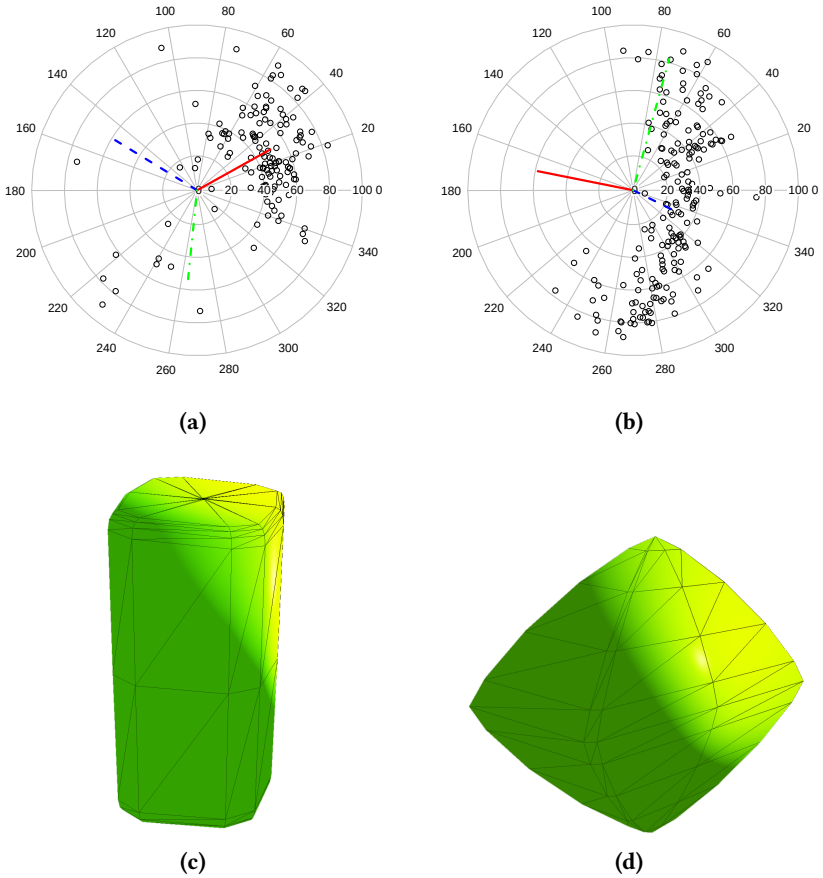


**Figure 4.4** – (a) Fibres orientation distributions in SFRC analysis: Positive uniaxiality (linear) and (c) the corresponding superellipsoidal glyph, (b) negative uniaxiality (ring-like) and (d) the corresponding glyph

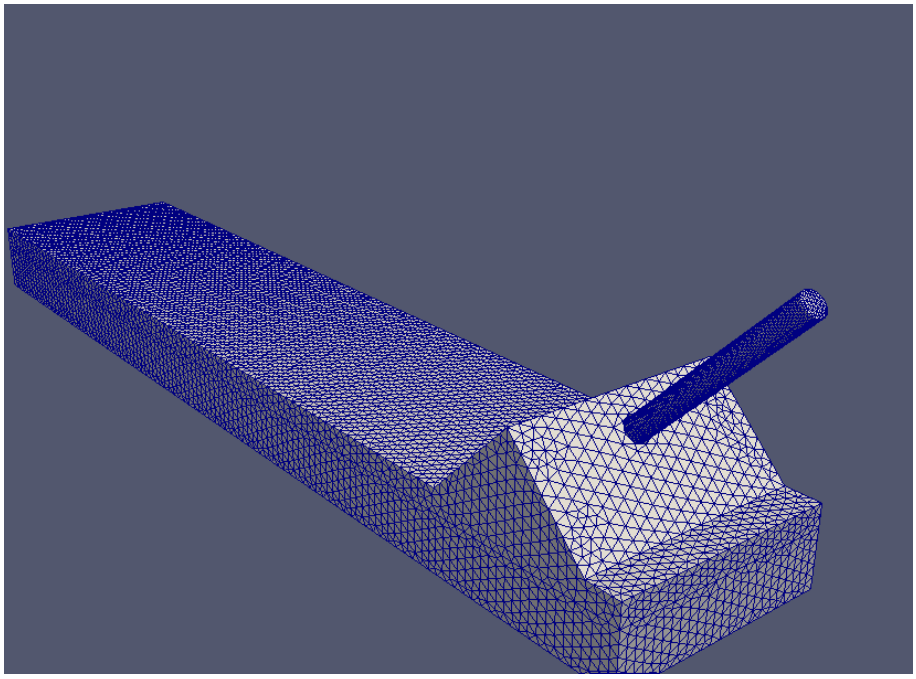

**Figure 4.5** – Mesh structure for the OpenFOAM-based CFD simulation.

in a box-shaped mould through a large pipe.

The first step to use the algorithms described in the previous section, that are tuned to traceless tensors, is to remove the trace from the orientation tensors (therefore converting them into alignment tensors).

In order to properly describe the simulation through superellipsoidal tensor glyphs, the 3D mesh of the simulation (depicted in Fig. 4.5) is divided into cells, each of them described by an Alpha ($\alpha$) value that represents the amount of concrete present in that given cell at a certain moment of the simulation. Only cells with a content of concrete sufficiently high are taken into account for the fibres orientation equation coupling.

The idea behind the A.C.T.I.V.E. software visualisation was therefore to represent each meaningful cell with an appropriate superellipsoidal glyph shape, describing the fibre orientation for each cell at each step of the process. By using the Jankun-Kelly,Mehta [17] method explained in the previous section, we extracted the necessary metrics from the tensors of each step of the simulation and used them to model the parametric surfaces of the superellipsoids in OpenGL.
In order to maintain a good scalability of the software with very large amounts

of tensor data (the test datasets contained approximately 80000 tensors) while preserving a very high visualisation quality (high vertex number in the glyphs resolution, dynamic lighting and specular shaders, etc.) some precautions where necessary.
The most influential choice for the performances was to separate the metrics computation from the visualisation itself. The whole set of algebraic operations on the tensors matrices (eigenvalues and eigenvectors extractions) might have represented a risky bottle-neck in the visualisation.

The whole calculation has therefore been outsourced to an external tool that takes the whole OpenFOAM simulation folder as input, and produces a file containing the metrics of each glyph. It is performed, single-threaded, in a total time of approximately 4 minutes for 20 time steps of animation of approximately 80000 tensors.
At this point, it was already possible to understand that a very large variety of glyphs, even though generated by slightly different tensors, would have had shape parameters differences so small to be invisible to the human eye. This led to the successive important optimisation step of A.C.T.I.V.E, that consisted of preparing a set of precomputed shapes covering the discretised range of the superellipsoidal domain.
By using the shape metrics extracted in the previous step as indices of the table, we select which shape better corresponds to the given tensor. Finally we apply the correct scaling and rotation and we position them in the 3D space.
The above sequence is repeated for each glyph of each time step during the animation display (as shown in Fig. 4.6). Due to such simplified operations, the software allows to modify in real time certain parameters of the visualisation (scaling, colors and thresholding according to the $\alpha$ value of each cell or amplification of certain axes for better visibility), with no influence on the performances.

Several lower level optimisation were also applied to the code by using innate properties of OpenGL and VRUI to reduce the number of draw calls by batching the vertices before each update of the frame.

Similar performances have been observed in the software on a single screen computer desktop (i5-3350 3.1GHz 4-cores CPU, 16GB RAM, Quadro600 GPU) and in multiscreen on the Kyb3 (Opteron 4284 3.0GHz 8-cores CPU, 64 GB RAM, Quadro4000 GPU).

With the addition of several further visualisation features already designed, A.C.T.I.V.E. is going to soon become one of the most important tools in our group. The understanding of a tensor field from numerical data, is a long and complex

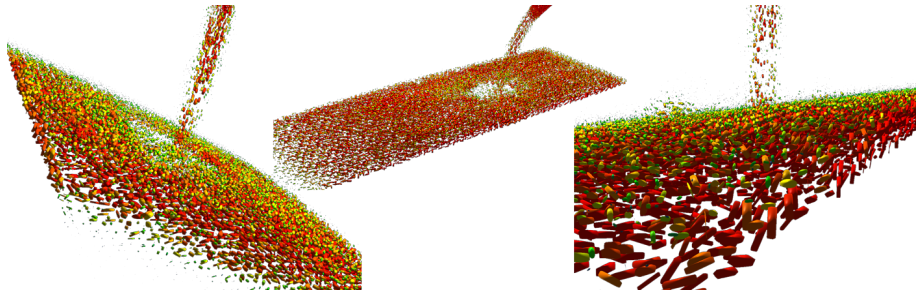

**Figure 4.6** – A.C.T.I.V.E. visualisation of an SFRC OpenFOAM-based CFD simulation.

process, only accessible to academic people with mathematical and physical backgrounds. The access to a tool able to reliably inspect a CFD simulation is therefore a valuable tool for researchers and for company engineers. It allows a much easier matching of cause-effect in the field of SFRC casting and working.
For an even more intuitive understanding, further extensions of the A.C.T.I.V.E. software will include mesh-based visualisation of the fibres, granting therefore an additional layer of similarity to the real concrete casting situation.

## 4.3 CHAPTER CONCLUSIONS

This chapter presented the development of A.C.T.I.V.E., a portable software for the visualization of CFD simulations of the casting of the SFRC. A.C.T.I.V.E. offers an effective and fast method to predict the distribution and orientation of the fibres in the material according to the different casting method used. Such data is invaluable in order to spare time and materials otherwise used to perform the same experiments in a real setup.
The following list summarizes the outcomes of the software:

- Computes CFD simulations of SFRC casting and visualizes them animated using superellipsoidal glyphs to display the fibres orientation tensors.
- Portable and scalable, offers the same functionalities on traditional desktop computer, immersive and semi-immersive VE.
- Optimized to displays animated simulations of large amounts of data smoothly also on low-performances systems.
- Offers full control of the visualization parameters to allow in-depth inspection of the data

- Released under open source license and available in the VisPar group repository (see section 1.2 for details)

# 5

## CONCLUSIONS AND FUTURE WORK

Despite the wide variety of topics covered by this dissertation, it is my hope that I made clear the common ground on which they all joined: scientific visualisation.
Designing and building the Kyb3 with specific constraints in mind and developing a software using a new and unique algorithm that made use of the VR system, for development and for the final display of the results, were the two main components of the work done.

By looking at the big picture, it should be evident that the whole research done during my doctoral studies aimed not only at the development of the separate components. We performed and reported the research work in a way to both highlight the place its parts have in the process and how each of them offers or receives benefits from scientific visualisation.

We developed the Kyb3 so that, as stated in the introduction, despite a specific visualisation aim in mind, it could allow a wide flexibility in use and development. The two different software presented, μTAnS-Fib for SFRC μCT analysis and A.C.T.I.V.E. for CFD simulations visualisation, already highlight two related but different uses that can be made of the Kyb3. Both of them share the same application field, the research and visualisation on complex materials, but from completely different points of view.

As described in detail in Publication II, visualisation-assisted development proved to be a unique asset in terms of time and quality assurance optimisation. It reduced the propagation of errors throughout the process, sped up the validation of partial and final results, and simplified the task of broadcasting the obtained results both to an academic and non-academic audience.

It is my opinion that such benefits were absolutely vital for the development of the SFRC software. Thanks to the VR visualisation on the Kyb3, a variety of

patterns, previously hidden in the data, have been detected and will soon be inspected. An example of that is for example represented by the different behaviour of the voxel orientation vectors at the extremities of a fibre. If they represent the real ends of a fibre they will be arranged in a 3d sunburst-like distribution (due to the amplification of the slightly rounded shape of the fibre's end caused by the Gaussian filtering), while in the case of cut fibres they will just fade away in the direction of the fibre segment next to the cut.

This is therefore how the separate topics of my research, from Virtual Reality to Complex Materials analysis, synergistically merge in the frame of Scientific Visualisation. Although each of the topics can represent a stand-alone field of research, it was the aim of my studies to use them together in order to highlight the advantages that such an interdisciplinary approach would generate.

Let us now evaluate the contributions in terms of novelty and results for each of its components.

Regarding the VR part of the research, that constituted the platform on which the following development were based on:

- The Kyb3 is a VE with a unique ratio of screen surface, occupied space and construction costs.
- It represents a novel concept of VE for Scientific Visualization and for VR-oriented development and prototyping.
- With a full documentation on design and construction, and with the use of opensource software only, the Kyb3 is a tool reproducible by any research institution in need of a similar VE.
- We designed and built a VE that, despite a specific scientific visualisation as its main scope, has the flexibility to start the research field in VR in Estonia and be used in several application fields.

In the SFRC part, the application field of our research:

- Our algorithm and software produces excellent results about fibres orientations in SFRC in much shorter times than the other existing ones (where timing is mentioned).
- The algorithm correctly handles the separation of touching fibres and partially cut fibres.
- The filtering component of the software allows the analysis to be run on very noisy datasets.

- We obtained additional information about the fibres' hooks contribution to the material properties of SFRC otherwise neglected by other software.
- Due to the lack of need for user interaction during the process, the uTAnS-fib software is able to process autonomously large batches of datasets.
- The A.C.T.I.V.E. software can, thanks to implementation optimisation, visualise in real time and with good quality very large amounts of tensor data (tested with up to 80000 tensors) also on low performances machines.

We consider the results of both the main components of the research to be very satisfactory and to have respected the premises with which we began the work.

Even if the Kyb3 and the developed software can be used separately for other application fields and on other platforms, I would like once again to highlight the great symbiosis that joined them in our research: a powerful analysis and visualisation tool used on a likewise powerful and intuitive visualisation system.

The whole work I brought on during my Doctoral studies with the help of my scientific advisor Dr. Heiko Herrmann though, was never meant as an arrival point, but more as a starting point. The Kyb3 and the developed software, aside from their specific uses, need to represent an example of the potential of such a visualisation approach. During my studies, we already drafted possible extensions of the work done that would open the way to new researches and new doctoral students works as well.

With the expertise earned through the development of the Kyb3, larger, CAVE-like systems can be built for the first time in Estonia, as well as a variety of other more specific ones, as L-benches and HMD-based systems, tuned to the needs of particular application fields. The Kyb3 itself, although fully functional, might be used as an experimental platform for different tracking systems (eg. optical ones) and, with the substitution of only a few components it could easily employ active polarised stereoscopic or a passive/active hybrid.
Moreover, thanks to the well exposed software infrastructure, almost all the existing VR software can be used immediately on it, or with only slight minor modifications.

In the SFRC/complex materials branch of our research, we believe to have opened up an even wider variety of future possibilities.
The existing software can be further enriched in features and improved in the already implemented ones.
We believe for example that the μTAnS-Fib SFRC μCT analysis software separ-

ation of fibres might benefit by a more detailed data mining processing of the peaks maps to further enhance fibres separation also in complex setup. Moreover, a better discretisation of the sphere for the polar coordinates clustering would enhance the research for separate peeks and minimise the approximation caused by spherical coordinates when the angles values are too close to the poles. It is our firm belief that the information describing the orientation of the fibre hook is contained in the peeks map as well. A method to extract it would provide additional insight and details about the datasets.

A possible approach to implement the mentioned development might probably use neural network algorithms. The same family of algorithms, moreover, properly trained, might further enhance the filtering process, possibly completely removing every need for user intervention on the input of parameters.
By using the VTK libraries for an optimised visualisation, it would be also possible to developed a graphical interface with interactive visualisation of the partial data, in order to further simplify the software user's familiarisation process.

The A.C.T.I.V.E. software, with its clean and well documented code, can be further extended in order to integrate additional information visualisation (flow fields, volumetric visualisation, casting mould meshes, etc). With the scalability and portability granted by the VRUI platform, I believe its potential, yet partially untapped, could grow into a very powerful tool in the future.

# BIBLIOGRAPHY

# BIBLIOGRAPHY


[1] K.-N. An, M.C. Jacobsen, L.J. Berglund, and E.Y.S. Chao. Application of a magnetic tracking device to kinesiologic studies. *Journal of Biomechanics*, 21(7):613 – 620, 1988. ISSN 0021-9290. doi: 10.1016/0021-9290(88)90225-4.

[2] A. Baak, M. Muller, G. Bharaj, H.-P. Seidel, and C. Theobalt. A data-driven approach for real-time full body pose reconstruction from a depth camera. In *Computer Vision (ICCV), 2011 IEEE International Conference on*, pages 1092–1099, Nov 2011. doi: 10.1109/ICCV.2011.6126356.

[3] A.H. Barr. Superquadrics and angle-preserving transformations. *Computer Graphics and Applications, IEEE*, 1(1):11–23, Jan 1981. ISSN 0272-1716. doi: 10.1109/MCG.1981.1673799.

[4] Tony Bernardin, Eric Cowgill, Oliver Kreylos, Christopher Bowles, Peter Gold, Bernd Hamann, and Louise Kellogg. Crusta: A new virtual globe for real-time visualization of sub-meter digital topography at planetary scales. *Computers and Geosciences*, 37(1):75 – 85, 2011. ISSN 0098-3004. doi: 10.1016/j.cageo.2010.02.006. Virtual Globes in Science.

[5] Herman J. Blinchikoff and Anatol I. Zverev. *Filtering in the Time and Frequency Domains*. Krieger Publishing Co., Inc., Melbourne, FL, USA, 1986. ISBN 0898749522.

[6] Carolina Cruz-Neira, Daniel J. Sandin, and Thomas A. DeFanti. Surround-screen projection-based virtual reality: The design and implementation of the CAVE. In *Proceedings of the 20th Annual Conference on Computer Graphics and Interactive Techniques*, SIGGRAPH '93, pages 135–142, New York, NY, USA, 1993. ACM. ISBN 0-89791-601-8. doi: 10.1145/166117.166134.

[7] Michael B. Dillencourt, Hanan Samet, and Markku Tamminen. A general approach to connected-component labeling for arbitrary image representations. *J. ACM*, 39(2):253–280, April 1992. ISSN 0004-5411. doi: 10.1145/128749.128750.

[8] Marika Eik, Karl Lohmus, Martin Tigasson, Madis Listak, Jari Puttonen, and Heiko Herrmann. DC-conductivity testing combined with photometry for measuring fibre orientations in SFRC. *Journal of Materials Science*, 48(10): 3745–3759, May 2013. ISSN 0022-2461. doi: 10.1007/s10853-013-7174-3.

[9] I. D. Faux and M. J. Pratt. *Computational Geometry for Design and Manufacture*. Halsted Press, New York, NY, USA, 1979. ISBN 047026473X.

[10] L. A. Feldkamp, L. C. Davis, and J. W. Kress. Practical cone-beam algorithm. *J. Opt. Soc. Am. A*, 1(6):612–619, Jun 1984. doi: 10.1364/JOSAA.1.000612.

[11] Liberato Ferrara, Marco Faifer, and Sergio Toscani. A magnetic method for non destructive monitoring of fiber dispersion and orientation in steel fiber reinforced cementitious composites part 1: method calibration. *Materials and Structures*, 45(4):575–589, 2012. ISSN 1359-5997. doi: 10.1617/s11527-011-9793-y.

[12] A. F. Frangi, W.J. Niessen, Paul J. Nederkoorn, J. Bakker, W.P.Th.M. Mali, and M.A. Viergever. Quantitative analysis of vascular morphology from 3d mr angiograms: in vitro and in vivo results. *Magnetic Resonance in Medicine*, 45: 311–322, 2001.

[13] S. Grunewald, F. Laranjeira, J.C. Walraven, A. Aguado, and C. Molins. Influence of fibre orientation on the performance of steel fibre-reinforced concrete. *8th RILEM International Symposium on Fiber Reinforced Concrete: challenges and opportunities (BEFIB 2012)*, pages 313 – 325.

[14] Gaël Guennebaud, Benoît Jacob, et al. Eigen v3. http://eigen.tuxfamily.org, 2010.

[15] Mario Gutierrez, F Vexo, and Daniel Thalmann. *Stepping into Virtual Reality*. Springer-Verlag TELOS, Santa Clara, CA, USA, 1 edition, 2008. ISBN 1848001169, 9781848001169.

[16] Amy Henderson. *The ParaView Guide: A Parallel Visualization Application*. Kitware, November 2004.

[17] T. J. Jankun-Kelly and Ketan Mehta. Superellipsoid-based, real symmetric traceless tensor glyphs motivated by nematic liquid crystal alignment visualization. In *IEEE Transactions on Visualization and Computer Graphics (Proceedings Visualization/Information Visualization 2006)*, pages 1197–1204, 2006. doi: 10.1109/TVCG.2006.181.

[18] Hans J. Johnson, M. McCormick, L. Ibáñez, and The Insight Software Consortium. *The ITK Software Guide*. Kitware, Inc., third edition, 2013. URL `http://www.itk.org/ItkSoftwareGuide.pdf`.

[19] D.F. Keefe and T. Isenberg. Reimagining the scientific visualization interaction paradigm. *IEEE Computer*, 46(5):51–57, 2013. ISSN 0018-9162. doi: 10.1109/MC.2013.178.

[20] Youngjun Kim, Martin van Velsen, and Randall W. Hill, Jr. Lecture notes in computer science. chapter Modeling Dynamic Perceptual Attention in Complex Virtual Environments, pages 266–277. Springer-Verlag, London, UK, UK, 2005. ISBN 3-540-28738-8. doi: 10.1007/11550617_23.

[21] G. Kindlmann. Superquadric tensor glyphs. In *Proceedings of IEEE TVCG/EG Symposium on Visualization 2004*, pages 147–154, May 2004.

[22] Gordon L. Kindlmann. Teem, 2008. URL `http://teem.sf.net`.

[23] Volodymyr V. Kindratenko. A survey of electromagnetic position tracker calibration techniques. *Virtual Reality*, 5(3):169–182, 2000. ISSN 1359-4338. doi: 10.1007/BF01409422.

[24] David Kirk. *Graphics gems III*. The graphics gems series. Academic Press, London, San Diego, 1992. ISBN 0-12-409673-5.

[25] Oliver Kreylos. Environment-independent VR development. In George Bebis, Richard Boyle, Bahram Parvin, Darko Koracin, Paolo Remagnino, Fatih Porikli, Jörg Peters, James Klosowski, Laura Arns, YuKa Chun, Theresa-Marie Rhyne, and Laura Monroe, editors, *Advances in Visual Computing*, volume 5358 of *Lecture Notes in Computer Science*, pages 901–912. Springer Berlin Heidelberg, 2008. ISBN 978-3-540-89638-8. doi: 10.1007/978-3-540-89639-5_86.

[26] Dirk-Jan Kroon. Hessian based Frangi vesselness filter, March 2010. URL `http://www.mathworks.com/matlabcentral/fileexchange/24409-hessian-based-frangi-vesselness-filter`.

[27] T.-H. Le, P.J.J. Dumont, L. Orgéas, D. Favier, L. Salvo, and E. Boller. X-ray phase contrast microtomography for the analysis of the fibrous microstructure of {SMC} composites. *Composites Part A: Applied Science and Manufacturing*, 39(1):91 – 103, 2008. ISSN 1359-835X. doi: 10.1016/j.compositesa.2007.08.027.

[28] G. Lehmann. Label object representation and manipulation with itk. `http://hdl.handle.net/1926/584`, 08 2007. ISSN 2327-770X.

[29] David F. McAllister. *Stereo and 3-D Display Technologies*. John Wiley and Sons, Inc., 2002. ISBN 9780471443391. doi: 10.1002/0471443395.img093.

[30] Evelyn Orman. Effect of virtual reality exposure and aural stimuli on eye contact, directional focus, and focus of attention. 2012.

[31] N. Ozyurt, T. O. Mason, and S. P. Shah. Non-destructive monitoring of fiber dispersion in frcs using ac-impedance spectroscopy. In MARIAS. KONSTAGDOUTOS, editor, *Measuring, Monitoring and Modeling Concrete Properties*, pages 285–290. Springer Netherlands, 2006. ISBN 978-1-4020-5103-6. doi: 10.1007/978-1-4020-5104-3_33.

[32] Thomas D. Parsons and Albert A. Rizzo. Neuropsychological assessment of attentional processing using virtual reality. *Annual Review of CyberTherapy and Telemedicine*, 6(1), 2008.

[33] Claudia Redenbach, Alexander Rack, Katja Schladitz, Oliver Wirjadic, and Michael Godehardt. Beyond imaging: on the quantitative analysis of tomographic volume data. *International Journal of Materials Research*, 2012(2): 217–227, 2012.

[34] Stephan Reichelt, Ralf Häussler, Gerald Fütterer, and Norbert Leister. Depth cues in human visual perception and their realization in 3d displays. volume 7690, pages 76900B–76900B–12, 2010. doi: 10.1117/12.850094.

[35] Whitman Richards. Stereopsis and stereoblindness. *Experimental Brain Research*, 10(4):380–388, 1970. ISSN 0014-4819. doi: 10.1007/BF02324765.

[36] Michael D. Robinson, Gary Sharp, and Jianmin Chen. *Polarization Engineering for LCD Projection.* Wiley, Santa Clara, CA, USA, 2005. ISBN 978-0-470-87105-8.

[37] Jannick P. Rolland, Yohan Baillot, and Alexei A. Goon. A survey of tracking technology for virtual environments, 2001.

[38] W. Rollmann. Zwei neue stereoskopische methoden. *Annalen der Physik*, 166(9):186–187, 1853. ISSN 1521-3889. doi: 10.1002/andp.18531660914.

[39] Jürgen Schnell, Katja Schladitz, and Frank Schuler. Richtungsanalyse von fasern in betonen auf basis der computer-tomographie. *Beton- und Stahlbetonbau*, 105(2):72–77, 2010. ISSN 1437-1006. doi: 10.1002/best.200900055.

[40] Will Schroeder, Kenneth M. Martin, and William E. Lorensen. *The Visualization Toolkit (2Nd Ed.): An Object-oriented Approach to 3D Graphics.* Prentice-Hall, Inc., Upper Saddle River, NJ, USA, 1998. ISBN 0-13-954694-4.

[41] Pierre Soille. *Morphological Image Analysis: Principles and Applications.* Springer-Verlag New York, Inc., Secaucus, NJ, USA, 2 edition, 2003. ISBN 3540429883.

[42] P. Stroeven and J. Hu. Review paper – stereology: Historical perspective and applicability to concrete technology. *Materials and Structures*, 39(1):127–135, 2006. ISSN 1359-5997. doi: 10.1617/s11527-005-9031-6.

[43] Jussi-Petteri Suuronen, Aki Kallonen, Marika Eik, Jari Puttonen, Ritva Serimaa, and Heiko Herrmann. Analysis of short fibres orientation in steel fibre reinforced concrete (SFRC) using x-ray tomography. *Journal of Materials Science*, 48(3):1358–1367, February 2013. ISSN 0022-2461. doi: 10.1007/s10853-012-6882-4.

[44] Russell M. Taylor, II, Thomas C. Hudson, Adam Seeger, Hans Weber, Jeffrey Juliano, and Aron T. Helser. VRPN: A device-independent, network-transparent VR peripheral system. In *Proceedings of the ACM Symposium on Virtual Reality Software and Technology*, VRST '01, pages 55–61, New York, NY, USA, 2001. ACM. ISBN 1-58113-427-4. doi: 10.1145/505008.505019.

[45] T. L. Turner and R. F. Hellbaum. Lc shutter glasses provide 3-d display for simulated flight. *Inf. Disp.*, 2(9):22–24, September 1986. ISSN 0362-0972.

[46] Andries van Dam, David H Laidlaw, and Rosemary Michelle Simpson. Experiments in immersive virtual reality for scientific visualization. *Computers and Graphics*, 26(4):535 – 555, 2002. ISSN 0097-8493. doi: 10.1016/S0097-8493(02)00113-9.

[47] Miguel A. Vicente, Dorys C. Gonzalez, and Jesus Manguez. Determination of dominant fibre orientations in fibre-reinforced high-strength concrete elements based on computed tomography scans. *Nondestructive Testing and Evaluation*, 29(2):164–182, 2014. doi: 10.1080/10589759.2014.914204.

[48] Xiaolin Wei, Peizhao Zhang, and Jinxiang Chai. Accurate realtime full-body motion capture using a single depth camera. *ACM Trans. Graph.*, 31(6):188:1–188:12, November 2012. ISSN 0730-0301. doi: 10.1145/2366145.2366207.

[49] H. G. Weller, G. Tabor, H. Jasak, and C. Fureby. A tensorial approach to computational continuum mechanics using object-oriented techniques. *Comput. Phys.*, 12(6):620–631, November 1998. ISSN 0894-1866. doi: 10.1063/1.168744.

[50] C.-F. Westin, S.E. Maier, H. Mamata, A. Nabavi, F.A. Jolesz, and R. Kikinis. Processing and visualization for diffusion tensor {MRI}. *Medical Image Analysis*, 6(2):93 – 108, 2002. ISSN 1361-8415. doi: 10.1016/S1361-8415(02)00053-1.

[51] Stefan Winkler and Dongbo Min. Stereo/multiview picture quality: Overview and recent advances. *Signal Processing: Image Communication*, 28(10): 1358 – 1373, 2013. ISSN 0923-5965. doi: 10.1016/j.image.2013.07.008.

[52] Craig M. Wittenbrink. Ifs fractal interpolation for 2d and 3d visualization. In *Proceedings of the 6th Conference on Visualization '95*, VIS '95, pages 77–, Washington, DC, USA, 1995. IEEE Computer Society. ISBN 0-8186-7187-4.

[53] J. Wuest, E. Denarié, E. Brühwiler, L. Tamarit, M. Kocher, and E. Gallucci. Tomography analysis of fiber distribution and orientation in ultra high–performance fiber-reinforced composites with high-fiber dosages. *Experimental Techniques*, 33(5):50–55, 2009. ISSN 1747-1567. doi: 10.1111/j.1747-1567.2008.00420.x.

[54] G. Zachmann. Distortion correction of magnetic fields for position tracking. In *Computer Graphics International, 1997. Proceedings*, pages 213–220, 251, Jun 1997. doi: 10.1109/CGI.1997.601306.

# CURRICULUM VITAE

**CURRICULUM VITAE**

1. Personal Data

Name : Emiliano Pastorelli
Date and place of Birth : 25th of May 1982, Sanremo (Italy)
Nationality : Italian

2. Contact Information

Address : Akadeemia Tee 21, 12618, Tallinn Estonia
Phone : +372 58390502
Email : pastorelli@cens.ioc.ee

3. Education

| Educational Institution | Graduation year | Education (Field of study/degree) |
|---|---|---|
| Universita' degli Studi di Genova, Genova (Italy) | 2009 | Information and Communication Technology with 3D Graphics and Image processing specialization/Bachelor degree |
| Universita' degli Studi di Genova, Genova (Italy) | 2011 | Information and Communication Technology with 3D Graphics and Image processing specialization/Master degree |

4. Language competence/skills

| Language | Level |
|---|---|
| Italian | Mother language |
| English | Fluent |
| Spanish | Fluent |
| French | Fluent |
| German | Average |
| Russian | Basic |
| Estonian | Basic |

5.Professional Employment

| Period | Organization | Position |
|---|---|---|
| 2012-... | Institute of Cybernetics at Tallinn University of Technology | Engineer |
| 2013-... | Portside Out Starboard Home Industries AB, Stockholm, Sweden | Multimedia 3D developer |

6. Scientific work

Pastorelli, Emiliano; Herrmann, Heiko (2013). A small-scale, low-budget semi-immersive virtual environment for scientific visualization and research. In: Procedia Computer Science. Volume 25 : 2013 International Conference on Virtual and Augmented Reality in Education, 14 - 22.

Herrmann, Heiko; Pastorelli, Emiliano. (2014). Virtual reality visualization for photogrammetric 3d reconstructions of cultural heritage. In: Augmented and Virtual Reality, First International Conference, AVR 2014, Lecce, Italy, September 17-20, 2014, Revised Selected Papers: (Toim.) De Paolis, Lucio Tommaso; Mongelli, Antonio. Cham: Springer, (Lecture Notes in Computer Science; 8853), 283 - 295.

Herrmann, H.; Padilla, M.; Pastorelli, E. (2014). A.C.T.I.V.E.: A scalable superellipsoid-based CFD visualization for virtual and desktop environments. EuroVR 2014 : Conference and Exhibition of the European Association of Virtual and Augmented Reality, Bremen, Germany, December 8th - 10th, 2014. (Toim.) Zachmann, G.; Perret, J.; Amditis, A.. EuroGOOS Office, 1 - 4.

Pastorelli, Emiliano; Herrmann, Heiko (2014). Complex materials analysis and visualization through Virtual Reality environments. In: Proceedings of the 8th Annual Conference of the Estonian National Doctoral School in Information and Communication Technologies : December 5-6, 2014, Rakvere: Tallinn: Tallinn University of Technology, 99 - 102.

Pastorelli, Emiliano; Herrmann, Heiko (2014). Virtual Reality Visualization for Short Fibre Orientation Analysis. In: Xplore IEEE BEC2014: Proceedings of the 14th Baltic Electronic Conference(Accepted).

Pastorelli, Emiliano; Herrmann, Heiko (2015). Time-efficient automated analysis for fibre orientation in Steel Fibre Reinforced Concrete. In: Proceedings of the Estonian Academy of Sciences(Accepted).

7. Defended Theses

Skeleton construction for Tethraedral meshes, Universita' degli Studi di Genova, Genova (Italy). Supervisor Prof.Enrico Puppo

Tensor Visualization with Virtual Reality Displays, Universita' degli Studi di Genova, Genova (Italy). Supervisors Prof.Paola Magillo, Dr.Heiko Herrmann (Institute of Cybernetics at Tallinn University of Technology)

8. Main area of work/Current research topics :

Virtual reality 3D visualization, Image processing and Scientific visualization for complex materials

**ELULOOKIRJELDUS**

1. Isikuandmed


Nimi : Emiliano Pastorelli
Sünniaeg ja -koht : 25. Mai 1982, Sanremo (Itaalia)
Kodakondsus : Itaalia


2. Kontaktandmed


Aadress : Akadeemia Tee 21, 12618, Tallinn
Telefon : +372 58390502
E-post : pastorelli@cens.ioc.ee


3. Hariduskäik

| Õppeasutus (nimetus lõpetamise ajal) | Lõpetamise aeg | Haridus (eriala/kraad) |
|---|---|---|
| Universita' degli Studi di Genova, Genova (Itaalia) | 2009 | Information and Communication Technology with 3D Graphics and Image processing specialization/Bachelor degree |
| Universita' degli Studi di Genova, Genova (Itaalia) | 2011 | Information and Communication Technology with 3D Graphics and Image processing specialization/Master degree |

4. Keelteoskus (alg-, kesk- või kõrgtase)

| Keel | Tase |
|---|---|
| Itaalia | emakeel |
| Inglise | kõrgtase |
| Hispaania | kõrgtase |
| Prantsuse | kõrgtase |
| Saksa | kesktase |
| Vene | algtase |
| Eesti | algtase |

5.Teenistuskäik

| Töötamise aeg | Tööandja nimetus | Ametikoht |
|---|---|---|
| 2012-... | TTÜ Küberneetika Instituut | Insener |
| 2013-... | Portside Out Starboard Home Industries AB, Stockholm, Rootsi | Multimedia 3D developer |

6. Teadustöö:

Pastorelli, Emiliano; Herrmann, Heiko (2013). A small-scale, low-budget semi-immersive virtual environment for scientific visualization and research. In: Procedia Computer Science. Volume 25 : 2013 International Conference on Virtual and Augmented Reality in Education, 14 - 22.

Herrmann, Heiko; Pastorelli, Emiliano. (2014). Virtual reality visualization for photogrammetric 3d reconstructions of cultural heritage. In: Augmented and Virtual Reality, First International Conference, AVR 2014, Lecce, Italy, September 17-20, 2014, Revised Selected Papers: (Toim.) De Paolis, Lucio Tommaso; Mongelli, Antonio. Cham: Springer, (Lecture Notes in Computer Science; 8853), 283 - 295.

Herrmann, H.; Padilla, M.; Pastorelli, E. (2014). A.C.T.I.V.E.: A scalable superellipsoid-based CFD visualization for virtual and desktop environments. EuroVR 2014 : Conference and Exhibition of the European Association of Virtual and Augmented Reality, Bremen, Germany, December 8th - 10th, 2014. (Toim.) Zachmann, G.; Perret, J.; Amditis, A.. EuroGOOS Office, 1 - 4.

Pastorelli, Emiliano; Herrmann, Heiko (2014). Complex materials analysis and visualization through Virtual Reality environments. In: Proceedings of the 8th Annual Conference of the Estonian National Doctoral School in Information and Communication Technologies : December 5-6, 2014, Rakvere: Tallinn: Tallinn University of Technology, 99 - 102.

Pastorelli, Emiliano; Herrmann, Heiko (2014). Virtual Reality Visualization for Short Fibre Orientation Analysis. In: Xplore IEEE BEC2014: Proceedings of the 14th Baltic Electronic Conference(Accepted).

Pastorelli, Emiliano; Herrmann, Heiko (2015). Time-efficient automated analysis for fibre orientation in Steel Fibre Reinforced Concrete. In: Proceedings of the Estonian Academy of Sciences(Accepted).

7. Kaitstud tööd:

Skeleton construction for Tethraedral meshes, Universita' degli Studi di Genova, Genova (Italy). Juhendaja Prof.Enrico Puppo

Tensor Visualization with Virtual Reality Displays, Universita' degli Studi di Genova, Genova (Italy). Juhendajad Prof.Paola Magillo, Dr.Heiko Herrmann (Institute of Cybernetics at Tallinn University of Technology)

8. Peamine uurimisteema/käesolev uurimisteema:

Virtual reality 3D visualization, Image processing and Scientific visualization for complex materials

# APPENDIX

PUBLICATION I

Pastorelli E., Herrmann H.
**A Small-scale, Low-budget Semi-immersive Virtual Environment for Scientific Visualization and Research.**
*Procedia Computer Science*, 25(iii-iv), pp. 14-22, September 2013

Available online at www.sciencedirect.com

ScienceDirect

Procedia Computer Science 25 (2013) 14 – 22

Procedia Computer Science

2013 International Conference on Virtual and Augmented Reality in Education

# A Small-scale, Low-budget Semi-immersive Virtual Environment for Scientific Visualization and Research

Emiliano Pastorelli [a,*], Heiko Herrmann [a,†]

[a] *Department of Mechanics and Applied Mathematics, Institute of Cybernetics, Tallinn University of Technology, Tallinn, 12618, Estonia*

**Abstract**

This paper describes the design concepts, the making of and some applications of the first Estonian Virtual Reality Environment. Using hardware only slightly above the threshold of consumer level, we built a virtual environment (VE) aimed at scientific visualization with the lowest possible space requirements (smaller than a cube with 2 m edge length in total) and budget (approximately below 30.000 €). The system is a fully functional visualization environment that replicates most of the features and properties of a real-sized CAVE-like System, therefore allowing further prototyping and research in the field of Virtual Reality.



*Keywords :* Virtual Reality; Stereoscopics; Estonia; Scientific visualization; Semi-Immersive; Magnetic Tracking

## 1. Introduction

### *1.1. Introduction to the Kyb3*

The decision process that led to the Kyb3 (kju:b) project originated from two main reasons.

The first one, specifically related to the research interests of the Institute of Cybernetics at Tallinn University of Technology (where the system has been built and by which it has been financed), was the need for a modern scientific visualization tool. The system has the dual aim of being a support for research and

* Emiliano Pastorelli, Tel.: +372-6204150. Fax. : +372-6204151. E-mail address : pastorelli@cens.ioc.ee
† Heiko Herrmann, Tel.: +372-6204228. Fax. : +372-6204151. E-mail address : hh@cens.ioc.ee


doi:10.1016/j.procs.2013.11.003

simulations, and to be used to display to non-scientists, in a visual and therefore more easily understandable way, the applications of the physical theories developed at the institute.

The second reason, more long-term but not less appealing, was to realize the first Virtual Reality project in Estonia. As this small Baltic country is currently reaching a European-wide fame for becoming the "Silicon valley of northern Europe" [1], our plan was to pioneer the research field of Virtual Reality with a low budget virtual environment (VE) that could be used to introduce researchers and industries to Virtual Reality concepts, to be eventually extended through a real sized CAVE™-like [2] system.

To achieve these aims, a small Virtual Reality system, able to reproduce most of the features available in room-sized CAVE™-like systems, was needed. The system should be designed in a way that, despite the constrained dimensions, it could easily illustrate the potential of such environments.

With the main (but not only) aim of the Kyb3 system to be applied to scientific visualization, it had to be powerful enough to manipulate large datasets but at the same time it had to be operated in a quite small room (approx. 3 x 5 meters), occupying no more than a 2 x 2 meter area and, being a prototype project, it had to be of limited costs.

The complete system, including frame, screens, projectors, mirrors, workstation and tracking system, has been built so that it can be assembled and disassembled relatively easily and transported in a small van or a large car. The total time necessary to assemble the Kyb3 (including projectors and mirrors alignment) is approximately 5 hours, while the overall weight does not exceed 150 kg.

The contributions of the Kyb3 are:

- Space and budget-constrained environment through an accurate use of short-throw projectors and mirrors and a single graphic workstation.
- Adoption of specific requirements for scientific visualization interaction.
- Opening the way to a completely new research field for Estonia representing a fully functional small scale prototype of a CAVE™-like System.
- Low-cost user tracking and interaction using Wintracker III magnetic tracker and Wiimote Plus.

### *1.2. CAVE™ Systems and small sized installations*

Despite the initial euphoria that followed Cruz-Neira's innovative concept in 1992 [2] the last decade witnessed a recession in the development of Virtual Reality Environments. The main reason was simply their high cost.

In spite of the availability of powerful low-cost hardware, a full-fledged full-sized VE can still reach costs that are unsustainable for small and medium sized research institutes, easily reaching several hundreds of thousands of euros, making it a definitely expensive research topic.

The high cost and the limited ongoing research consequently imposed also a strong constraint on the applications of VE in the private sector.

In its wider definition [3], a semi-immersive VE is a computer-generated environment mainly composed of interactive computer graphics, designed to physically and/or psychologically immerse one or more users in an alternative reality. A CAVE™-like system is a room-sized semi-immersive VE with the number of rear-projected bounding surfaces ranging from 3 to 6 (eventually including floor and ceiling). The user position inside the VE is tracked through an optical or magnetic-based system which enables the presentation of the correct perspectives and the correct stereoscopic effect.

Despite being visually impressive, the full sized CAVE-like systems have, as we mentioned before, two main problems: cost and size. We already spent some words on the price ranges that they can reach, but what about the needed space? With a traditional back-projection (mirror endowed), a typical prerequisite is to have at

least 3 meters of free space behind each screen (including floor and ceiling). This requirement, summed up with the size of the VE itself, usually enclosed in a 3 x 3 x 3 meter cube, results in a huge space requirement of a cube with a 9 meter edge length for a 6-wall CAVE™-like system.

Several research projects have been dealing with space and cost limitations, examples of this are the miniCAVE at the Anhalt University of Applied Science in Köthen, Germany [4] and the PIT CAVE at the University of North Carolina at Chapel Hill [5]. Our approach, however, even if somehow inspired by those projects, presents several differences.

As we said in the introduction, we intended to realize a system for multiple users and demonstration of scientific visualization issues and we also wanted at the same time to implement on a smaller scale most of the features present in a room-sized CAVE™, to have a prototype on which to learn, and to be used to open the way to research in Estonia towards more complex virtual environments.

## 2. The Kyb3

### *2.1. Frame and screens*

The Kyb3 Virtual Environment is composed by three rear-projection screens (two walls and one table screen), each one illuminated by a pair of short-range projectors driven by a multiple-GPU graphics workstation.

Due to the rectangular shape of the screens, and to eventually save additional space, one of the two wall screens, the one adjacent to the shorter edge of the table screen, has been slid back so that part of its surface (approx. 30 cm) will remain hidden (Fig. 1a). This will give a more compact external look to the system, and will moreover allow us to additionally support the screens from inside the frame.

The proper scene alignment using this particular frame positioning will be compensated through software configuration.

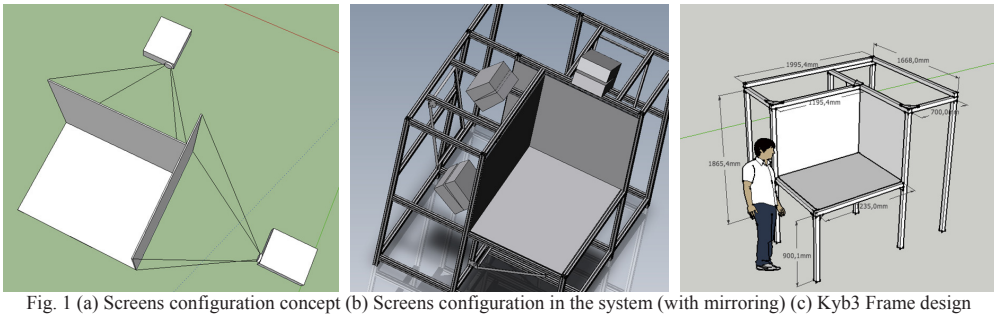


Fig. 1 (a) Screens configuration concept (b) Screens configuration in the system (with mirroring) (c) Kyb3 Frame design

The whole system is encased in a custom-made aluminium frame (built by OÜ Dimentio, Tallinn, Estonia) that supports the three screens and the movable parts that allow the positioning of the projectors and mirrors (Fig. 1b, 2b).

Additionally, the structure can be eventually disassembled to be moved. The whole structure is 1.90 m tall and 2 m x 1.70 m large, with the table floor suspended approximately 90 cm from the floor of the room (Fig. 1c). The height of the whole system has been chosen after several experimental setups (Fig. 2a) to allow a proper use of the table screen for above inspection of data, and so that the wall screens are taller than the average user height, therefore reducing the chance that the gaze of the user will float outside their boundaries, destroying the immersive feeling upon contact with the room. After multiple tests with different users, it has

been shown that the data is mostly kept in the corner between the three screens or on the lower part of the side screens.

The users tend to constantly look down with an angle that is approximately always between 30° and 45°, making therefore the chosen setup the ideal one.

The reason for the choice of aluminium versus steel as building material was related to the intention of using electromagnetic tracking sensors, and therefore the need to avoid the interferences caused by ferromagnetic materials [6]. Wood was ruled out due to its tendency to deform (wooden structures are considered to be sort-of "alive").

Fig. 2 : (a) Experimental test setup (b) Kyb3 final setup

For the screens we chose polymer-made acryl glass middle-grey polarization-preserving rigid back-projection ones of 92 x 122 cm of size.

### *2.2. Projectors and mirrors*

We mentioned in Section 1 the need for a space-saving system and we have shown in section 2.1 the small size achieved by the system (a cuboid of dimensions 2 x 1.7 x 1.9 m). To achieve an image of the proper size (approx. 92 x 122 cm) with such a limited available space behind the screens (70 cm), two necessary requirements were short throw projectors and a mirror system.

After a long search we decided to use the Acer S5201B DLP projectors. With a 3000 lumen brightness and a 4500:1 contrast ratio on a 1024 x 768 resolution, they represented one the best compromises between quality and price of the systems available in Estonia, but what really made them the favourite ones was the extremely short throw range.

With a throw range of approximately 60 cm for an image of 100 cm of base, they were definitely the best option to achieve a large bright image while using as small space as possible. Using the online Acer calculator first, and performing some direct measurements afterwards, we obtained that the necessary distance to achieve the projection size we needed was approximately between 75 and 85 cm, but it had to take into account the need for applied keystoning to compensate the double projectors, and also the size of the projectors, whose length including cables is approximately 35 cm.

Summing it up with the necessary distance stated above, would have required a space behind the screens of approximately 120-140 cm, far too much for what we had available. From that, imperatively, arose the need to use mirrors to reduce that distance.

Through the use of short-range lenses and optical mirrors, the required image size is obtained with only 70 cm of space necessary behind each screen.

However, a very precise alignment of the projectors that uses the smallest possible amount of keystone effect was necessary for every screen due to the properties of short-ranged projectors, with which every fraction of degree of rotation, and every millimetre of relocation have an amplified strong effect on the image. This heavily influenced the design of the frame that we therefore designed and built with custom-made full movable mountings that allow the multi-directional configuration of each projector (as a pair and individually) and of the related mirror (Fig. 3a, 3b, 3c).

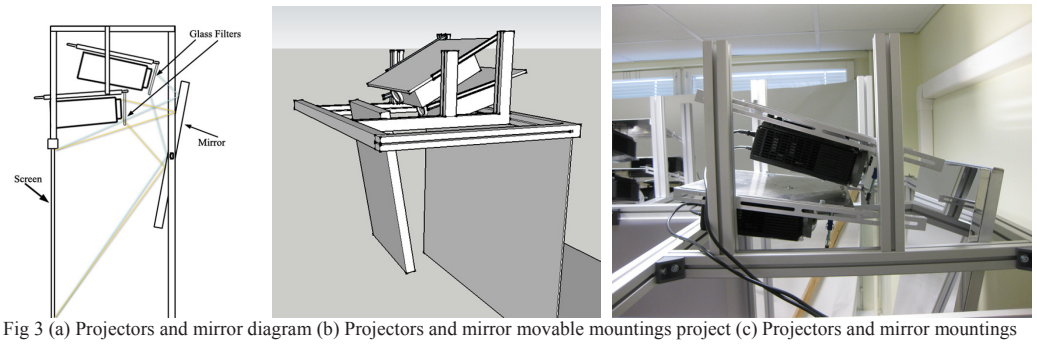


Fig 3 (a) Projectors and mirror diagram (b) Projectors and mirror movable mountings project (c) Projectors and mirror mountings

To complete the projector mounting, we built one small glass frame for each projector to hold the circular polarizing filters, for each pair of projectors the left eye filter and the right eye filter.

### *2.3. Kyb3 Workstation*

While most of the real-sized CAVE-like systems run on a distributed network of multiple computers (usually at least one computer for every screen), this choice would have conflicted with our space and budget requirements and, as all the most commonly used VE software can also run on a single computer with multiple displays, we decided to choose this solution. The Kyb3 workstation has:

- Dual 8-Core Opteron 4284 3.0 GHz
- 64 Gb ECC Registered 1666 MHz RAM
- 4x Nvidia Quadro 4000 Graphic Cards
- Intel SSD 300 GB HDD

Three of the graphics card are used to drive the projectors (two projectors per card) while the fourth one is used for a control display external to the system.

While also a weaker computer might have been able to drive a demonstration system, scientific visualization, our main aim, has a very high demand for resources that a smaller machine would not support. The machine is furthermore equipped with an InfiniBand 40Gb card that will allow a direct high speed connection (40Gb/s) with the second graphic workstation in the same room (and that is used to control a Planar SD2220W 3D display). The Institute of Cybernetics new computer cluster can be accessed via 10Gb/s Ethernet for additional computational power. The operating system running on the graphic machines is Debian 7.1 “Wheezy”.

### 2.4. User tracking and interaction

One of the main prerequisites of a usable multi-screen semi-immersive system is the user interaction management. To maintain a correct perspective, a realistic stereoscopic 3D and to allow the user to properly interact with the scene, it is necessary to implement a reactive and precise system to track the position and orientation of the head and of the interaction devices in the three-dimensional space.

We analysed the advantages and disadvantages of the two main approaches (magnetic and optical tracking) and in the end, with both of them fitting our needs, we decided in favour of the electromagnetic tracking as our main user tracking system, buying a VR-Space Wintracker III device (Fig. 4a). The reason for this choice was first of all budget-related. Despite not being widely common, for a price of 1500€, limited compared to that of most of the other devices, the Wintracker III offered three tracked sensors with a high degree of precision (0.01 cm and 0.1°), with an output of approximately 90 values per second (divided among the number of sensors in use) and an effective range of up to 150 cm.

Fig. 4 (a) Wintracker III with transmitter and 3 sensors; (b) Tracked polarized glasses (c) Tracked Wiimote plus wand

The drawback of working with a low cost almost unknown tracking device was that there were almost no documentation or user experiences available online about it, and there was no support software for testing under Linux. Also VRPN [7], our choice for input devices management, had no server class for the Wintracker III.

As a first step we therefore wrote a VRPN Server for the device (now part of the main VRPN trunk). Taking advantage of the fact that the Wintracker III is an HID (Human Interface Device), we encoded in the server not only the data reading and proper conversion into VRPN standards, but also the possibility of sending a list of HIDAPI library (http://www.signal11.us/oss/hidapi/) commands to the device when the VRPN server is started.

Through the configuration file it is therefore now possible to select how many and which sensors have to be activated, which hemisphere of the transmitter has to be used (the front one or the upper one) and if the optional range extender has to be activated or not. We installed one of the sensors on top of the polarized glasses, and we completed our first working head-tracking system (Fig. 4b).

As further progress, we introduced a Wiimote Plus want as the main interaction tool, and we decided to adopt VRUI [8] as the main framework for applications and development. A first experimental attempt made with the Wiimote+ IR camera and a IR self-built LED beacon proved the IR tracking to be too limited in freedom for the size of our system and too unreliable. We therefore decided to couple the Wiimote controller with one of the Wintracker III sensors through a VRUI Device Daemon to provide the position and orientation (Fig. 4c). This combination proved to be an ideal low-cost interaction tool, due to the 11 buttons and a practical handle of the Wiimote and the precise tracking of the magnetic sensor.

## 3. Applications of the Kyb3

In Section 1.1 we mentioned that the Kyb3 VE has been built with the double goal of being employed as a scientific visualization tool and of being a development workbench for further research in Estonia about Virtual Reality and 3D Visualization. In this section we will narrow the focus on the two directions, giving some highlights on the applications fields on which the institute is working with the Kyb3, either as a tool or as an autonomous research subject.

### *3.1. Scientific visualization*

The main multipurpose scientific visualization tool used since the beginning in the Kyb3 environment has been ParaView [9]. One of the main ongoing research directions in the Department of Mechanics and Applied Mathematics of the Institute of Cybernetics at TUT is related to micro-structured materials. One of the investigated materials is Steel Fibres Reinforced Concrete (SFRC) [10] [11]. The understanding of the influence of the orientation distribution of the fibres on the material properties is of crucial importance for safe usage of this construction material. 3D visualization is an important tool to achieve this goal.

Among the steps taken in the analysis was scanning cylinder samples of SFRC taken from full-scale floor slabs through a Computer Tomography. The volumetric data was filtered, segmented and skeletonized and afterwards the orientation of each object was analysed [10]. It was necessary to visually inspect the correctness of the analysis, especially of the correct separation of the touching fibres, for which a new algorithm had been developed. This inspection could not be performed on a 2D computer screen, due to the large number of thin objects. Therefore this was performed using stereoscopic visualization, using ParaView. In ParaView visual thresholding of the volumetric data has been performed, in order to isolate the fibres from the concrete and gravel in the 3D visualization (Fig. 5a).

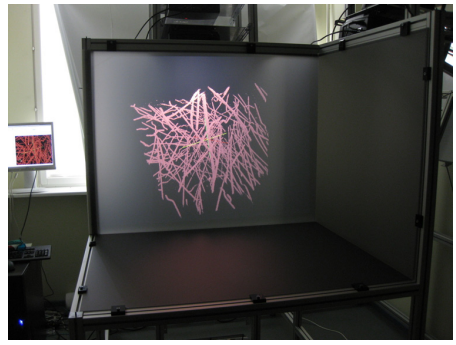

Fig. 5 Steel fibres reinforced concrete volumetric 3D Visualization

While the visualization was possible with the Planar 3D Passive Polarized Monitor, there was still room for improvement.

We therefore chose ParaView, the only one among the software used in our lab being able to support a multi-screen tracked environment to visualize the fibres data on the Kyb3. Using our self written VRPN server for the head-tracking (Section 2.4) jointly with the VRUI Device Daemon for the Wiimote wand interaction (Section 2.4), we configured the interaction environment, while the screen positions and sizes could be configured directly from ParaView internal configuration files. The resulting level of visual understanding of the data was for all the test users much higher than the expectations. The size of the screens, joined with the 3D

depth perception and a natural way of interaction with the data (scaling, moving and rotation) given by the wand, fully satisfied the need of the user for a deeper interaction with the dataset. Here the system also proved its use to disseminate research results: the thresholded volume images have been shown to civil engineers, both from a university and a company, to demonstrate the problem of fibre alignment (or non-alignment). The possibility to "stick one's head into the data" helped a lot in the explanation and understanding. Furthermore the visualization of fibre orientation distribution using tensor glyphs [12] [13] is under development. Ongoing research employs ParaView to visualize the simulation particle-laden flows performed with OpenFOAM. Of special interest are Computational Fluid Dynamics simulations of fibre distribution and alignment for different concrete casting methods.

In addition to the fibre-oriented visualization issues, several other software packages have been set up and are being investigated, to widen the range of scientific fields whose visualization might be managed through the Kyb3. VMD [14] has been installed and configured for molecule and molecular dynamics visualization; jReality [15] for mathematical surface visualization and a whole suite of software developed on VRUI for an even wider choice of datasets (e.g. LiDAR data, mesh objects, volumetric data).

### *3.2. Development*

The second and more open-ended target was, as we said, the starting and pursuit of research focused on Virtual Reality techniques improvements and the development of software made and optimized to run on multiscreen VE. This research is currently branched in two different directions.

The first one, closely related to the scientific visualization issues described in Section 3.1, is aiming at the development of VE-based software able to fulfil some specific needs of the researchers at the Institute of Cybernetics. Employing OpenFOAM for the simulation of the flow of concrete together with the transport of cylindrical particles, we are currently designing and developing a visualization tool for VE, based on VRUI, for the visualization of the fluid flow together with the orientation distribution of the fibres by tensor glyphs. Therefore, the software under development will not only be dealing with the animated visualization of the CFD simulation, but also simultaneously extracting data from the simulations and performing a quantitative analysis on it, allowing therefore also the visualization of the tensor glyphs.

The second direction taken by our research team deals with developments related to VR itself, its techniques and methods and possible improvements. Currently, several topics have been proposed as BSc and MSc theses with the intent to create for the first time a generation of VR researchers in Estonia and to find students with an interest in the subject. The main development effort is being aimed towards the investigations on a low-cost and marker-free user-tracking system based on consumer-hardware, e.g., using multiple MS Kinect cameras.

## 4. Concluding remarks

With the Kyb3 we believe we have managed to obtain the results we were aiming for. That is, with a really low budget compared to the cost of traditional semi-immersive VE, we built a system that while fulfilling its own purpose as a scientific visualization tool, also allowed the Institute of Cybernetics at Tallinn University of Technology to start a complete new field of research, with several possibilities both as an autonomous or as a cross-disciplinary one.

The system, in addition to a really low price/performance ratio, has also been tailored to a very small space, obtainable only through a special self-made frame and the use of short-throw projectors and mirrors.

All in all the above mentioned results exactly fit with the objectives we established two years ago, and the first step of the creation of a 3D Scientific Visualization and Virtual Reality group is therefore complete, with the way now open for many more related further research topics.

**Acknowledgements**

Compiled with the assistance of the Tiger University Program of the Estonian Information Technology Foundation (VisPar project, EITSA grants 10-03-00-24, 12-03-00-11, 13030009 and 13030031). This research was supported by the European Union through the European Regional Development Fund, in particular through funding for the "Centre for Nonlinear Studies" as an Estonian national centre of excellence. This research was also supported by the European Social Fund's Doctoral Studies and Internationalisation Programme DoRa 4 (through a long time stipend for Emiliano Pastorelli).

**References**

[1] Runnel P, Pruulmann-Vengerfeldt P, Reinsalu K. The Estonian Tiger Leap from Post-Communism to the Information Society: From Policy to Practice. *Journal of Baltic Studies* 2009; **40**:29-51.
[2] Cruz-Neira C, J.Sanding D, DeFanti TA. Surround-screen projection-based virtual reality: the design and implementation of the CAVE in: Proceedings of the 20th annual conference on Computer graphics and interactive techniques *SIGGRAPH '93*, 1993, pp. 135-142.
[3] Gutierrez M, Vexo F, Thalmann, D. *Stepping into Virtual Reality.* Springer, 2008
[4] Schlechtweg S. miniCAVE: a fully immersive display system using consumer hardware, in: Proceedings of the 14th Eurographics conference on Virtual Environments EGVE'08, 2008, pp. 73-80.
[5] Arthur K, Preston T, II RT., Jr. FB, Whitton M, Wright W. Designing and building the PIT : A head tracked stereo workspace for two users, in: Proceedings of 2nd Int. Immersive Projection Technology Workshop, 1998.
[6] Zachmann G. Distortion Correction of Magnetic Fields for Position Tracking, in: Proceedings of the 1997 Conference on Computer Graphics International CGI '97, 1997, pp 2103-220.
[7] Taylor II, Russell M, Hudson TC, Seeger A, Weber H, Juliano J, Helser, AT. VRPN: A Device-Independent, Network-Transparent VR Peripheral System, in Proceedings of the ACM symposium on Virtual reality software and technology VRST '01, 2001, pp. 55-61.
[8] Kreylos O. Environment-Independent VR Development, in G. Bebis et al. (Eds.), Advances in Visual Computing. Springer Berlin Heidelberg, 2008. p. 901-912.
[9] Henderson A. ParaView Guide, A Parallel Visualization Application. Kitware, 2007.
[10] Suuronen J-P, Kallonen A, Eik M, Puttonen J, Serimaa R, Herrmann, H. Analysis of short fibres orientation in Steel Fibre Reinforced Concrete (SFRC) using X-ray tomography. *Journal of Materials Science* 2013; **48**:1358-1367.
[11] Eik M, Herrmann, H. Raytraced Images for Testing the Reconstruction of Fibre Orientation Distributions. *Proceedings of the Estonian Academy of Sciences* 2012; **61**:128-136.
[12] Kindlmann G. Superquadric Tensor Glyphs, in: Proceedings of IEEE TVCG/EG Symposium on Visualization, 2004, pp. 147-154.
[13] Schultz T, Kindlmann G. Superquadric Glyphs for Symmetric Second-Order Tensors. *IEEE Trans. on Visualization and Computer Graphics* 2010; **16**:1595-1604.
[14] Humphrey W, Dalke A, Schulten K. VMD -- Visual Molecular Dyanamics. *Journal of Molecular Graphics* 1996; 14:33-38.
[15] Weißmann S, Gunn C, Brinkmann P, Hoffmann T, Pinkall, U. jReality: a java library for real-time interactive 3D graphics, in: Proceedings of the 17th ACM international conference on Multimedia MM '09, 2009, pp. 927-928.

PUBLICATION II

Pastorelli E., Herrmann H.
**Virtual Reality Visualization for Short Fibre Orientation Analysis.**
*Proceedings of the 14th Biennial Baltic Electronics Conference (BEC 2014)*, pp. 201-204, Tallinn, Estonia, Oct. 2014

# Virtual Reality Visualization for Short Fibre Orientation Analysis

Emiliano Pastorelli and Heiko Herrmann
Institute of Cybernetics at Tallinn University of Technology Akadeemia tee 21
12618 Tallinn, Estonia
Email: pastorelli@cens.ioc.ee, hh@cens.ioc.ee

***Abstract*—The paper investigates the beneficial contribution of visual feedback in the development of an algorithm for the automatized analysis of fibre orientations in short fibre reinforced composites. Of special interest was steel fibre reinforced concrete (SFRC), a multi-disciplinary research area involving material sciences, physics and civil engineering. More in detail, this paper explains how scientific visualization techniques, employed on a Virtual Reality environment, contribute to the understanding of the SFRC properties, both for research and educational aims. Furthermore, the analysis algorithm to obtain fibre orientation distributions from noisy tomography scans is presented.**

## I. Introduction

In the last years, with the increasing availability of cost-accessible hardware components, several researchers all over the world started relying heavily on scientific visualization techniques for the validation and understanding of numerical results. With the growing size and complexity of simulations, the visual aspects of the scientific investigation are becoming, in several fields, a priceless asset for the research.
Our interest in Virtual Reality Scientific Visualization arose from research on complex materials like liquid crystals [1]–[4] and short fibre reinforced building materials [5]–[7]. The main difficulty with 2D visualization and typical "3D"-ish visualization on 2D computer screens is, that the depth impression is very difficult to achieve with thin and elongated objects like fibres. Some 3D impression is possible, if the scene is rotated, but as soon as the rotation stops, the depth impression is lost. A solution is provided by use of 3D stereoscopic screens, like the one used in our lab since 2010. However, the wish and need for a larger system which provided user tracking soon became apparent.

### A. The VR visualization system "Kyb3"

Designed and built in the beginning of 2013 at the Institute of Cybernetics at TUT, the Kyb3 [8] is the first Virtual Reality Environment (VE) ever build in Estonia.
With a visualization surface of approximately $2.6\mathrm{m}^2$, distributed on three joined rear-projection screens, the Kyb3 makes use of passive circular polarization filters and glasses to generate a realistic 3-dimensional feeling of the displayed 3D scene.
The system keeps track of the position and rotation of the user's head through a sensor connected to an electromagnetic tracking system. The scene adjusts itself to the user, constantly recalculating the correct perspective and point of view, to grant a complete immersive feeling. The interaction is managed through two tracked wands, with 8 buttons and an analogic joystick each, and optionally a tracked data-glove, to grant the widest possible choice of control configurations. Built to be an affordable VE aimed at a scientific visualization use, the Kyb3 has also been designed to present all the features that characterize the room-sized high-cost CAVE-like systems [9]. The reason for that choice was to have not only a tool aimed at a specific application, but a prototyping system on which to undertake the first steps to start a field of research in IT still completely new for Estonia.
The Kyb3 VE was designed with two main constraints in mind: space and budget. The idea was to build a VR system that, differently from the big CAVE-like ones, could fit in a normal room (while the traditional ones usually need an approximate area of 9x9 meters) and could be affordable for a normal research institution (while for CAVE-like systems usually the prices range from about 200.000 € to several million Euro). The full cost of the Kyb3 was kept below 40.000 €. This choice influenced every single decision in the design of the system even though, despite the budget limitations, the worksation running the Kyb3 has two 8-core processors, 64GB of RAM and 4 high-end NVIDIA QUADRO 4000 graphic cards, making it a powerful machine on which to run simulations. More complete details on the design and features of Kyb3 can be found in [8].

### B. Analysis of short fibre orientations

SFRC is a relatively new construction material, introduced to substitute in certain situations the traditional steel bars reinforced concrete. Compared to the traditional one, it uses short steel fibres (of varying lengths) mixed in the concrete and then cast together with it.
The properties and performance of SFRC depend on several factors such as shape, aspect ratio, size, surface characteristics and, as in all the fibre composite materials, strongly on the orientation of the fibres within the matrix. The characteristics of the composite tend to be often heterogeneous and anisotropic, due to the non-uniform and non-isotropic distribution of the fibres within the matrix. Among the most modern techniques to analyze the properties of the SFRC [6] is the X-ray computed microtomography [5], [10] of concrete samples extracted from large structural members. The reconstructed voxel image of the volume (Fig. 2), allows then a wide choice of possibilities on

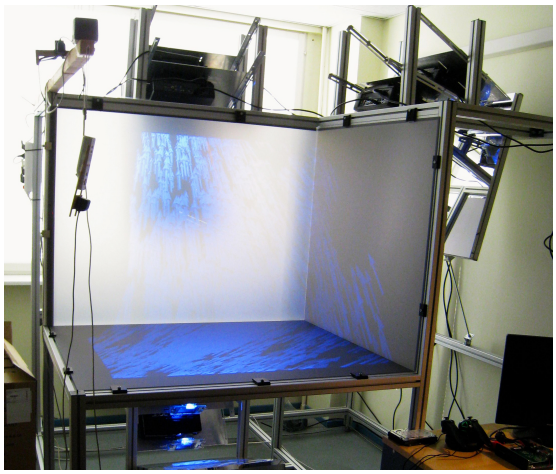

Fig. 1. The Kyb3 virtual environment

how to proceed with the analysis. Each of the analyzed sample cylinders was scanned in three subsets (top, middle, bottom), each of them represented by a regular grid of approximately $800 \times 800 \times 600$ elements, that means almost 400 millions grayscale voxels describing the absorption values in the sub-volume's dataset.
Extracting information out of this type of dataset can be performed through several different paths, but with the size of the data, it appears obvious that some sort of visual feedback is necessary to validate the correctness of the obtained information.
Throughout the whole data analysis procedure, it might happen, in several parts of the development, to come across parts of the algorithm that seem to perform correctly but whose results are instead wrong. A simple textual printout of the results, was often not sufficient to determine the correctness of the process.

Due to the complex structure of SFRC and the differences, its use requires in the construction process from the traditional techniques, the visualization of the theoretical results provides also an additional value in the education of construction company managers and workers. To obtain optimal distribution and alignments of the fibres, the casting process need to be undertaken with specific approaches, and specially when dealing with non-academic people, a 3-dimensional visualization, representing a tangible example of real-world behavior of the material, can be in several occasions worth much more than words and numbers.

## II. A new Short Fibre Orientation Analysis Algorithm

The target was to implement/develop an algorithm, which can automatically detect the fibre orientations with as little user-interaction as possible. The requirement of non-interactivity is derived from the wish to minimize user errors. Typical methods, like skeletonization, require a skilled user, and respectively training of the staff. To enable a wide-spread use of the software not only in research and development, but also in quality control, there should be as minimal as possible user skills necessary.
The idea was to implement an analysis similar to [11], based on the hessian analysis. In this approach, the direction of the smallest change in gray-level is determined from the eigenvectors and eigenvalues of the hessian matrix. This direction should point in the direction of the fibre axis. However, the algorithm in [11] was derived for dense fibre suspensions, while in SFRC the fibre content is usually around three vol.-%, and the large contribution of the isotropic matrix —together with a noisy dataset and a strong cupping effect— spoils the analysis.
The filtering process was fundamental for the success of the analysis of the SFRC sample. By employing the 3-dimensional Frangi vesselness filter approach [12], usually employed in detecting blood vessels in medical tomographies, we identified and highlighted tubular shaped structures in the dataset. This way, we compensated the cupping effect, a typical problem in tomography that manifests itself when the low frequencies of the X-ray are absorbed earlier, therefore causing an intensity drop of the gray values in the internal parts of the scanned objects, hampering a uniform traditional thresholding of the dataset, Fig. 2. The filtering also removed noise areas that had the same gray values as the fibres from the dataset.
The filtering was applied to the dataset by using the Insight Segmentation and Registration Toolkit library (ITK) [13], while the rest of the algorithm is self-implemented in C++:

Phase 1 : Filtering
load nhdr+raw volume
apply itk::HessianRecursiveGaussianImageFilter
apply itk::Hessian3DToVesselnessMeasureImageFilter
apply itk::MedianImageFilter
apply itk::BinaryThresholdImageFilter
apply itk::OpeningByReconstructionImageFilter
apply itk::BinaryImageToShapeLabelMapFilter to extract separate fibres and save the labels
apply itk::SmoothingRecursiveGaussianImageFilter

Phase 2 : Analysis
**for all** voxel $\in$ label mask **do**
  calculate the Hessian matrix for each voxel belonging to a fibre and save the eigenvector corresponding to the smallest eigenvalue (by absolute value)
**end for**
**for all** region $\in$ labeled fibres regions **do**
  Convert all the vector to polar coordinates and cluster them in a $90 \times 360$ matrix
  Detect the highest peak for each region, convert back to cartesian coordinates and save to VTK file
**end for**

After loading the original raw volume obtained from the scan, we proceed, as mentioned above, first of all by filtering the data in order to extract the features of interest. By applying the Hessian 3D Vesselness Measure filter we highlight the cylindrical structures in the dataset and exclude the background noise. By means of a Median filter and a Binary Threshold, we then remove almost completely all the remaining noise, and keep in the filtered dataset only the elements representing fibres. At this point, we branch the data into two different processes, that will be both necessary for the orientation

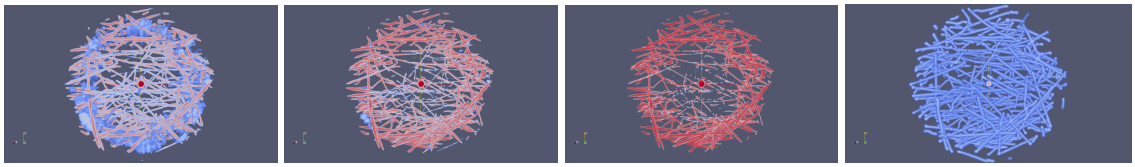

(a) (b) (c) (d)

Fig. 2. An SFRC tomography image seen from top with different thresholds, the "cupping effect" (beam hardening) is visible (a),(b),(c). (d) shows how the Frangi algorithm solved the problem.

analysis. On the first of them we apply a Smoothing Recursive Gaussian filter to the binary data and we save to file the obtained dataset, on the other one we apply a Binary to Shape Label Map in order to identify each separate non-connected region (fibre) and label the voxel composing it with different values. We load the smoothed data on the second part of the software and we perform the real orientation analysis. For each voxel in the volume we calculate the Hesse matrix on the gray values and we find the eigenvector of the smallest (according to amount) eigenvalue of the Hesse matrix. Finally, we average the orientation vectors of the whole volume and we calculate the overall orientation tensor.

Due to some unexpected results of the main C++ software, an additional prototype was implemented in GNU Octave [14], [15] using the image toolbox [16]. In our case several functions from [17] have been used. However, both independent implementations give the same results (up to rounding errors).

As the results of the algorithm seemed to be correct but were still different from the ones obtained by the skeletonization algorithms [5], we undertook a detailed visual investigation of the dataset by comparing the results for smaller subvolumes and for self-built single fibre test datasets. The investigation revealed that the voxel by voxel analysis was indeed correct, but that the presence of the small hook structures in each fibre was influencing the results enough to cauce a noticeable difference in the results, as the orientation describing the main shaft of each fibre was averaged with the orientation of the vectors describing the hooks. Even though this unexpected result revealed further properties related to the uncracked state of SFRC otherwise not shown by the skeletonization approach, we developed the algorithm further to also extract the fibre orientation through an analysis of each separate fibre (by using the labels extracted in the first part of the algorithm). Fig. 3 shows a fibre orientation peak in its polar coordinates representation (Theta on the $Z$-axis, Phi on the $X$-$Y$-plane).

The new part of the algorithm works as follows: For each fibre the local orientation vectors of each voxel are converted to spherical coordinates, after, they are grouped into 5 degree bins. The highest peak is determined and converted back into cartesian coordinates. This peak value describes the orientation of the shaft of each fibre. For each fibre the orientation and the position, determined by the region centroid, are saved. These can be visualized together with the local orientation vectors, see Fig. 5.

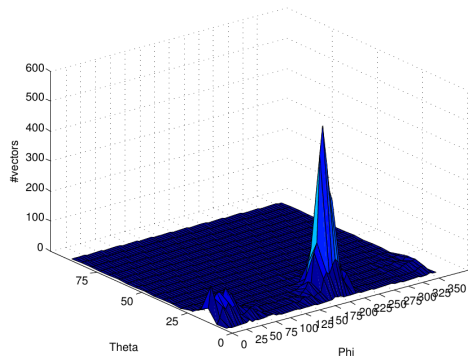


Fig. 3. Orientation peaks for a single fibre region; Theta is the inclination angle with respect to the $Z$-axis, Phi is the $X$-$Y$-in-plane angle.

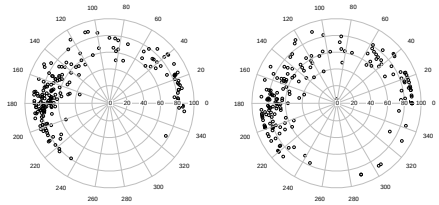

(a) (b)

Fig. 4. (a) Scatterplot of test volume orientation distribution using skeletonization. (b) Scatterplot of test volume orientation distribution using the algorithm described in this paper. Radius: Theta, Circumference: Phi

## III. Performances and correctness of the algorithm

Although some further improvements of the algorithm and optimizations of the software are being currently still developed, the first results given where extremely satisfactory in terms of performances and correctness of the results. In Fig. 4 it is possible to see the results of the algorithm (Fig. 4(b)) compared to those obtained with the skeletonization approach from [5], [10] (Fig. 4(a)). Despite some minor differences, the two orientation distribution scatterplots show an almost identical pattern. Regarding the performances, the algorithm is producing the results in approximately one third of the skeletonization method, that means two hours less. Further optimization will probably improve the computation speed.

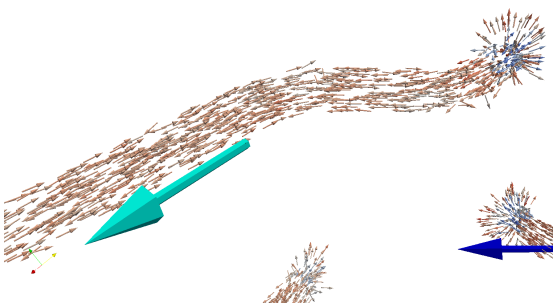

Fig. 5. Voxel orientation vectors (brown) and main fibre orientation vectors (colored)

## IV. Using the VR system for feedback to test the performance of the algorithm

A crucial point was the assessment of the filtering of the image, here the 3D visualization proved to be invaluable to distinguish artefacts from fibres and to investigate how well touching fibres had been separated. The successful reconstruction of the Frangi vesselness filter features with different values and the validation of the labeling mask results were also only possible through a visual inspection of partial and final results (Fig. 5). Furthermore, the visualization of the results, displayed unexpected patterns in the dataset. An example is a completely different behavior in the eigenvalues corresponding to the voxel vector in the real ends of the fiber or in the points in which the fiber is cut. That sort of patterns would have probably never emerged from the simple analysis of the values, but thanks to the visualization of the analysis, our group will further investigate them, in order to write even more specialized information extraction algorithms.

## V. Conclusion

Throughout the whole development process, the visualization feedback of partial and final results proved to be a unique, fundamental asset for the final successful results. The constant inspection of the data through the Kyb3 displays (using ParaView) allowed to locate and correct conceptual and implementation faults that showed up while applying techniques usually used in medical image processing to SFRC. The successful bond between a natural system interaction and a wide choice of visualization options throughout the process proved that the expectation we had when we built the Kyb3 VR were indeed correct. The process will now continue by following the same guideline and by expanding the visualization system with further price-accessibile components and by further developing the SFRC analysis software to extract and visualize an even wider range of features.

## Acknowledgment

The paper was compiled with the assistance of the Tiger University Program of the Estonian Information Technology Foundation (VisPar system, EITSA/HITSA Tiigriülikool grants 10-03-00-24, 12-03-00-11, 13030009).
This research was supported by the European Union through the European Regional Development Fund, in particular through funding for the "Centre for Nonlinear Studies" as an Estonian national centre of excellence. This research was also supported by the European Social Fund's Doctoral Studies and Internationalisation Programme DoRa 4 (through a long time stipend for E.P.). Further, the IT Akadeemia 2013/2014 grant for E.P.'s studies is gratefully acknowledged.

## References

[1] O. Lehmann, "Über fliessende Krystalle," *Zeitschrift für Physikalische Chemie*, vol. 4, pp. 462–472, 1889.

[2] ——, *Flüssige Krystalle*. Leipzig: Wilhelm Engelmann, 1904.

[3] W. Muschik, C. Papenfuss, and H. Ehrentraut, "Mesoscopic theory of liquid crystals," *Journal of Non-Equilibrium Thermodynamics*, vol. 29, no. 1, pp. 75–106, 2004.

[4] H. Herrmann and J. Engelbrecht, "Comments on mesoscopic continuum physics: Evolution equation for the distribution function and open questions," *Proceedings of the Estonian Academy of Sciences*, vol. 61, no. 1, pp. 71–74, Jan. 2012.

[5] J.-P. Suuronen, A. Kallonen, M. Eik, J. Puttonen, R. Serimaa, and H. Herrmann, "Analysis of short fibres orientation in steel fibre reinforced concrete (SFRC) using x-ray tomography," *Journal of Materials Science*, vol. 48, no. 3, pp. 1358–1367, Feb. 2013.

[6] M. Eik, K. Lõhmus, M. Tigasson, M. Listak, J. Puttonen, and H. Herrmann, "DC-conductivity testing combined with photometry for measuring fibre orientations in SFRC," *Journal of Materials Science*, vol. 48, no. 10, pp. 3745–3759, May 2013.

[7] H. Herrmann and M. Eik, "Some comments on the theory of short fibre reinforced material," *Proceedings of the Estonian Academy of Sciences*, vol. 60, no. 3, pp. 179–183, Jul. 2011.

[8] E. Pastorelli and H. Herrmann, "A small-scale, low-budget semi-immersive virtual environment for scientific visualization and research," *Procedia Computer Science*, vol. 25, no. iii–iv, pp. 14–22, Sep. 2013.

[9] C. Cruz-Neira, D. J. Sandin, and T. A. DeFanti, "Surround-screen projection-based virtual reality: The design and implementation of the CAVE," in *Proceedings of the 20th Annual Conference on Computer Graphics and Interactive Techniques*, ser. SIGGRAPH '93. New York, NY, USA: ACM, 1993, pp. 135–142. [Online]. Available: http://doi.acm.org/10.1145/166117.166134

[10] J. Schnell, K. Schladitz, and F. Schuler, "Richtungsanalyse von Fasern in Betonen auf Basis der Computer-Tomographie," *Beton- und Stahlbetonbau*, vol. 105, no. 2, pp. 72–77, 2010. [Online]. Available: http://dx.doi.org/10.1002/best.200900055

[11] C. Redenbach, A. Rack, K. Schladitz, O. Wirjadic, and M. Godehardt, "Beyond imaging: on the quantitative analysis of tomographic volume data," *International Journal of Materials Research*, vol. 2012, no. 2, pp. 217–227, 2012.

[12] Y. Sato, S. Nakajima, H. Atsumi, T. Koller, G. Gerig, S. Yoshida, and R. Kikinis, "3d multi-scale line filter for segmentation and visualization of curvilinear structures in medical images," in *CVRMed-MRCAS'97*, ser. Lecture Notes in Computer Science, J. Troccaz, E. Grimson, and R. Mösges, Eds. Springer Berlin Heidelberg, 1997, vol. 1205, pp. 213–222. [Online]. Available: http://dx.doi.org/10.1007/BFb0029240

[13] T. S. Yoo, M. J. Ackerman, W. E. Lorensen, W. Schroeder, V. Chalana, S. Aylward, D. Metaxas, and R. Whitaker, "Engineering and algorithm design for an image processing api: A technical report on itk - the insight toolkit," in *Proc. of Medicine Meets Virtual Reality*, J. Westwood, Ed. Amsterdam: IOS Press, 01 2002, pp. 586–592.

[14] "GNU Octave." [Online]. Available: https://www.gnu.org/software/octave/

[15] J. W. Eaton, D. Bateman, and S. Hauberg, *GNU Octave Manual Version 3*. Network Theory Limited, 2008.

[16] "Octave-forge image package." [Online]. Available: http://octave.sourceforge.net/image/

[17] D.-J. Kroon, "Hessian based Frangi vesselness filter," Mar. 2010. [Online]. Available: http://www.mathworks.com/matlabcentral/fileexchange/24409-hessian-based-frangi-vesselness-filter

PUBLICATION III

Herrmann H., Padilla M., Pastorelli E.

**A.C.T.I.V.E.: A scalable superellipsoid-based CFD visualization for virtual and desktop environments.**

*Eurographics Proceedings of EuroVR 2014 : Conference and Exhibition of the European Association of Virtual and Augmented Reality, Bremen*, pp. 1-4, Bremen, Germany, Dec. 2014

Conference and Exhibition of the European Association of Virtual and Augmented Reality (2014)
G. Zachmann, J. Perret, and A. Amditis (Editors)

# A.C.T.I.V.E.: A scalable superellipsoid-based CFD visualization for virtual and desktop environments

H. Herrmann[1] and M. Padilla[2] and E. Pastorelli[1]

[1]Institute of Cybernetics at Tallinn University of Technology, Estonia
[2]Institut für Mathematik, TU Berlin, Germany

**Abstract**

*The paper presents a flexible software (A.C.T.I.V.E.) able to visualize the superellipsoidal glyphs describing the orientation of short fibres during the dynamic process of casting Short Fibre Reinforced Composite in a container. The software is designed to run on the VRUI framework and it features an optional face-tracking to grant a more natural interaction also on standard non-3D displays. Due to its flexibility it can be used on a wide range of environments, from desktop computer to multi-screen CAVE-like systems.*

Categories and Subject Descriptors (according to ACM CCS): I.3.3 [Computer Graphics]: Picture/Image Generation—Line and curve generation

## 1. Introduction

Virtual Reality Environments (VE) are nowadays more and more a fact, not only for a niche of researchers and rich private institutions, but also for more limited budgets and for the public. What no less than ten years ago could have only been achieved with a budget of hundreds of thousands of Euro, is now available for a small fraction of that price. With consumer HMD and 3D Screens getting lower in prices and available in a wider offer, simple personal VEs are now a reality often only slightly more expensive than common desktop computer. Obvious and unavoidable differences in size and performances between small VEs and the large ones exist, but the gap between them is slowly being filled by the advancements in hardware technologies.

### 1.1. Our VRE

At the visualization group of the Institute of Cybernetics of Tallinn, we began our way towards Virtual Reality in 2010 with a graphic workstation endowed with a 3D Planar Display (linear polarization) to explore 3-dimensional data, to continue in 2012/2013 with the design of construction of our CAVE-like [CNSD*92] system, the Kyb3 Fig. 1 [PH13].

Conceived to abide to strict constraints of budget and space, with an occupied space of only 2.35m × 2.04m × 1.77m, the Kyb3 features three 1.1m × 0.8m screens and a full magnetic tracking of the user position and interaction, for a total cost of approximately € 35000. The Kyb3 is currently used at the Institute of Cybernetics for a wide of scientific applications.

### 1.2. Short Fibre Reinforced Composites and Tensor Visualization

Short fibre reinforced composites are very popular in many application areas from glass fibre plastics to steel fibre reinforced concrete (SFRC) in civil engineering. The mechanical properties of these composites strongly depend on the distribution of the fibres, i.e. they depend on both the spatial and *orientational* distribution [HEBP14, SKE*13, PH14]. Therefore simulations of the production process, e.g. injection molding, are necessary. These simulations involve the CFD simulation of the matrix material (plastic, concrete, metal, etc) and the fibres, which can be either included as individual particles or by use of a tensorial equation. The orientation distribution of the fibres can be characterized by orientation tensors or alignment tensors (the traceless part of the orientation tensors).

Therefore the visualization of the orientation tensors is important for the analysis of the computer simulations. The second order tensors can be visualized using superquadric or superellipsoid glyphs [Kin04, JM06, SK10]. To be able to visualize a large number of tensors in a VRE, the visualization of the parametric glyph surfaces needs to be fast, this is

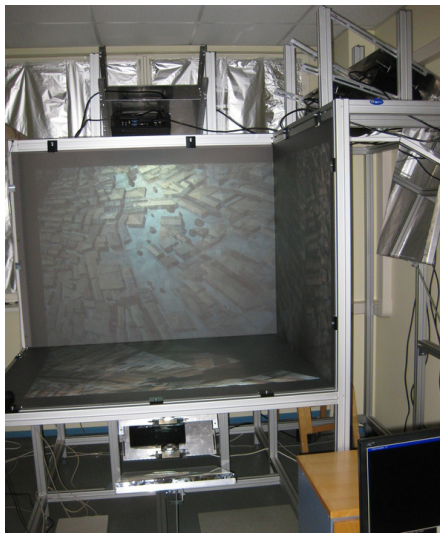

**Figure 1:** *The Kyb3 VRE at IoC*

a problem of several of the available visualization tools. A reason for this can be, that the shape of the glyph, and the vertices to display, is calculated on-the-fly.

## 2. A.C.T.I.V.E.: Anisotropic Composite Tensor Interactive Visualization Environment

Our goal for this project was to visualize datasets of tensor fields for visual inspection and analysis, while making the process reproducible on many machines with different Virtual Reality set-ups such as different displays and trackers. Additionally we wanted to extend the possibilities of experiencing (in a limited way), a partial data immersivity on any Desktop setup, by creating a 3D-tracker that could work on many common desktop set-ups. In the end we wanted a cost effective visualisation with a virtual experience that could run on a wide range of system, such as CAVE-like environments, 3D monitors, HMD or regular displays (the latter with anaglyphic stereo). As one of the main research fields involving the visualization of data and results through the Kyb3 VE, is the study of Micro-structured composite materials and their physical properties [PH14], the data used for the visualization is obtained from an OpenFOAM simulation [Fig. 2]. representing the casting of SFRC (steel fibre reinforced concrete) into a box-shaped container. The fibres themselves are not represented as single elements in the simulation, but their orientation equation is coupled with the fluid rheology. The simulation allows us to obtain, for each time step, a tensor field describing the properties of the fibres orientation in the concrete.

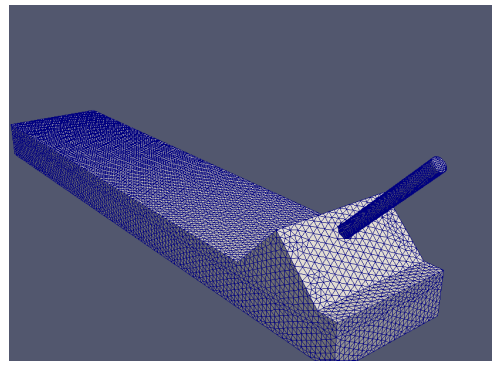

**Figure 2:** *The OpenFOAM SFRC casting setup (including the pipe through which the concrete flows in the container)*

Each tensor is used to calculate the shape metrics from which the parametrization of the corresponding superellipsoid glyph is determined. OpenGL is eventually used to draw the parametric surfaces of the glyphs in the 3D space, Fig. 3. Due to the high amount of small Glyphs with different sizes and shapes visualized for each time step of the simulation, it becomes increasingly hard to see their 3D relative positions towards each other on a static 2D screen. As a solution, we ported our OpenGL code to the VRUI (Virtual Reality User Interface) [**?**] framework, mainly in order to take advantage of its ability to hide the characteristics of the system on which it will be executed from the developer. User input and tracking, 3D stereoscopy and scene manipulation are also directly managed by VRUI . Additionally, in its last release, VRUI also embeds the possibility to be used with HMD as well, for example with the Oculus Rift.

### 2.1. Superellipsoidal glyphs

Superellipsoids, whose definition is often ambiguously mixed with that of superquadrics, are a group of solids whose domain partly intersect the domain of the superquadrics but also extends towards a range of different shapes. Although also built through the use of two parameters (one defining the exponent of the super-ellipses representing their horizontal section and the second the exponent of the ones constituting their vertical sections) as for the superquadrics, the shapes obtained in the extremes of the domain range of superellipsoids, tend to be more easily identifiable, less prone to visual ambiguities and to allow a smoother and recognizable transition among shapes [JM06]. Due to this properties, each glyph can be more expressive about the properties of the related Tensor at the given location. To speed up the computation, since the datasets involves the plotting of several thousand glyphs for each timeframe of the simulation, we created a discrete set of pre-

computed super ellipsoid vertices with a range of parameters fine enough for the human eye not to notice. From the OpenFOAM simulation data we compute the positions, orientations and parameters of the glyph once and store them in separate files.

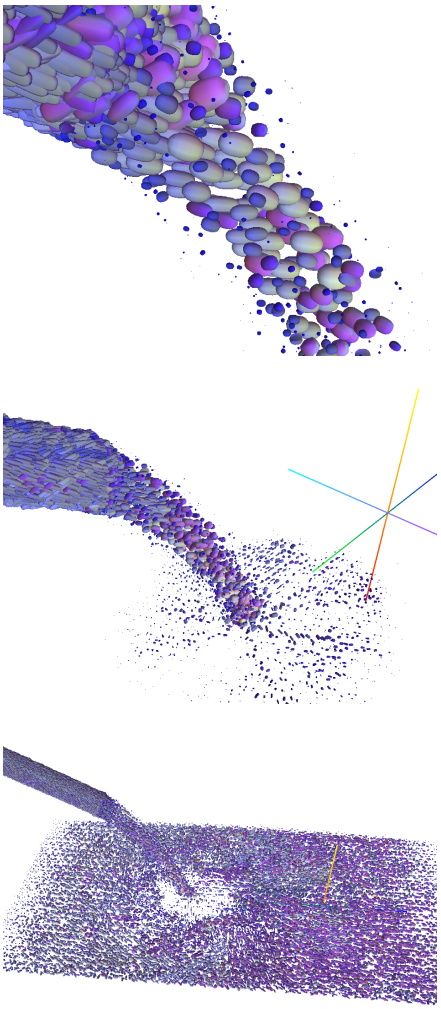

**Figure 3:** *A.C.T.I.V.E. Tensor Glyphs Visualization*

### 2.2. User tracking on desktop environments

The A.C.T.I.V.E. software can be used on anything from a full-size CAVE-like environment over Oculus Rift, over desktop 3D monitors down to standard 2D monitors. However, the degree of immersivity is obviously reduced. On 2D screens it is still possible to obtain a 3D impression, if the scene is rotated or adjusted to changes is the user position. However, the adjustment to the changes is user position require the user to be tracked.

The traditional stereoscopic effect of showing the user two different images, one for each eye, is usually only effective for a single user set in a specified location. To produce the best possible 3-dimensional effect, we need the camera in the scene to be in sync with every yet so slightly movement of the users head. This implies at least one display per user, but allows him to look beyond the edges of the usually static viewing volume. By tweaking the view frustum with the input of a head tracker we can create the illusion of looking through a window. To reach a true virtual reality we will always need both: stereoscopic views and a tracker for the user's eyes. While this doesn't represent an issue on our Kyb3 system, where the user head position and rotation is constantly tracked by electromagnetic sensors, the same feature was not available for our 3D planar display and other normal desktop posts. Luckily, the fact that a human head can never be held perfectly still came to our benefit. Every small head movement results indeed in small changes to our perspective of our surrounding; causing closer objects to shift farther than further once. We decided to implement this subtle yet important effect to the common desktop experience by tracking the position of the face of the user in front of the display.

### 2.3. Camera Facetracking

Tracking hardware is usually quite expensive and not yet widespread enough. Therefore, for the convenience of all users we decided to create a tracker that only relies on a device easily accessible for every laptop and desktop computer : a front facing camera parallel to the display. This means that most users would probably not require any additional hardware to benefit of this feature of our software. To implement the whole face-tracking component, we relied on the OpenCV library features [Bra00] and its including features detections in images, by continuously reading the pixel location and pixel size of the biggest face found in the camera. With knowledge of the pixel resolutions, the field of view angle of the camera and approximate height of the face we can estimate the absolute position of the eyes in the face relative to the camera itself, Fig. 4.

The tracker has been implemented in C++ and is endowed with configurable smoothers for the raw pixel data and the final tracking data. If the tracking was successful in the last frame, we also predict the size of the face and focus on the area of the image where we expect the face to be next. All of these features result in a smooth tracking experience that is reliable and fast when used in a common desktop environment. The limitations that this approach holds are that

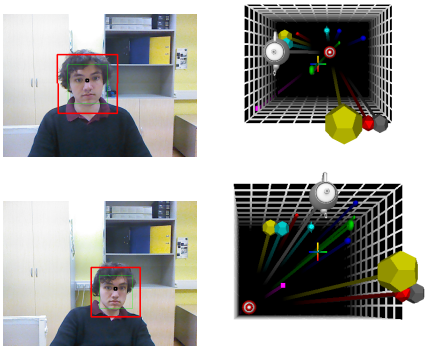

**Figure 4:** *Face tracking*

it only tracks 3D positions and not rotations and that the facial detection is limited to frontal and profile faces. However, the detection protocols are easily swappable in the configuration file and can therefore be easily updated when better ones become available [VJ01]. The framerate is kept at 60 fps, which is essential since a high frame rate is always necessary to have a comfortable tracking experience. It is not meant to track a user walking around a room or complex motions, the user has to stay in the camera viewing volume and show his face to the camera without rotating or his head too far.

Finally, in order to grant the face-tracking component the maximum flexibility of use, we created a VRPN (Virtual-Reality Peripheral Network) [THS*01] server using our face-tracking features for the convenience to easily connect it to any client that reads VRPN tracker inputs. VRPN is a very helpful tool to connect multiple tracker, analog and button input devices with client software while maintaining a simple interface for clients and being available on windows and linux. VRUI, that we used as a framework for our tensor field visualisation, can launch a device daemon specifically for any VRPN input.

## Conclusions

The A.C.T.I.V.E software represents one of our several subprojects aimed towards building a complete research environment for Micro-structured composite materials analysis and visualization. Other software elements composing the full final system [PH14] are being developed or are already functional, and all of them are meant for flexibility and portability among different types of platforms.

## Acknowledgments.

The paper was compiled with the assistance of the Tiger University Program of the Estonian Information Technology Foundation (VisPar system, EITSA/HITSA Tiigriülikool grants 10-03-00-24, 12-03-00-11, 13030009).
This research was supported by the European Union through the European Regional Development Fund, in particular through funding for the "Centre for Nonlinear Studies" as an Estonian national centre of excellence. This research was also supported by the European Social Fund's Doctoral Studies and Internationalisation Programme DoRa 4 (through a long time stipend for E.P.). Further, the IT Akadeemia 2013/2014 grant for E.P.'s studies is gratefully acknowledged, and the DAAD Rise Worldwide Internship grant for M.P.

## References

[Bra00] BRADSKI G.: The opencv library. *Dr. Dobb's Journal of Software Tools* (2000). 3

[CNSD*92] CRUZ-NEIRA C., SANDIN D. J., DEFANTI T. A., KENYON R. V., HART J. C.: The cave: audio visual experience automatic virtual environment. *Commun. ACM 35*, 6 (June 1992), 64–72. 1

[HEBP14] HERRMANN H., EIK M., BERG V., PUTTONEN J.: Phenomenological and numerical modelling of short fibre reinforced cementitious composites. *Meccanica 49*, 8 (Aug. 2014), 1985–2000. 1

[JM06] JANKUN-KELLY T. J., MEHTA K.: Superellipsoid-based, real symmetric traceless tensor glyphs motivated by nematic liquid crystal alignment visualization. In *IEEE Transactions on Visualization and Computer Graphics (Proceedings Visualization/Information Visualization 2006)* (2006), pp. 1197–1204. 1, 2

[Kin04] KINDLMANN G.: Superquadric tensor glyphs. In *Proceedings of IEEE TVCG/EG Symposium on Visualization 2004* (May 2004), pp. 147–154. 1

[PH13] PASTORELLI E., HERRMANN H.: A small-scale, low-budget semi-immersive virtual environment for scientific visualization and research. *Procedia Computer Science 25*, iii–iv (Sept. 2013), 14–22. 1

[PH14] PASTORELLI E., HERRMANN H.: Virtual reality visualization for short fibre orientation analysis. Baltic Electronics Conference 2014, Oct. 2014. accepted. 1, 2, 4

[SK10] SCHULTZ T., KINDLMANN G.: Superquadric glyphs for symmetric second-order tensors. *IEEE Trans. on Visualization and Computer Graphics 16*, 6 (2010), 1595–1604. 1

[SKE*13] SUURONEN J.-P., KALLONEN A., EIK M., PUTTONEN J., SERIMAA R., HERRMANN H.: Analysis of short fibres orientation in steel fibre reinforced concrete (SFRC) using x-ray tomography. *Journal of Materials Science 48*, 3 (Feb. 2013), 1358–1367. 1

[THS*01] TAYLOR II R. M., HUDSON T. C., SEEGER A., WEBER H., JULIANO J., HELSER A. T.: VRPN: A device-independent, network-transparent VR peripheral system. In *Proceedings of the ACM Symposium on Virtual Reality Software and Technology* (New York, NY, USA, 2001), VRST '01, ACM, pp. 55–61. 4

[VJ01] VIOLA P. A., JONES M. J.: Rapid object detection using a boosted cascade of simple features. In *CVPR (1)* (2001), IEEE Computer Society, pp. 511–518. 4

PUBLICATION IV

Pastorelli E., Herrmann H.

**Time-efficient automated analysis for fibre orientations in Steel Fibre Reinforced Concrete**

*Proceedings of Estonian Academy of Sciences*, 2015, *Accepted*

# Time-efficient automated analysis for fibre orientations in Steel Fibre Reinforced Concrete

Emiliano Pastorelli[a], Heiko Herrmann[a,b]

[a] Centre for Nonlinear Studies, Institute of Cybernetics at Tallinn University of Technology, Akadeemia tee 21, 12618 Tallinn, Estonia
[b] Institut für Physik, Technische Universität Chemnitz, Chemnitz, Germany
E-mail: hh@cens.ioc.ee

**Abstract.** One of the most important factors to determine the mechanical properties of a fibre composite material is the orientation of the fibres in the matrix. Their orientation might differ in distinct parts of the structural element as dependent from the casting techniques and mould materials. This paper presents an algorithm to retrieve the single fibre's orientation information out of SFRC samples scanned through a $\mu$CT scanner. The software implemented with the algorithm includes a data filtering component to remove the noise from the datasets and prepare them correctly for the analysis. Due to its short computational times and its almost complete lack of need for external user intervention, the software is able to process and analyse large batches of data in short periods by providing results in a variety of visual and numerical formats.

**Key words:** computer engineering, image analysis, tomography, steel fibre reinforced concrete, fibre orientation.

## 1. Introduction

Steel Fibre Reinforced Concrete (SFRC) is a cementitious composite material made of cement and aggregate, that incorporates discrete discontinuous fibres. Also thanks to its advantages in terms of production speed and required labour force, SFRC is probably going to gradually supplement or substitute the traditional metal bars or grids reinforced concrete in several construction industry applications.
The need to reinforce concrete arises from the nature of the material itself. Unreinforced concrete is brittle and with a low tensile strength and low strain capacity. In order to perform properly it needs a way to bridge the micro cracks that propagate in its structure to prevent sudden failure.
That method is represented, in the specific case of SFRC described in this paper, by incorporating into the mixture a certain amount of steel fibres with hooked ends, 50 mm long and 1 mm thick. Their presence is fundamental in order to improve the mechanical property of the material. They help the concrete in bearing part of the tensile stress and chemically and mechanically transfer the remaining part to more stable regions of the matrix. Multiple factors influence the efficiency of the fibres: shape, volume fraction, aspect ratio, their surface properties and their orientation [1, 2].
As the orientation distribution of the fibres within the matrix is non-uniform, the properties of the system often tend towards anisotropy. A number of investigations [3–7] demonstrated the strong influence that the orientation has on the material properties.

## 2. Motivation of the research

Several methods already exist in order to extract orientation information from X-ray tomographies of SFRC concrete [8–11]. Most of them are based on approaches very different from each other, among which are: skeletonisation [8], linear regression [10] and separate regions labeling [11].
For several of them though, the use of commercial software and libraries prevented the disclosure of the detailed implementation of the methods. Additionally, most of the methods require either long processing times or the user interaction along the process or even both. This prevents the overnight processing of large batches of datasets, slowing down the whole research process and increasing the possibility for mistakes.
In order to find a solution to the above mentioned problems, we decided to design and implement our own algorithm. The choice was made with the need in mind to have a flexible fast system for the analysis that

could be progressively expanded and improved according to new needs that might arise during our research.

## 3. Introduction to the analysis

The development of the algorithm was initially inspired by [12] and by their use of the Hessian matrix to detect cylindrical shapes in the volumes.
Its pure application though, being developed for higher density straight fibres could not perform correctly in order to analyse the sparsely distributed hooked-end fibres of our samples.
Our specific datasets provided moreover a variety of additional challenges that required a more complex combined approach. The first step of the process was to filter them in order to optimize the data to be fed to the analysis. Filtering was done with the Insight Toolkit (ITK) libraries [13] in order to flag on the volume all the voxels that would not be of interest for the analysis. This meant for the analysis to ignore all the voxels belonging to the matrix (cement, aggregate and air bubbles), all the scanning artefacts and noise.
In better formed datasets (i.e. with no touching fibres), this phase might have also be sufficient to already isolate and label each fibre separately. Unfortunately it was not the case for our data. Due to the tomographic reconstruction and partly as a by-product of the data filtering to isolate cylindrical shapes with the Frangi Vesselness filter [14], it is very rare to have completely separated fibres. Most of them have indeed contact points with other fibres, quite often forming chains of fibres of three or more elements. Only two input parameters are needed in order to perform the data filtering: the thickness of the fibres (in voxels) and the threshold for the binarisation. The first one depends on the properties of the specific type of SFRC analysed and the scanner resolution. The second one depends on the properties of the scanner, of the analysed material and the volume reconstruction. Both the parameters remain constant for all the samples belonging to a batch of the same material scanned with the same technique and devices and using the same parameters for the volume reconstruction.

## 4. Analysis

The data prepared for the analysis after the filtering phase is:

- Cleared of all the voxels not belonging to fibres,
- Binarised,
- The non touching regions have been labeled uniquely [15] and their indices stored to file and
- Smoothed with a Gaussian 3D filter.

The last step, in particular, was necessary in order to use the Hessian-based method mentioned in the previous section.
The Hessian matrix is the square matrix of the second-order partial derivatives of a function. When such a matrix is calculated for each pixel/voxel of a greyscale image (be it 2- or 3-dimensional), its eigenvalues and eigenvectors contain an important set of information about the input element: the variation of intensity of the grey level in all the directions. Equations (1)–(4) and Figure 1 show the construction of the matrix on

a 2D image:

$$(H)_{ij} = \left(\frac{\partial^2 f}{\partial i \partial j}\right), \text{where } i,j = x,y \tag{1}$$

$$\frac{\partial^2 f(x,y)}{\partial x \partial x} \approx \frac{f(x+1,y) - 2f(x,y) + f(x-1,y)}{h^2}, \tag{2}$$

$$\frac{\partial^2 f(x,y)}{\partial y \partial y} \approx \frac{f(x,y+1) - 2f(x,y) + f(x,y-1)}{k^2}, \tag{3}$$

$$\frac{\partial^2 f(x,y)}{\partial x \partial y} \approx \frac{f(x+1,y+1) - f(x+1,y-1) - f(x-1,y+1) + f(x-1,y-1)}{4hk}, \tag{4}$$

here $h$ and $k$ are the pixel (voxel) sizes in $x$ and $y$ directions respectively. In 3D, $i,j = x,y,z$ and corresponding equations for $z$ would be added. In order to be constructed correctly, the matrix requires the cylindrical elements to have a grey level gradient from the inside (high values) to the outside (lower values).

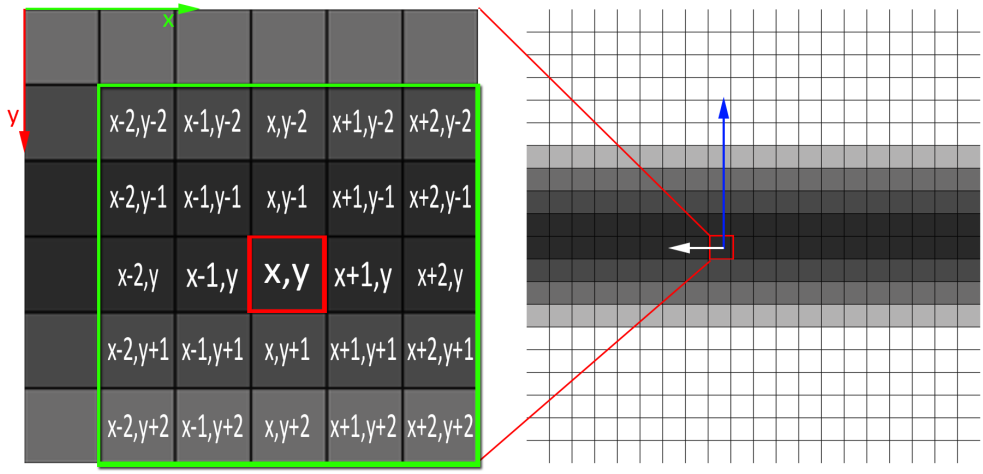


Figure 1. Pixels used for the construction of the 2D greyscale-based Hessian matrix. The direction of the eigenvectors of the matrix in one point is also indicated.

A problem related to our specific datasets arose from the scanning devices not being prepared to process so large concrete samples (10 cm diameter). Because of that, the reconstructed volumes presented a cylindrically shaped artefact, see Fig. 2, in their middle. This artefact contaminated the analysis for multiple reasons.

It connected multiple touching fibres regions making their following separation even more complex, but it also would have been recognised by the analysis as a very large fibre (due to the cylindrical shape), and would have been therefore difficult to manage in the automated analysis.

In order to avoid problems, we filtered the data prior the analysis by coring out the voxels belonging to a parallelepiped-shaped region wrapping the artefact. The results with the core removed immediately proved to be much better than the ones with it still in the volume.

For each voxel belonging to a fibre (using the labels stored during the filtering) the algorithm calculates the Hessian matrix and extracts its eigenvectors. The smallest of them represents the direction of the fibre in that specific voxel (Fig. 1). The orientation vectors for each of the regions are then stored together for the next phase of the analysis. The data gathered so far though, does not represent the fibres' main shaft

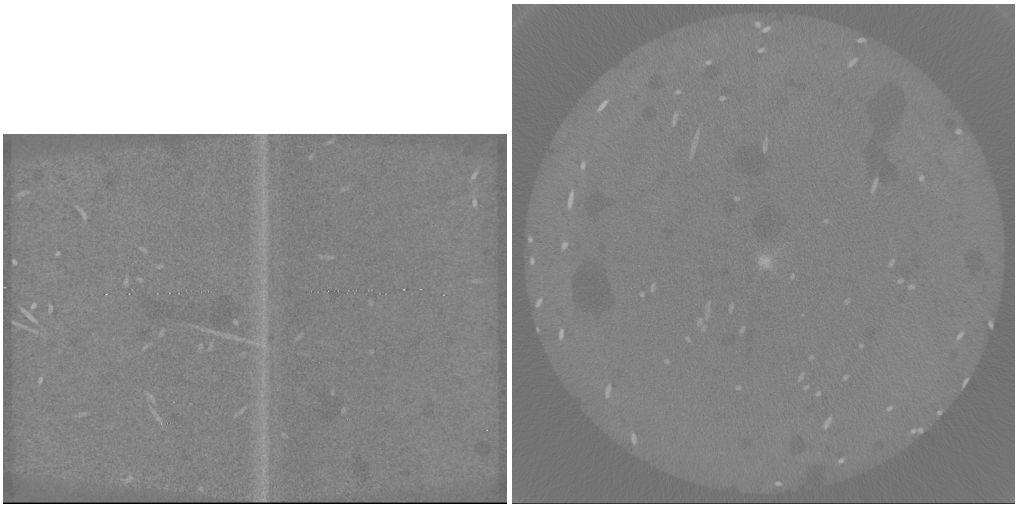

(a) horizontal (b) vertical

Figure 2. Slice images of the tomography showing the artefact in the middle

contribution (i.e. the important one to determine the fibres' contribution at crack time) due to the presence of those vectors belonging to the hooked ends (Fig. 3). In the next section we explain the algorithm we developed to extract the main orientation of the fibres.

## 5. Separation of Touching Fibres

The next step was the most important one of the algorithm in order to identify the orientation of the single fibres.

The idea came from the observation of the voxel vectors visualised on the Kyb3 system, our Virtual Reality environment [16]. Even in case of chains of touching fibres it was quite obvious from the visual inspection that the majority of orientation vectors was aligned along the shafts of the fibres. Therefore the distribution of the orientation vectors of the voxels should show peaks corresponding to the main shafts of each fibre. Unless two fibres of the chain would have identical orientation (in which case they would be seen as a single very large peak), this behaviour had to be isolated and analysed properly.

To cast the data into a more easily analysable format, we converted the voxel orientation vectors from cartesian to spherical coordinates. This operation suffers of some of the weaknesses of the spherical coordinates for angles very close to the poles of the sphere, but allows clustering to be done more easily on a $90 \times 360$ 2D matrix. As for the indices of the matrix we used the Theta ($\vartheta$) angle to represent the rotation on the $z$ axis (polar angle) and the Phi ($\varphi$) angle for the rotation on the $x$-$y$-plane (azimuthal angle).

In order to clean the results from noise and facilitate peak detection we smoothed the whole matrix with a simple Gaussian filtering.

The analysis of a single fibre (a rare occurrence in the dataset) generates a single dominating peak and represents no particular problem for the detection (Fig. 4(a)). Slightly more complex was the case of multiple touching fibres. The angles corresponding to the main fibres orientation, though, generated peaks of such a size to be easily identifiable in the matrix (Fig. 4(b)). To ignore the noise and the much smaller peaks resulting from the hooked ends of the fibre, we thresholded the data proportionally to the highest peaks in the matrix.We then proceeded to isolate the separate clusters through a connected regions labelling algorithm [17].

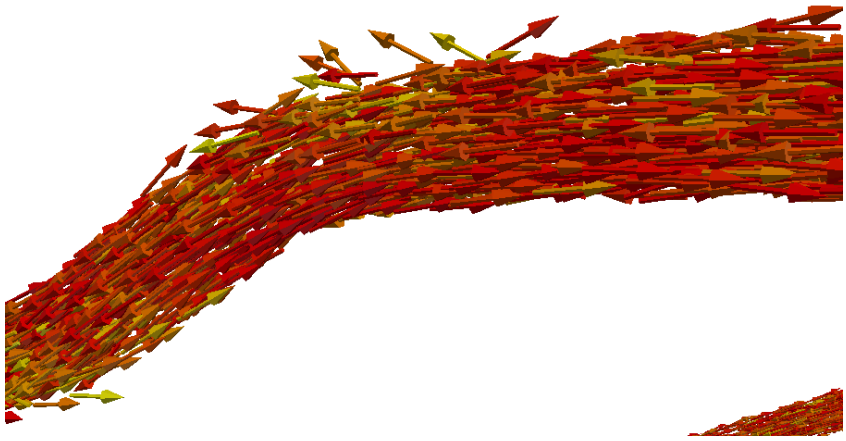

Figure 3. Detail on the voxel vectors in proximity of one of the hooked ends of a fibre

In each of the clusters, we proceeded then by locating the highest local peak, i.e. the one corresponding to the fibre shaft orientation.
As the last step we converted back the angles from spherical to cartesian coordinates. The outcome is that for each fibre, we now had the centre point (obtained by averaging the coordinates of all the voxels belonging to the peak) and the orientation.

## 6. Performances and timings

While the filtering process can be expensive in terms of resources (the ITK Frangi Vesselness filter [18] applied to a $900 \times 900 \times 576$ volume requires up to 32GB of RAM) and takes approximately 23 to 25 minutes per volume, the analysis component of the software is, by contrast, very fast and lightweight.
Thanks to the labels provided by the filtering phase, only the relevant voxels are analysed while all the others are completely skipped and speeds up computation up additionally.
A series of optimisation in the data structure's use, allows to run the whole process on a $900 \times 900 \times 576$ dataset in a time that ranges between 2 and 3.5 minutes depending on the amount of fibres in the volume. The RAM consumption for the analysis barely reaches 4GB and requires absolutely no additional input from the user.
The whole filtering and analysis process for a single dataset can be therefore performed in approximately 25 to 28 minutes.

## 7. Validation of results

The validation of the algorithm and its implementation has been made in two ways: visually and numerically. The visual feedback was used throughout the whole development for a quick testing of the correctness of all the steps (Fig. 4), from filtering until the final analysis was performed.

Throughout software execution, we saved a variety of data describing each step's outcome in formats easy to read and visualise. This allowed a constant correctness control and the possibility to quickly detect

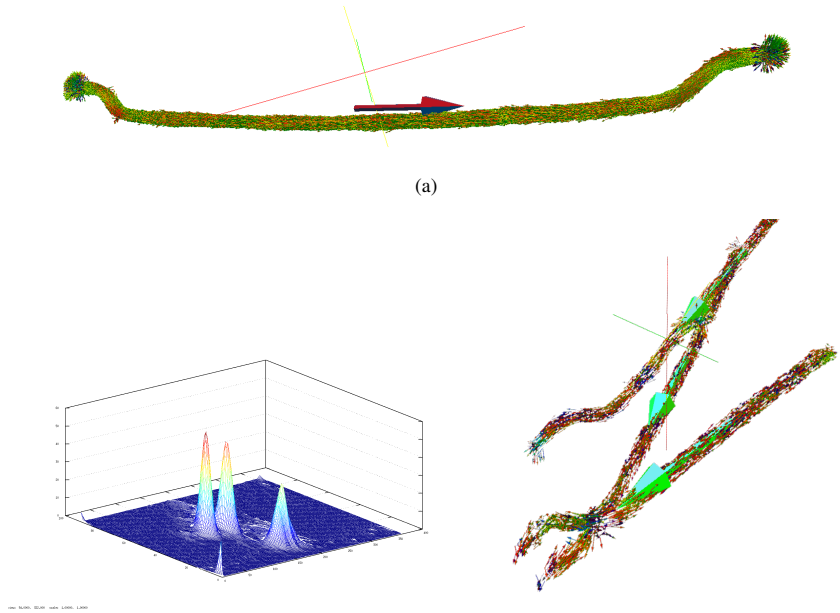

(a)

(b) (c)

Figure 4. (a) a single fibre orientation extraction, (b) the peaks describing three touching fibres, (c) the three touching fibres separate orientations after the analysis of the regions peaks map.

and correct algorithmic and implementation mistakes. The data produced at the end of the whole analysis consisted of:

- Volume file (in the NRRD/NHDR format [19]; header+raw volume) containing the filtered and smoothed volume showing only the fibres,
- a VTK [20] point based visualisation file containing all the voxel vectors of all fibres (Fig. 5),
- a VTK file containing the single fibre orientation vectors correctly positioned in space.

As it can be seen in Fig. 3, Fig. 4 and Fig. 5, the voxel vectors and fibre orientation vectors show unambiguously the correctness of the algorithm and the software.
In order to perform a numerical validation, we compared the results of the analysis with those provided by the skeletonisation approach [8] on the same datasets. Aside from small differences depending on a variety of factors, the two analyses were very similar in the results. The scatterplots in Fig. 6 show the superposition of the fibre orientation angles as obtained by skeletonisation (Fig. 6(a)) and by our method (Fig. 6(b)). The comparison performed correctly on all the 15 datasets . By using the same equations described in [6, 8], we calculated from the data the order parameter and director describing the orientation of the fibres in the sample.

The director is the eigenvector corresponding to the largest eigenvalue (according to absolute value: $|\lambda_1| \geq |\lambda_2| \geq |\lambda_3|$) of the second order alignment tensor $\mathbf{A}$ that is described as:

$$\mathbf{A} = \frac{1}{N}\sum_{i=1}^{N} \overline{\mathbf{n}_i \otimes \mathbf{n}_i} \tag{5}$$

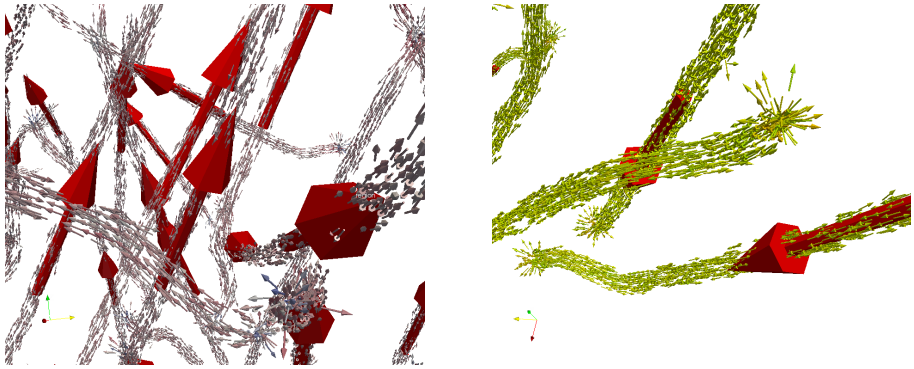

(a) (b)

Figure 5. (a) full orientation extraction, voxel and fibres vectors, (b) orientation extraction detail on single fibre.

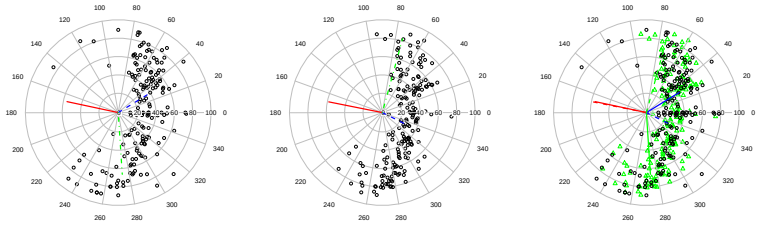

(a) (b) (c)

Figure 6. Scatterplot describing the orientation angles in a sample: (a) with the skeletonisation method [8], (b) with the method described in this paper, and (c) the superposition of the two results.

$\mathbf{n}_i$ represents the direction of the $i$-th fibre, $N$ the total amount of fibres and $\overline{\mathbf{n}_i \otimes \mathbf{n}_i}$ the symmetric traceless tensor product. The order parameter is given as

$$S = \frac{3}{2}\lambda_1 \tag{6}$$

or as

$$S = \left\langle \frac{3}{2}\cos^2\alpha - \frac{1}{2} \right\rangle \tag{7}$$

with $\lambda_1$ the largest eigenvalue of $\mathbf{A}$ and $\alpha$ is the angle between the individual fibre and the director.

The director of the sample displayed in Fig. 6 (expressed in $\vartheta$, $\varphi$ angles) is $(\varphi = 169, \vartheta = 59)$ for the skeletonisation approach and $(\varphi = 168, \vartheta = 57)$ with our method.
The order parameter is $S = -44$ for the skeletonisation, and $S = -41$ for our algorithm. The differences among the parameters is sufficiently small to validate the results.

## 8. Conclusion

Although still under improvement, the described method and software already proved to provide very reliable results.
The limited human interaction and very fast processing times minimize the possibility for human errors and allow the autonomous analysis of large batches of data.
The software builds its own structured directories in order to store all the output orderly and process the numeric data further for additional analyses. With further steps towards an even more precise analysis of the peaks in order to succeed also in case of very similarly aligned fibres and a more easily usable graphical interface, we strongly believe that the software has a chance to become a widespread tool for SFRC analysis.

## Acknowledgement

This research was supported by the European Union through the European Regional Development Fund, in particular through funding for the "Centre for Nonlinear Studies" as an Estonian national centre of excellence. Compiled with the assistance of the Tiger University Program of the Estonian Information Technology Foundation (VisPar/Kyb3 visualization system, EITSA/HITSA grants 10-03-00-24, 12-03-00-11 and 13030009). This research was supported by European Social Fund's Doctoral Studies and Internationalisation Programme DoRa T4, which is carried out by Archimedes Foundation (scholarship for E.P.). E.P. also gratefully acknowledges the ICT doctoral school for the study grant for the academic year 2014/2015.

## References

1. Bentur A, Mindess S. Fibre reinforced cementitious composites. London and New York: Taylor & Francis; 2007.
2. Tejchman J, Kozicki J. Experimental and theoretical investigations of steel-fibrous concrete. 1st ed. Springer series in geomechanics and geoengineering. Springer; 2010.
3. Grünewald S, Laranjeira F, Walraven JC, Aguado A, Molins C. Influence of fibre orientation on the performance of steel fibre-reinforced concrete. 8th RILEM International Symposium on Fiber Reinforced Concrete: challenges and opportunities (BEFIB 2012). 2013;p. 313 – 325.
4. Wuest J, Denarie E, Bruhwiler E, Tamarit L, Kocher M, Gallucci E. Tomography analysis of fiber distribution and orientation in ultra high-performance fiber-reinforced composites with high-fiber dosages. Experimental Techniques. 2009;33(5):50–55.
5. Le TH, Dumont PJJ, Orgeas L, Favier D, Salvo L, Boller E. X-ray phase contrast microtomography for the analysis of the fibrous microstructure of SMC composites. Compos Part A: Appl Sci Manuf. 2008;39(1):91–103.
6. Herrmann H, Eik M, Berg V, Puttonen J. Phenomenological and numerical modelling of short fibre reinforced cementitious composites. Meccanica. 2014 Aug;49(8):1985–2000.
7. Eik M, Puttonen J, Herrmann H. An orthotropic material model for steel fibre reinforced concrete based on the orientation distribution of fibres. Composite Structures. 2015;121(0):324–336.
8. Suuronen JP, Kallonen A, Eik M, Puttonen J, Serimaa R, Herrmann H. Analysis of short fibres orientation in Steel Fibre Reinforced Concrete (SFRC) using X-ray tomography. J Mater Sci. 2013 Feb;48(3):1358–1367.
9. Schnell J, Schladitz K, Schuler F. Richtungsanalyse von Fasern in Betonen auf Basis der Computer-Tomographie. Beton- und Stahlbetonbau. 2010;105(2):72–77.
10. Vicente MA, Gonzalez DC, Minguez J. Determination of dominant fibre orientations in fibre-reinforced high-strength concrete elements based on computed tomography scans. Nondestructive Testing and Evaluation. 2014;29(2):164–182.
11. Ponikiewski T, Katzer J, Bugdol M, Rudzki M. Steel fibre spacing in self-compacting concrete precast walls by X-ray computed tomography. Mater Struct. 2014;p. 1–12.
12. Redenbach C, Rack A, Schladitz K, Wirjadic O, Godehardt M. Beyond imaging: on the quantitative analysis of tomographic volume data. Int J Mater Res. 2012;2012(2):217–227.
13. Johnson HJ, McCormick M, Ibanez L, Consortium TIS. The ITK Software Guide; 2013. Available from: `http://www.itk.org/ItkSoftwareGuide.pdf`.
14. Frangi AF, Niessen WJ, Nederkoorn PJ, Bakker J, Mali WPTM, Viergever MA. Quantitative analysis of vascular morphology from 3D MR angiograms: in vitro and in vivo results. Magnetic Resonance in Medicine. 2001;45:311–322.
15. Lehmann G. Label object representation and manipulation with ITK; 2007. `http://hdl.handle.net/1926/584`.

16. Pastorelli E, Herrmann H. A small-scale, low-budget semi-immersive Virtual Environment for Scientific Visualization and Research. Procedia Computer Science. 2013 Sep;25(iii–iv):14–22.
17. Dillencourt MB, Samet H, Tamminen M. A General Approach to Connected-component Labeling for Arbitrary Image Representations. J ACM. 1992 Apr;39(2):253–280. Available from: http://doi.acm.org/10.1145/128749.128750.
18. Kroon DJ. Hessian based Frangi Vesselness filter; 2010. http://www.mathworks.com/matlabcentral/fileexchange/24409-hessian-based-frangi-vesselness-filter.
19. Kindlmann G, Bigler J, Van Uitert D. NRRD file format; 2008. Available from: http://teem.sourceforge.net/nrrd/format.html.
20. Schroeder W, Martin KM, Lorensen WE. The Visualization Toolkit (2nd Ed.): An Object-oriented Approach to 3D Graphics. Upper Saddle River, NJ, USA: Prentice-Hall, Inc.; 1998.

# DISSERTATIONS DEFENDED AT TALLINN UNIVERSITY OF TECHNOLOGY ON *INFORMATICS AND SYSTEM ENGINEERING*

1. **Lea Elmik**. Informational Modelling of a Communication Office. 1992.

2. **Kalle Tammemäe**. Control Intensive Digital System Synthesis. 1997.

3. **Eerik Lossmann**. Complex Signal Classification Algorithms, Based on the Third-Order Statistical Models. 1999.

4. **Kaido Kikkas**. Using the Internet in Rehabilitation of People with Mobility Impairments – Case Studies and Views from Estonia. 1999.

5. **Nazmun Nahar**. Global Electronic Commerce Process: Business-to-Business. 1999.

6. **Jevgeni Riipulk**. Microwave Radiometry for Medical Applications. 2000.

7. **Alar Kuusik**. Compact Smart Home Systems: Design and Verification of Cost Effective Hardware Solutions. 2001.

8. **Jaan Raik**. Hierarchical Test Generation for Digital Circuits Represented by Decision Diagrams. 2001.

9. **Andri Riid**. Transparent Fuzzy Systems: Model and Control. 2002.

10. **Marina Brik**. Investigation and Development of Test Generation Methods for Control Part of Digital Systems. 2002.

11. **Raul Land**. Synchronous Approximation and Processing of Sampled Data Signals. 2002.

12. **Ants Ronk**. An Extended Block-Adaptive Fourier Analyser for Analysis and Reproduction of Periodic Components of Band-Limited Discrete-Time Signals. 2002.

13. **Toivo Paavle**. System Level Modeling of the Phase Locked Loops: Behavioral Analysis and Parameterization. 2003.

14. **Irina Astrova**. On Integration of Object-Oriented Applications with Relational Databases. 2003.

15. **Kuldar Taveter**. A Multi-Perspective Methodology for Agent-Oriented Business Modelling and Simulation. 2004.

16. **Taivo Kangilaski**. Eesti Energia käiduhaldussüsteem. 2004.

17. **Artur Jutman**. Selected Issues of Modeling, Verification and Testing of Digital Systems. 2004.

18. **Ander Tenno**. Simulation and Estimation of Electro-Chemical Processes in Maintenance-Free Batteries with Fixed Electrolyte. 2004.

19. **Oleg Korolkov**. Formation of Diffusion Welded Al Contacts to Semiconductor Silicon. 2004.

20. **Risto Vaarandi**. Tools and Techniques for Event Log Analysis. 2005.

21. **Marko Koort**. Transmitter Power Control in Wireless Communication Systems. 2005.

22. **Raul Savimaa**. Modelling Emergent Behaviour of Organizations. Time-Aware, UML and Agent Based Approach. 2005.

23. **Raido Kurel**. Investigation of Electrical Characteristics of SiC Based Complementary JBS Structures. 2005.

24. **Rainer Taniloo**. Ökonoomsete negatiivse diferentsiaaltakistusega astmete ja elementide disainimine ja optimeerimine. 2005.

25. **Pauli Lallo**. Adaptive Secure Data Transmission Method for OSI Level I. 2005.

26. **Deniss Kumlander**. Some Practical Algorithms to Solve the Maximum Clique Problem. 2005.

27. **Tarmo Veskioja**. Stable Marriage Problem and College Admission. 2005.

28. **Elena Fomina**. Low Power Finite State Machine Synthesis. 2005.

29. **Eero Ivask**. Digital Test in WEB-Based Environment 2006.

30. **Виктор Войтович**. Разработка технологий выращивания из жидкой фазы эпитаксиальных структур арсенида галлия с высоковольтным p-n переходом и изготовления диодов на их основе. 2006.

31. **Tanel Alumäe**. Methods for Estonian Large Vocabulary Speech Recognition. 2006.

32. **Erki Eessaar**. Relational and Object-Relational Database Management Systems as Platforms for Managing Softwareengineering Artefacts. 2006.

33. **Rauno Gordon**. Modelling of Cardiac Dynamics and Intracardiac Bio-impedance. 2007.

34. **Madis Listak**. A Task-Oriented Design of a Biologically Inspired Underwater Robot. 2007.

35. **Elmet Orasson**. Hybrid Built-in Self-Test. Methods and Tools for Analysis and Optimization of BIST. 2007.

36. **Eduard Petlenkov**. Neural Networks Based Identification and Control of Nonlinear Systems: ANARX Model Based Approach. 2007.

37. **Toomas Kirt**. Concept Formation in Exploratory Data Analysis: Case Studies of Linguistic and Banking Data. 2007.

38. **Juhan-Peep Ernits**. Two State Space Reduction Techniques for Explicit State Model Checking. 2007.

39. **Innar Liiv**. Pattern Discovery Using Seriation and Matrix Reordering: A Unified View, Extensions and an Application to Inventory Management. 2008.

40. **Andrei Pokatilov**. Development of National Standard for Voltage Unit Based on Solid-State References. 2008.

41. **Karin Lindroos**. Mapping Social Structures by Formal Non-Linear Information Processing Methods: Case Studies of Estonian Islands Environments. 2008.

42. **Maksim Jenihhin**. Simulation-Based Hardware Verification with High-Level Decision Diagrams. 2008.

43. **Ando Saabas**. Logics for Low-Level Code and Proof-Preserving Program Transformations. 2008.

44. **Ilja Tšahhirov**. Security Protocols Analysis in the Computational Model – Dependency Flow Graphs-Based Approach. 2008.

45. **Toomas Ruuben**. Wideband Digital Beamforming in Sonar Systems. 2009.

46. **Sergei Devadze**. Fault Simulation of Digital Systems. 2009.

47. **Andrei Krivošei**. Model Based Method for Adaptive Decomposition of the Thoracic Bio-Impedance Variations into Cardiac and Respiratory Components. 2009.

48. **Vineeth Govind**. DfT-Based External Test and Diagnosis of Mesh-like Networks on Chips. 2009.

49. **Andres Kull**. Model-Based Testing of Reactive Systems. 2009.

50. **Ants Torim**. Formal Concepts in the Theory of Monotone Systems. 2009.

51. **Erika Matsak**. Discovering Logical Constructs from Estonian Children Language. 2009.

52. **Paul Annus**. Multichannel Bioimpedance Spectroscopy: Instrumentation Methods and Design Principles. 2009.

53. **Maris Tõnso**. Computer Algebra Tools for Modelling, Analysis and Synthesis for Nonlinear Control Systems. 2010.

54. **Aivo Jürgenson**. Efficient Semantics of Parallel and Serial Models of Attack Trees. 2010.

55. **Erkki Joasoon**. The Tactile Feedback Device for Multi-Touch User Interfaces. 2010.

56. **Jürgo-Sören Preden**. Enhancing Situation – Awareness Cognition and Reasoning of Ad-Hoc Network Agents. 2010.

57. **Pavel Grigorenko**. Higher-Order Attribute Semantics of Flat Languages. 2010.

58. **Anna Rannaste**. Hierarcical Test Pattern Generation and Untestability Identification Techniques for Synchronous Sequential Circuits. 2010.

59. **Sergei Strik**. Battery Charging and Full-Featured Battery Charger Integrated Circuit for Portable Applications. 2011.

60. **Rain Ottis**. A Systematic Approach to Offensive Volunteer Cyber Militia. 2011.

61. **Natalja Sleptšuk**. Investigation of the Intermediate Layer in the Metal-Silicon Carbide Contact Obtained by Diffusion Welding. 2011.

62. **Martin Jaanus**. The Interactive Learning Environment for Mobile Laboratories. 2011.

63. **Argo Kasemaa**. Analog Front End Components for Bio-Impedance Measurement: Current Source Design and Implementation. 2011.

64. **Kenneth Geers**. Strategic Cyber Security: Evaluating Nation-State Cyber Attack Mitigation Strategies. 2011.

65. **Riina Maigre**. Composition of Web Services on Large Service Models. 2011.

66. **Helena Kruus**. Optimization of Built-in Self-Test in Digital Systems. 2011.

67. **Gunnar Piho**. Archetypes Based Techniques for Development of Domains, Requirements and Sofware. 2011.

68. **Juri Gavšin**. Intrinsic Robot Safety Through Reversibility of Actions. 2011.

69. **Dmitri Mihhailov**. Hardware Implementation of Recursive Sorting Algorithms Using Tree-like Structures and HFSM Models. 2012.

70. **Anton Tšertov**. System Modeling for Processor-Centric Test Automation. 2012.

71. **Sergei Kostin**. Self-Diagnosis in Digital Systems. 2012.

72. **Mihkel Tagel**. System-Level Design of Timing-Sensitive Network-on-Chip Based Dependable Systems. 2012.

73. **Juri Belikov**. Polynomial Methods for Nonlinear Control Systems. 2012.

74. **Kristina Vassiljeva**. Restricted Connectivity Neural Networks based Identification for Control. 2012.

75. **Tarmo Robal**. Towards Adaptive Web – Analysing and Recommending Web Users` Behaviour. 2012.

76. **Anton Karputkin**. Formal Verification and Error Correction on High-Level Decision Diagrams. 2012.

77. **Vadim Kimlaychuk**. Simulations in Multi-Agent Communication System. 2012.

78. **Taavi Viilukas**. Constraints Solving Based Hierarchical Test Generation for Synchronous Sequential Circuits. 2012.

79. **Marko Kääramees**. A Symbolic Approach to Model-based Online Testing. 2012.

80. **Enar Reilent**. Whiteboard Architecture for the Multi-agent Sensor Systems. 2012.

81. **Jaan Ojarand**. Wideband Excitation Signals for Fast Impedance Spectroscopy of Biological Objects. 2012.

82. **Igor Aleksejev**. FPGA-based Embedded Virtual Instrumentation. 2013.

83. **Juri Mihhailov**. Accurate Flexible Current Measurement Method and its Realization in Power and Battery Management Integrated Circuits for Portable Applications. 2013.

84. **Tõnis Saar**. The Piezo-Electric Impedance Spectroscopy: Solutions and Applications. 2013.

85. **Ermo Täks**. An Automated Legal Content Capture and Visualisation Method. 2013.

86. **Uljana Reinsalu**. Fault Simulation and Code Coverage Analysis of RTL Designs Using High-Level Decision Diagrams. 2013.

87. **Anton Tšepurov**. Hardware Modeling for Design Verification and Debug. 2013.

88. **Ivo Müürsepp**. Robust Detectors for Cognitive Radio. 2013.

89. **Jaas Ježov**. Pressure sensitive lateral line for underwater robot. 2013.

90. **Vadim Kaparin**. Transformation of Nonlinear State Equations into Observer Form. 2013.

92. **Reeno Reeder**. Development and Optimisation of Modelling Methods and Algorithms for Terahertz Range Radiation Sources Based on Quantum Well Heterostructures. 2014.

93. **Ants Koel**. GaAs and SiC Semiconductor Materials Based Power Structures: Static and Dynamic Behavior Analysis. 2014.

94. **Jaan Übi**. Methods for Coopetition and Retention Analysis: An Application to University Management. 2014.

95. **Innokenti Sobolev**. Hyperspectral Data Processing and Interpretation in Remote Sensing Based on Laser-Induced Fluorescence Method. 2014.

96. **Jana Toompuu**. Investigation of the Specific Deep Levels in *p*-, *i*- and *n*-Regions of GaAs $p^+$-*pin*-$n^+$ Structures. 2014.

97. **Taavi Salumäe**. Flow-Sensitive Robotic Fish: From Concept to Experiments. 2015.

98. **Yar Muhammad**. A Parametric Framework for Modelling of Bioelectrical Signals. 2015.

99. **Ago Mõlder**. Image Processing Solutions for Precise Road Profile Measurement Systems. 2015.

100. **Kairit Sirts**. Non-Parametric Bayesian Models for Computational Morphology. 2015.

101. **Alina Gavrijaševa**. Coin Validation by Electromagnetic, Acoustic and Visual Features. 2015.